FATIGUE ANALYSIS OF RC SLABS WITH PLAIN BARS AND FRP STRENGTHENING BASED ON BRIDGING STRESS DEGRADATION CONCEPT

Ahmed Attia Mahmoud Drar

Division of Engineering and Policy for Sustainable Environment
Graduate School of Engineering
Hokkaido University
Sapporo, Japan

September, 2016

FATIGUE ANALYSIS OF RC SLABS WITH PLAIN BARS AND FRP STRENGTHENING BASED ON BRIDGING STRESS DEGRADATION CONCEPT

Ahmed Attia Mahmoud DRAR

A DISSERTATION SUBMITTED IN PARTIAL FULFILLMENT
OF THE REQUIREMENTS FOR THE DEGREE
OF DOCTOR OF PHILOSOPHY
IN ENGINEERING

Examination Committee:

Prof. Takashi MATSUMOTO
Prof. Hiroshi YOKOTA
Prof. Shunji KANIE

Division of Engineering and Policy for Sustainable Environment
Graduate School of Engineering
Hokkaido University
Sapporo, Japan

September, 2016

ACKNOWLEGEMENTS

First and foremost, I wish to express my deep, sincere thanks to my supervisor, Professor Takashi Matsumoto for his guidance, supervisions, instructions, valuable advices suggestions, and necessary assistances throughout the three-year study period at the Laboratory of Bridge and Structural Design Engineering, Hokkaido University. Without his patient assistance, it would not be possible for me to complete my Ph.D. study. His guidance helped me in all time of research, writing papers, and writing of this thesis. I could not have imagined having a better advisor and mentor for my Ph.D. study.

Besides my supervisor, I would like to thank the rest of my thesis committee members: Professor Hiroshi Yokota and Shunji Kanie, for their insightful comments and encouragement, but also for their question which incited me to widen my research from various perspectives.

From the bottom of my heart, I also wish to express my gratitude to Professor Toshiro Hayashikawa for his advice and motivation. He provided me an opportunity to join the research team in the laboratory meetings. I also would like to extend many thanks to Professor Xingwen He, who gives me many useful advices and comments for my study.

I thank my laboratory colleagues in for stimulating discussions, for the sleepless nights we were working together before deadlines, and for all the fun we have in the last three years.

In order to have today achievements, I would like to express my deep gratitude to the Japanese Government for their support of financial assistance as the scholarship during my study period in Japan.

On this occasion, I wish to express my greatest gratitude to my lovely wife, Taghreed Ahmed Mahmoud, my daughter, Rhf Ahmed, and my son Mohammed Ahmed for their care, encouragement, and moral support throughout the time I have lived and learned in Sapporo.

Last but not the least, I would like to send my special thanks for to my parents: Attia Mahmoud Drar and Amal Amir Ahmed, for their supporting and motivations in my life in general. I would like to give this achievement, Ph.D., to my family, including my parents and my brothers.

ABSTRACT

The safety of construction in the long-term performance is the main goal of structural designers. An example is seen in reinforced concrete (RC) bridge deck slabs that have been subjected to a large number of load repetitions. Therefore, many numerical and experimental studies have been conducted to predict the fatigue life of these slabs. Most of these studies focused on the modeling of fatigue behaviors of RC slabs reinforced with deformed bars. Until 1965, plain bars were used for reinforcing RC bridge slabs in a part of Japan. The fatigue damage of those slabs is more significantly observed than that of slabs reinforced with deformed bars. Moreover, old slabs were economically designed by small thickness without considering the fatigue resistance. Until 1965, plain bars were used for reinforcing RC bridge slabs in a part of Japan. The fatigue damage of those slabs is more significantly observed than that of slabs reinforced with deformed bars. Therefore, it is important to predict the fatigue behaviors of these slabs to decide a suitable repairing method.

For the main goal of this research, a numerical method based on the bridging stress degradation concept is presented in this study to simulate the fatigue behaviors of RC slabs reinforced with plain bars under a moving load. Moreover, this study provides a numerical investigation to understand the fatigue failure and the improvement mechanism of fiber reinforced polymer (FRP) strengthening.

Finite element method (FEM) is used to solve a slab model of smeared crack elements. The cracked elements are modified according to the bridging stress degradation concept. This concept can be defined as the reduction of transferred stress across a crack plane under repetitive loading due to crack opening and closing process. Reinforcing bars are modeled as a smeared reinforcement according to its ratio in all directions. For plain reinforcing bars, the bond-slip effect between a reinforcing bar and its surrounding concrete is taken into consideration by adding equivalent bond strain to plain bar strain. To verify the numerical method, this study will be divided to three parts as follows.

In the first part, plain concrete beam is analyzed under static and fixed pulsating load. Moreover, RC beams are analyzed using this numerical method under fixed pulsating and moving load. The numerical method succeeded in describing the propagation of cracked elements for fixed pulsating and moving load. The numerical results are compared with the experimental results to examine the applicability of this method for plain and reinforced concrete beams.

In the second part, three RC slabs reinforced with plain bars are conducted using the proposed numerical method. Moreover, one RC slab reinforced with deformed bars is analyzed to compare with that reinforced with plain bars. The numerical model is verified using previous experimental data. This model is also able to capture the cracking pattern, change in displacement and rebar strain. The numerical results provide a good agreement with the experimental ones. In this part, a successful explanation of fatigue failure mechanism is existed. The effect of plain reinforcing bars on the fatigue behaviors is described.

In the last, three full scale RC slabs reinforced with plain bars under moving load are analyzed using a proposed numerical method to simulate their fatigue behaviors. two of them were strengthened with externally bonded FRP sheets in longitudinal and transverse directions on slab bottom surface. The interfacial bond behavior between FRP sheet and concrete surface

with its degradation due to fatigue loading are integrated to obtain appropriate numerical results. The propagation of cracked elements, center displacement evolution, cracking pattern and FRP strain are presented in this study. According to the results, FRP sheets play an important role to restrict the major crack opening. This leads to a slow degradation, longer fatigue life and smaller deformations for the strengthened RC slab. These numerical results are compared with the experimental results, and this comparison provides a good agreement.

TABLE OF CONTENTS

ACKNOWLEGEMENTS i
ABSTRACT ii
TABLE OF CONTENTS iv
LIST OF TABLES vii
LIST OF FIGURES viii
CHAPTER 1 GENERAL INTRODUCTION 1
1.1 Background and motivation 1
1.2 Brief review of previous studies 2
1.3 Objectives and scope of study 4
1.4 Organization of the thesis 4
CHAPTER 2 FATIGUE ANALYSIS METHOD BASED ON BRIDGING STRESS DEGRADATION 6
2.1 Introduction 6
2.2 Concrete 6
2.2.1 Nonlinear constitutive laws for concrete 6
2.2.2 Crack formation of concrete 8
2.2.3 Shear transfer for cracked concrete 9
2.2.4 Biaxial stress failure criterion of concrete 10
2.2.5 Bridging stress degradation and concrete behavior under cyclic loading 11
2.2.6 Concrete stiffness matrices 13
2.2.6.1 Uncracked concrete 13
2.2.6.2 Cracked concrete 13
2.3 Reinforcing bar 14
2.3.1 Modified stress-strain relationship according to bond-slip effect 15
2.3.2 Cyclic behavior of reinforcing bar 17
2.3.3 Smeared reinforcement stiffness matrix 18
2.4 FRP and interfacial bond element 18
2.4.1 FRP 19
2.4.2 Interfacial bond element 19
2.4.3 Interfacial bond behavior under cyclic loading. 22
CHAPTER 3 FATIGUE ANALYSIS OF PLAIN AND REINFORCED CONCRETE BEAMS 25
3.1 Introduction 25
3.2 Plain concrete beam 25

3.2.1 Static analysis of plain concrete beam 26
3.2.2 Fatigue analysis of plain concrete beam 27
3.3 Reinforced concrete beam 29
3.3.1 Static analysis of RC beam 30
3.3.2 Fatigue analysis of RC beam 31
3.3.3 Comparison between fixed pulsating and moving load 31
3.4 Deciding a reinforcing model technique 35
3.4.1 Analytical model of the tested RC beam 36
3.4.2 Results and discussions 38
3.5 Summary and conclusions 40
CHAPTER 4 FATIGUE ANALYSIS OF RC SLABS REINFORCED WITH PLAIN BARS 42
4.1 Introduction 42
4.2 RC slab modeling and analytical procedure 42
4.3 Static analysis results 43
4.3.1 Load-maximum displacement relation due to static loading 43
4.3.2 Maximum principle tensile strain distribution 45
4.3.3 Longitudinal and transverse displacement distribution 45
4.4 Fatigue analysis results 45
4.4.1 Propagation of cracked elements 45
4.4.2 Center displacement evolution 47
4.4.3 Fatigue life and S-N relationship 47
4.4.4 Cracking patterns 47
4.4.5 Fatigue failure mechanism 50
4.4.6 Reinforcing bar strain 52
4.5 Summary and conclusions 55
CHAPTER 5 FATIGUE ANALYSIS OF STRENGTHENED RC SLABS WITH FRP SHEETS 57
5.1 Introduction 57
5.2 Geometry and numerical model 57
5.3 Static analysis results 62
5.4 Fatigue analysis results 63
5.4.1 Propagation of cracked elements 63
5.4.2 Center displacement evolution 64
5.4.3 Cracking pattern and strain distribution at fatigue failure 67
5.4.4 Transverse FRP sheet strain 73

5.4.5 Fatigue behavior improvement due to FRP strengthening. 73
5.5 The separated and uniform cracked zones on fatigue analysis 78
5.6 Conclusions and summary 78
CHAPTER 6 CONCLUSIONS AND FUTURE WORKS 81
6.1 Major conclusions 81
6.2 Future works 82
APPENDIX A- PUBLICATION LISTS 83
REFERENCES 84

LIST OF TABLES

Table 3.1 Material properties [29] 29
Table 3.2 Percentages of cracked element volume and average degradation ratio..... 33
Table 3.3 materials properties of tested beam [32] 36
Table 3.4 Cracking load and displacement for analyzed beam 39

Table 4.1 RC slabs details 43
Table 4.2 The percentage of the cracked elements volume 49
Table 4.3 Fatigue life of RC slabs 49

Table 5.1 Details of analyzed RC slabs 58
Table 5.2 Materials properties [8] 59
Table 5.3 Applied moving load for all analyzed slabs 61
Table 5.4 The percentages of cracked elements volumes of analyzed slabs 66

LIST OF FIGURES

Fig. 1.1 Deformed and plain bar 1
Fig. 1.2 Shuen-Bridge (National Highway Route 334, Shari, Hokkaido, Japan)..... 1
Fig. 1.3 CFRP strengthening..... 2
Fig. 1.4 Cracking pattern for RC slab under moving load showing a punching shear failure [2]..... 3
Fig. 1.5 Moving load test 3

Fig. 2.1 Uniaxial stress-strain relation for concrete 7
Fig. 2.2 Crack formation: **(a)** initiation of a first crack; **(b)** three perpendicular crack formations..... 8
Fig. 2.3 Shear transfer model for one-directional crack..... 9
Fig. 2.4 Biaxial failure criterion of concrete 10
Fig. 2.5 Crack propagation due to bridging stress: (a) the first cycle; (b) after N cycles 12
Fig. 2.6 Concrete behavior under cyclic loading 12
Fig. 2.7 Principal and global stress-strain directions 14
Fig. 2.8 Smeared reinforced concrete elements 14
Fig. 2.9 Modified stress-strain relationship for reinforcing bar 16
Fig. 2.10 Stress and strain distribution of a cracked RC element in bending 16
Fig. 2.11 Giuffre-Menegotto-Pinto model [20]..... 17
Fig. 2.12 (a) FRP sheets and **(b)** Epoxy resin adhesive 18
Fig. 2.13 FRP installation..... 19
Fig. 2.14 Stress-strain relationship for FRP 19
Fig. 2.15 Strengthened RC slab..... 20
Fig. 2.16 Comparison between springs and 8-node interfacial element approaches..... 20
Fig. 2.17 Interfacial bond-slip model..... 20
Fig. 2.18 8-ndoe interface element..... 22
Fig. 2. 19 Bond stress versus slip displacement relationships under cyclic loading for Specimen S1-3 of Dai et al. [23] 23
Fig. 2.20 the degradation of interfacial bond stiffness due to cyclic loading..... 23

Fig. 3.1 three-point bending beam 25
Fig. 3.2 Load-midspan displacement relationships..... 26
Fig. 3.3 Stress and strain distributions at midspan section..... 27
Fig. 3.4 Cracking pattern at maximum load (point B) 27
Fig. 3.5 Cracked elements propagation..... 28
Fig. 3.6 Stress distributions at midspan of the beam at different number of cycles..... 28
Fig. 3.7 Relationships of maximum load level and fatigue life for numerical and experimental results 29
Fig. 3.8 Beam details and numerical model..... 30
Fig. 3.9 Load-midspan displacement relationships for numerical and experimental results 30
Fig. 3.10 Propagation of cracked elements due to fixed pulsating load equaling 80%..... 32
Fig. 3.11 Strain and stress distribution curves along the beam section at midspan (0~200 mm) 32
Fig. 3.12 Midspan displacement evolution of RC beam under fixed pulsating load equaling 80% 32
Fig. 3.13 Schematic moving load path on numerical model..... 33
Fig. 3. 14 Comparison between the propagation of cracked elements for RC beam under fixed pulsating load and that under the moving load..... 34
Fig. 3.15 Maximum and minimum midspan displacement evolution for RC beam under fixed pulsating load and that under moving load..... 34

Fig. 3. 16 Models for Reinforcement: (a) discrete; (b) embedded; and (c) smeared [27] 35
Fig. 3.17 detail for control beam reinforcement (all dimensions in mm) [28] 37
Fig. 3.18 (a) Volumes created in ANSYS; **(b)** Reinforcement configuration [29] 37
Fig. 3.19 Finite element meshing of a beam in embedded model by ATENA 38
Fig. 3.20 Numerical model using smeared reinforcement approach 38
Fig. 3.21 Load-displacement relationships for analyzed beam 39

Fig. 4.1 RC slab geometery and reinforcement arrengment 44
Fig. 4.2 Analytical procudure for fatigue analysis 44
Fig. 4.3 Maximum principal tensile strain on slab bottom surface at load equaling 309 kN 46
Fig. 4.4 Load-maximum displacement curves 46
Fig. 4.5 Displacement distribution for longitudinal and transverse direction 46
Fig. 4.6 Propagation of cracked elements 48
Fig. 4.7 Center displacement evolutions 48
Fig. 4.8 S-N relationships for RC slabs reinforced with plain bars 49
Fig. 4.9 Cracking patterns on bottom surface for analytical and experimental RC slabs at fatigue failure 51
Fig. 4.10 Maximum principal strain distribution on bottom surface and inner cracking pattern at fatigue failure in transverse direction for RC slabs under moving load 53
Fig. 4.11 Lower rebar strain evolution at the slab center 54
Fig. 4.12 Strain distribution at slab center 54

Fig. 5.1 RC slab geometry, upper and lower reinforcing bars arrangement (all dimensions in mm) ... 58
Fig. 5.2 FRP configuration (dimensions in mm) 59
Fig. 5.3 Moving load path 60
Fig. 5.4 Moving load pattern 61
Fig. 5.5 (a) Strengthened RC slab **(b)** Isotropic and Orthotropic approaches 62
Fig. 5.6 Load-center displacement curves 63
Fig. 5.7 Propagation of cracked elements for analyzed slabs 65
Fig. 5.8 Center displacement evolutions 66
Fig. 5.9 (a) Numerical and experimental [8] cracking pattern **(b)** maximum principal strain distribution at fatigue failure for RC slab S0 69
Fig. 5.10 Numerical and experimental [8] cracking pattern at fatigue failure for S450 70
Fig. 5.11 (a) maximum principal strain distribution **(b)** Shear strain distribution for interfacial bond elements at fatigue failure for S450 70
Fig. 5.12 Numerical and experimental [8] cracking pattern at fatigue failure for S330 72
Fig. 5.13 (a) maximum principal strain distribution **(b)** Shear strain distribution for interfacial bond elements at fatigue failure for S330 72
Fig. 5.14 Transverse FRP strain at slab center for S330 74
Fig. 5.15 Transverse FRP strain at slab center for S450 74
Fig. 5.16 Longitudinal and transverse FRP sheets overlapping 75
Fig. 5.17 Transverse strain distribution of concrete on the bottom slab surface at slab center 76
Fig. 5.18 Transverse strain distribution of concrete at different sheet location for S450 and S0 at fatigue failure 76
Fig. 5.19 Cracked zone propagation according to separated cracked zones concept for strengthened RC slab S450 77
Fig. 5.20 Comparison between separated and uniform cracked zones concepts on the center displacement evolutions 79

Fig. 5.21 Bridging stress degradation for plain and reinforced cracked concrete elements..... 79

CHAPTER 1

GENERAL INTRODUCTION

1.1 Background and motivation

Researchers and structural designers are concerned about the safety of construction in the long-term. Reinforced concrete (RC) bridge-deck slabs are subjected to a repetition of moving loads. These structures are required to avoid the fatigue failure. Therefore, there is a growing necessity to know fatigue life and performance of RC slabs. Accurate modeling of the fatigue behaviors of RC slabs is considered to be essential for the prediction of fatigue life.

Until 1965, the plain bars (**Fig. 1.1**) are used for reinforcing RC bridge slabs. These slabs have been serviced more than 50 years. An example of RC slab reinforced with plain bars is seen in Shuen-Bridge (National Highway Route 334, Shari, Hokkaido, Japan) which was built in 1964 as shown in **Fig. 1.2**. This bridge is suffering from fatigue damage due to a huge number of moving load repetitions and also from environmental damage. The fatigue damage is more significantly observed in the RC slab reinforced with plain bars than that reinforced with deformed bars. Therefore, it is essential to find a method for prediction of fatigue life and choosing a repairing strategy for RC slabs reinforced with plain bars.

Fig. 1.1 Deformed and plain bar

Fig. 1.2 Shuen-Bridge (National Highway Route 334, Shari, Hokkaido, Japan)

Fig. 1.3 CFRP strengthening

In recent years, carbon fiber-reinforced polymer (CFRP) sheets have been widely used for repairing and strengthening RC structures. This material is lightweight, bendable and high tensile strength. One of the common CFRP strengthening methods is using an externally bonded CFRP sheets technique. In this strengthening technique, CFRP sheets are bonded to the bottom concrete surface of RC slab with an epoxy resin. **Fig. 1.3** shows an example of strengthened RC slabs by using CFRP sheets in longitudinal and transverse directions.

Most of the previous studies focused on the modeling of fatigue behaviors of RC slabs reinforced with deformed bars. However, many RC slabs in use today are reinforced with plain bars, and they are suffering from fatigue damages. Moreover, it is beneficial to predict the improvement on fatigue life and performance of RC slabs reinforced with plain bars due to CFRP strengthening.

1.2 Brief review of previous studies

Many research groups have conducted experiments to investigate the fatigue behaviors of RC slabs. Previous studies [1, 2] found that the fatigue life of RC slabs under a moving load is lower than that under a fixed pulsating load. In these experimental studies, the most common mode of fatigue failure was by punching shear mode as shown in **Fig. 1.4**. Recently, numerical studies have been presented regarding RC structures subjected to repetitive loading to predict fatigue behaviors.

Ueda et al. [3] analyzed the fatigue strength of steel-concrete sandwich beams using the finite element method. Tailored constitutive models were employed according to fatigue effects by reducing stiffness and strength of material models. This reduction is mainly based on the empirical formulations from previous experimental analyses. This investigation indicated that the effect of reduction in compressive stiffness was found to be negligible.

Maekawa et al. [4] presented a numerical fatigue simulation of RC slabs under a moving load. This numerical method used a direct path-integral scheme with fatigue constitutive models for concrete tension, compression and crack surfaces shear. The fatigue deterioration of RC slabs under moving load is significant when the concrete fatigue modeling based on a reduction of shear transfer and tension stiffness is considered.

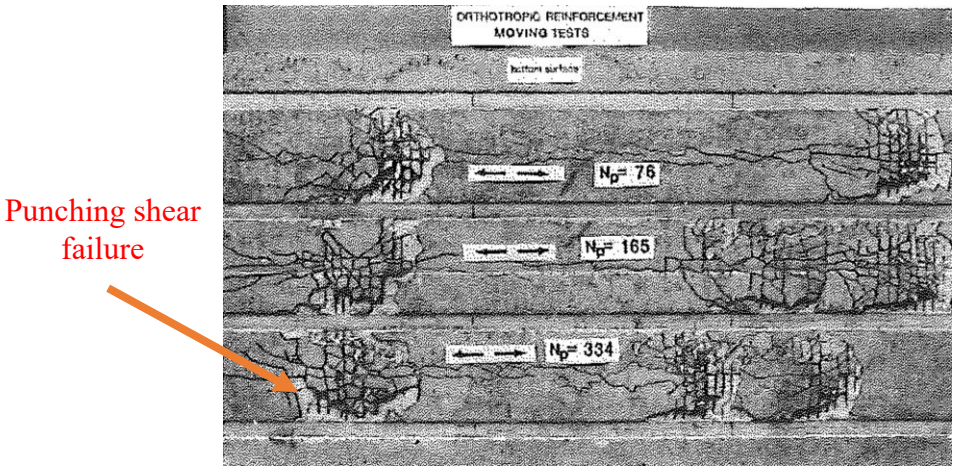

Fig. 1.4 Cracking pattern for RC slab under moving load showing a punching shear failure [2]

Fig. 1.5 Moving load test

The above-mentioned works concluded that the tension fatigue modeling for concrete plays an important role in predicting the fatigue behaviors of RC slabs. Therefore, understanding a mechanism of fatigue crack propagation is essential to evaluate concrete fatigue representation in tension. The bridging stress degradation concept was introduced for the first time by Li and Matsumoto [5] as a principal cause of fatigue crack propagation in concrete and fiber reinforced concrete beams. Suthiwarapirak and Matsumoto [6] used this concept in their numerical model to predict the fatigue behaviors of RC slabs. This study successfully provided a fatigue analysis of RC slabs under moving and fixed pulsating loads.

For RC slabs reinforced with plain bars, an experimental study on the fatigue durability was conducted by Shakushiro et al. [7] to propose an empirical formula for the fatigue life evaluation of these slabs. Although many existing RC slabs in use are reinforced with plain bars, analytical study for the fatigue life of these slabs has been rarely conducted. Therefore, it is necessary to accurately simulate fatigue behaviors numerically and develop the method of fatigue life prediction for the RC slabs reinforced with plain bars.

An experimental [8] study was conducted by Civil Engineering Research Institute for Cold Region (CERI) to evaluate the fatigue life of strengthened RC slabs with CFRP sheets under a moving load as shown in **Fig. 1.5**. The experimental study provided a significant improvement in fatigue life and deformations for repaired RC slabs.

1.3 Objectives and scope of study

The objectives of this thesis can be listed as follows.

1. This study mainly presents a numerical method to simulate the fatigue behaviors of the RC slabs reinforced with plain bars under a moving load. This method will be verified using the experimental results.

2. The bond-slip effect between a plain reinforcing bar and its surrounding concrete is carefully taken into consideration.

3. This method examines the applicability of the bridging stress degradation concept to analyze the fatigue behaviors of plain and reinforced concrete beams under pulsating and moving load.

4. This study presents a proposed method to numerically evaluate the CFRP strengthening on RC slabs reinforced with plain bars. Moreover, this study provides a numerical investigation to understand the fatigue failure and strengthening improvement mechanism.

1.4 Organization of the thesis

The thesis contents are organized in six chapters, which are further divided into several sections and subsections. The chapters have individual introduction, which give brief orientations of the subject under investigation. For a detailed discussion of various aspects of the subject, many references have been included in each chapter. The specific objectives of each chapter are as follows:

Chapter 1 provides the general introduction, review of previous studies and motivating objectives of this research.

Chapter 2 presents the numerical method of fatigue analysis based on bridging stress degradation. This chapter shows the constitutive laws of concrete and reinforcement. In the fatigue analysis, the bridging stress degradation of concrete leads to the propagation of cracked elements resulting a deterioration of structural stiffness. The bond-slip effect between a plain reinforcing bar and its surrounding concrete is employed in this method.

In **Chapter 3**, the investigation of flexural fatigue analysis is presented to analyze the fatigue behavior of plain and reinforced concrete beams under pulsating and moving load. The numerical results are compared with the experimental ones.

Chapter 4 presents the fatigue analysis of RC slabs reinforced with plain bars under different moving load levels. This chapter focus on the effect of bond-slip between a plain reinforcing bar and its surrounding concrete for fatigue behaviors. The obtained results are discussed and verified with the experimental results.

In **Chapter 5**, RC slabs with plain bars strengthened by externally bonded CFRP sheets are analyzed using a proposed numerical method to simulate their fatigue behaviors. The interfacial bond behavior between FRP sheet and concrete surface with its degradation due to fatigue loading are integrated to obtain accurate numerical results. The propagation of cracked elements, center displacement evolution, cracking pattern and FRP strain are presented in this chapter. These results are compared with the experimental results for verification.

All of these chapters lead to the conclusions and further developments in the final chapter, **Chapter 6**.

CHAPTER 2

FATIGUE ANALYSIS METHOD BASED ON BRIDGING STRESS DEGRADATION

2.1 Introduction

Using finite elements method (FEM) has been the preferred method to study the behavior of concrete. This method is economic way than the experimental tests. Many previous studies developed this method according the material behaviors of concrete to present an accurate static analysis.

To provide a numerical method for predicting fatigue behaviors, these studies can be used as a starting point for this research. The main goal of this study is numerical studying of the fatigue behaviors of RC slabs reinforced with plain bars. Therefore, the bridging stress degradation of concrete is integrated in this numerical method to simulate the deterioration effect due to fatigue loading. Moreover, the bond-slip effect between plain reinforcing bar and its surrounding concrete is considered in this numerical method. The numerical results are significantly influenced with this effect in the RC structures reinforced with plain bars.

In this chapter, the description of the proposed numerical method is presented. This chapter divided to two parts; concrete model and reinforcing bar model.

2.2 Concrete

Concrete is different than other homogenous materials because it contains a mixture of different components with different stiffness. Therefore, it exhibits a large number of micro cracks at the interface between the aggregates and mortar. The propagation of these cracks during loading contributes to the nonlinear behavior due to the difference in stiffness between aggregates and mortar. Moreover, the aggregate-mortar interface is the weakest link in the composite system. This is the primary reason for the low tensile strength of concrete.

The concrete material includes the flowing effects of its behavior:

- non-linear behavior in compression including hardening and softening,
- fracture of concrete in tension based on the nonlinear fracture mechanics,
- biaxial strength failure criterion,
- reduction of compressive strength after cracking,
- tension stiffening effect,
- reduction of the shear stiffness after cracking,
- and fixed crack direction model.

2.2.1 Nonlinear constitutive laws for concrete

In describing the uniaxial stress-strain behavior of concrete, many empirical formulas have been proposed. **Fig. 2.1** shows the most familiar nonlinear model by Maekawa et al. [9]. This relationship can be divided to 4 parts to indicate the damage state of concrete.

In this section, the stress-strain function (σ, ε) for each part will be described as the following. The modulus of elasticity and compressive strength of concrete can be assumed as E_c and $f_c^{'}$, respectively.

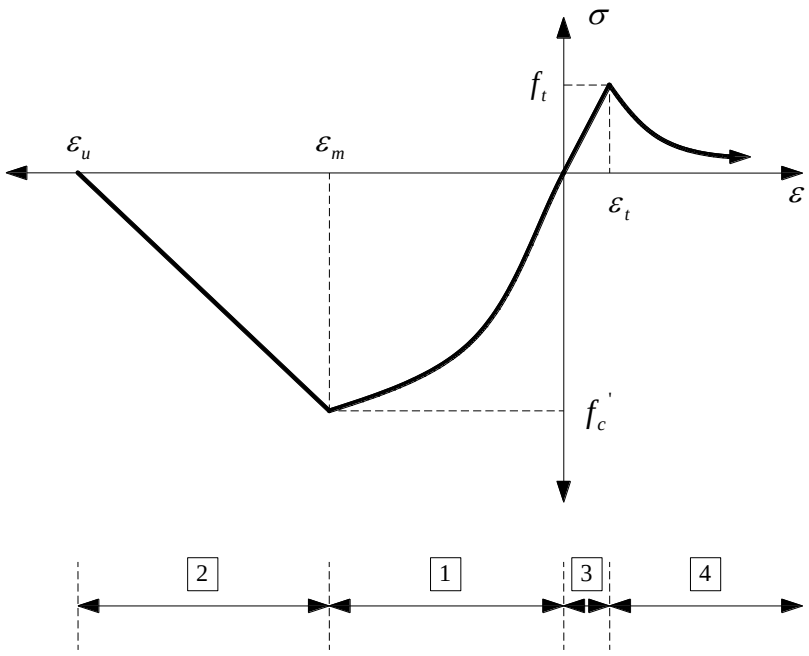

Fig. 2.1 Uniaxial stress-strain relation for concrete

First part is compression before peak stress. The following formula has been adopted for the ascending branch of the concrete stress-strain law in compression as shown in **Fig. 2.1**. This formula enables wide range of curve forms, from linear to curved, and is appropriate for normal as well as high strength concrete.

$$\sigma = f_c' \frac{\varepsilon}{\varepsilon_m}\left(2 - \frac{\varepsilon}{\varepsilon_m}\right), \qquad \text{at} \quad 0 \geq \varepsilon \geq \varepsilon_m \tag{2.1}$$

$$\varepsilon_m = 2\frac{f_c'}{E_c}, \tag{2.2}$$

where ε_m is concrete strain corresponding f_c'.

Second part is compression after peak stress. In this part, the softening law in compression is linearly descending based on local strain softening. The stress-strain relationship in this part can be adopted as the following equation. The slope of the softening part of the stress-strain diagram is defined by two points: a peak of the diagram at the maximal stress and a limit compressive strain ε_u at the zero stress.

$$\sigma = f_c' \frac{\varepsilon_u - \varepsilon}{\varepsilon_u - \varepsilon_m}, \qquad \text{at} \quad \varepsilon_m \geq \varepsilon \geq \varepsilon_u \tag{2.3}$$

$$\varepsilon_u = 3 \cdot \varepsilon_m, \tag{2.4}$$

Third part is tension before cracking. In this part, the behavior of concrete in tension without cracks is assumed linear elastic as shown in the following equation. This behavior continues until the effective tensile strength, f_t. The equation of the effective tensile strength is adopted from Japanese standard specifications for concrete structures.

$$\sigma = E_c \cdot \varepsilon, \qquad \text{at} \qquad \varepsilon_t \geq \varepsilon \geq 0 \tag{2.5}$$

$$\varepsilon_t = \frac{f_t}{E_c}, \tag{2.6}$$

$$f_t = 0.23 \cdot f_c'^{2/3} \tag{2.7}$$

where ε_t is cracking strain of concrete.

Fourth part is tension after cracking. The following formula simulates the cracking behavior of concrete. In smeared crack model, strain is derived from the crack opening displacement according to the crack band theory as shown in equation **(2.9)**. The crack formation takes place in the process zone of a potential crack with decreasing tensile stress on a crack face due to a bridging effect of the aggregate. This function is adopted using an exponential relationship by Maekawa et al. [9].

$$\sigma = f_t \left(\frac{\varepsilon_t}{\varepsilon} \right)^{0.4}, \qquad \text{at} \qquad \varepsilon > \varepsilon_t \tag{2.8}$$

$$\varepsilon = \frac{\delta_{cr}}{l}, \tag{2.9}$$

where δ_{cr} is crack opening displacement and l is element size.

2.2.2 Crack formation of concrete

Crack propagation characteristics of concrete are adapted by 8-node 3D smeared crack elements with multiple fixed crack concepts (Rots and Blaauwendraad 1989). For cracked elements, the first crack is assumed to start perpendicular to the direction of the maximum principal strain in the concrete matrix when tensile strain is larger than the cracking strain as shown in **Fig. 2.2 (a)**.

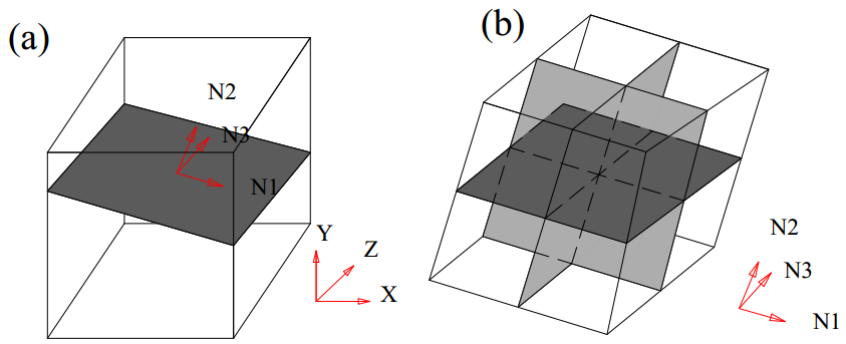

Fig. 2.2 Crack formation: **(a)** initiation of a first crack; **(b)** three perpendicular crack formations

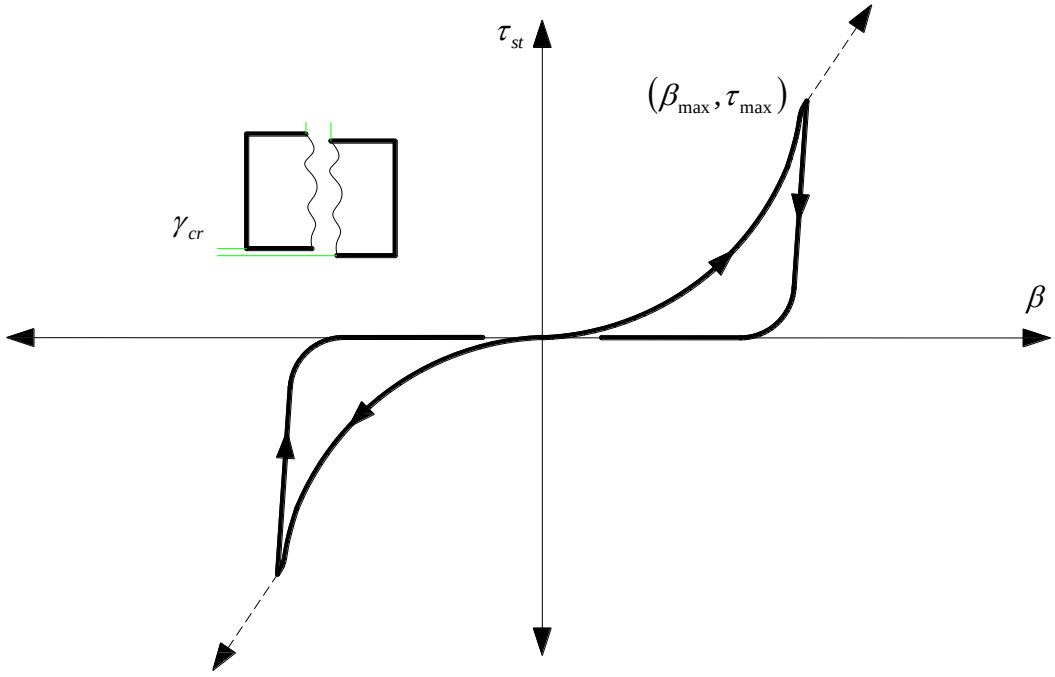

Fig. 2.3 Shear transfer model for one-directional crack

After the first crack appears, the second crack can propagate perpendicular to the first crack when the second tensile strain component exceeds the cracking strain. In addition, the third crack can form perpendicularly to the existing two cracks as shown in **Fig. 2.2 (b)**.

2.2.3 Shear transfer for cracked concrete

When the generation of a crack in concrete is determined by the maximum principal stress, shear stress and strain are zero at the crack plane perpendicular to the maximum principal stress direction at the moment of cracking. At increasing of applied load, the principal axes of stress and strain rotate and eventually lead to the formation of a new crack. At the same time, the existing crack is subjected to shear strain since it is no longer normal to the current principal direction. Therefore, the fixed crack approach needs to explicitly address shear transfer along crack interface. The solution of contact density model between cracks surface can be derived for monotonic loading path using an envelope curve as shown in **Fig. 2.4**. The simplified shear transfer model can be expressed as following.

a) Loading at $\beta \leq \beta_{\max}$

$$\tau_{st} = \tau_0 \frac{\beta^2}{1+\beta^2}, \quad \textbf{(2.10)}$$

$$\tau_0 = 3.8 \cdot f_c'^{1/3} \quad \textbf{(2.11)}$$

$$\beta = \frac{\gamma_{cr}}{\varepsilon_{t1}} \quad \textbf{(2.12)}$$

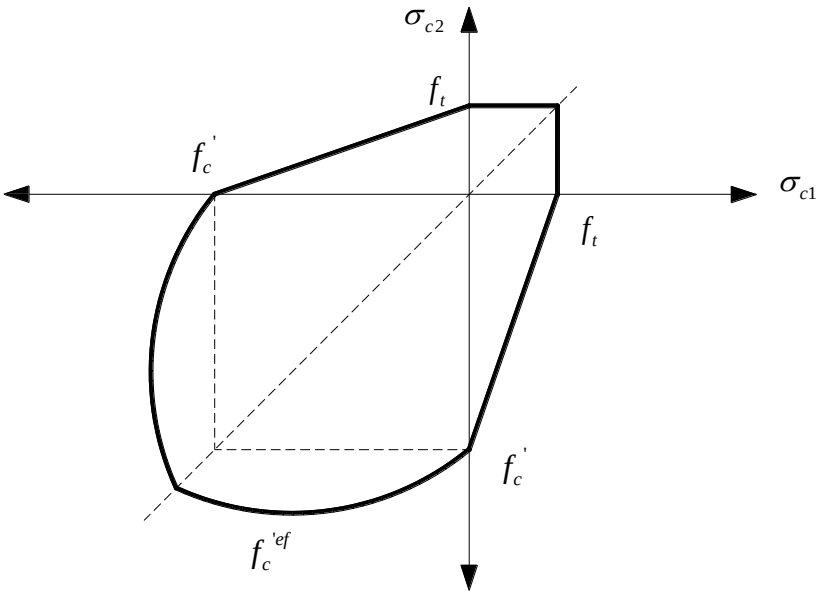

Fig. 2.4 Biaxial failure criterion of concrete

b) Unloading/reloading at $0.9\,\beta_{max} \le \beta < \beta_{max}$

$$\tau_{st} = \frac{\tau_{max}}{0.15\beta_{max}}\left(\beta - 0.85\beta_{max}\right), \tag{2.13}$$

$$\tau_{max} = \tau_0 \cdot \beta_{max}, \tag{2.14}$$

c) Unloading/reloading at $\beta < 0.9\,\beta_{max}$

$$\tau_{st} = \tau_{max}\left(\frac{0.05}{0.15}\right)\cdot\left(\frac{\beta}{0.9\beta}\right)^9, \tag{2.15}$$

$$\tau_{max} = \tau_0 \cdot \beta_{max}, \tag{2.16}$$

where τ_0 is the shear transfer strength, γ_{cr} is the shear strain due to crack, ε_{t1} is the tensile strain normal to crack and β is normalized shear strain.

2.2.4 Biaxial stress failure criterion of concrete

A biaxial stress failure criterion according to Kupfer et al. [10] is used as shown in **Fig. 2.4**. In the compression-compression stress state the failure function, $f_c'^{ef}$, is

$$f_c'^{ef} = f_c' \frac{1 + 3.65\dfrac{\sigma_{c1}}{\sigma_{c2}}}{\left(1 + \dfrac{\sigma_{c1}}{\sigma_{c2}}\right)^2}, \tag{2.17}$$

where σ_{c1} and σ_{c2} are the principal stresses in concrete. In the biaxial stress state, the strength of concrete is predicted under the assumption of a proportional stress path.

In the tension- compression state, the failure function continues linearly from the point $\sigma_1 = 0$ and $\sigma_2 = f_c'$ into the tension-compression region with the linearly decreasing strength:

$$f_c'^{ef} = f_c' r_{ec}, \tag{2.18}$$

$$r_{ec} = \left(1 + 5.3278 \frac{\sigma_{c1}}{f_c'}\right), \qquad \text{at } 1.0 \geq r_{ec} \geq 0.9 \tag{2.19}$$

where r_{ec} is the reduction factor of the compressive strength in the principal direction 2 due to the tensile stress in the principal direction 1.

2.2.5 Bridging stress degradation and concrete behavior under cyclic loading

The bridging stress degradation characteristic of concrete under a repetitive load is the most important part in the current fatigue analysis. A crack starts with length, *a*, and width, *w*, due to the first loading as shown in **Fig. 2.5 (a)**. Repetitive loading leads to the reduction of bridging stress, because the crack is subjected to a process of opening and closing. Therefore, this crack propagates with additional length, *da*, and additional width, *dw*, as shown in **Fig. 2.5 (b)**. This reduction is defined as the bridging stress degradation concept, and it is assumed to depend on two parameters: maximum tensile strain, $\varepsilon_{t\max}$, and number of cycles, *N* [5]. The equation of bridging stress degradation can be expressed as [11]:

$$\frac{f_{tN}}{f_t} = 1 - (d_0 + k\varepsilon_{t\max} l)\log(N), \tag{2.20}$$

where *l* is cracked element size, d_0 is stress degradation factor, *k* is slope of the linear relation between the bridging degradation factor and maximum tensile strain, $\varepsilon_{t\max}$, f_{tN} and f_t are bridging stress at the *N*th and the first cycle, respectively. Zhang et al. [11, 12] analyzed a large number of experimental data to conclude that the degradation of crack bridging stress under cyclic load is controlled by the number of cycle and the maximum and minimum crack opening. This degradation can be fitted by a linear model as a function of the logarithm of the number of cycles as shown in equation **(2.20)**. As Zhang et al. [11, 12], this factor can be approximately related to the maximum crack opening. Through their studies, it is found that $d_0 = 0.08$ and $k = 4$ mm^{-1} when the crack opening ≤ 0.016 mm and $d_0 = 0.014$ and $k = 0.12$ mm^{-1} when the crack opening > 0.016 mm. For smeared crack elements, the bridging stress degradation occurs by multiple cracks. Therefore, first range (the crack opening ≤ 0.016 mm) is applicable in this study [6].

The bridging stress in concrete is mainly influenced by the maximum particle size and surface texture of aggregate. The effect of aggregate size on bridging stress was studied by Wolinski et al. [13]. This study found that the maximum bridging stress and fracture energy are almost the same for concrete comprising mixes with maximum aggregate particle size of 8 mm, 16 mm and 32 mm. Therefore, this equation can be used to verify the experimental results by Shakushiro et al. [14] which used aggregate of maximum aggregate particle size of 20 mm.

Fig. 2.6 shows concrete behaviors under cyclic loading. The nonlinear path-dependency is considered in modeling the unloading and reloading paths to account for energy absorption under cyclic loading. The loading curve, indicated with black line, is adopted according to previous description in section 2.2.1. The unloading curve is expressed as a polynomial connecting the point where unloading starts ($\varepsilon_{\max}$, $\sigma_{\max}$) to point ($\varepsilon_{\min}$, $\sigma_{\min}$). This function

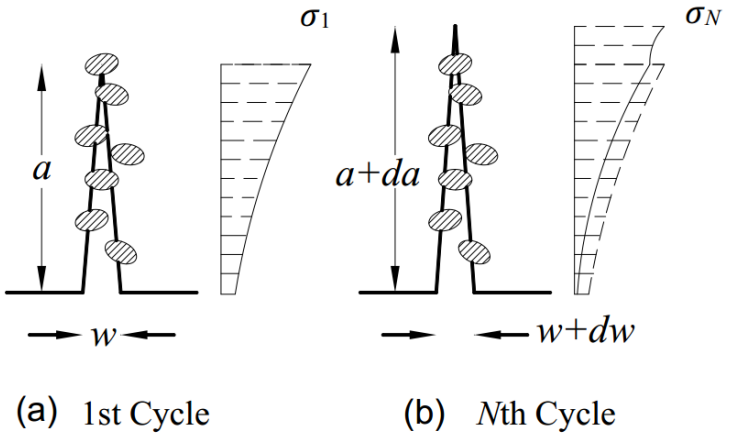

Fig. 2.5 Crack propagation due to bridging stress: (a) the first cycle; (b) after N cycles

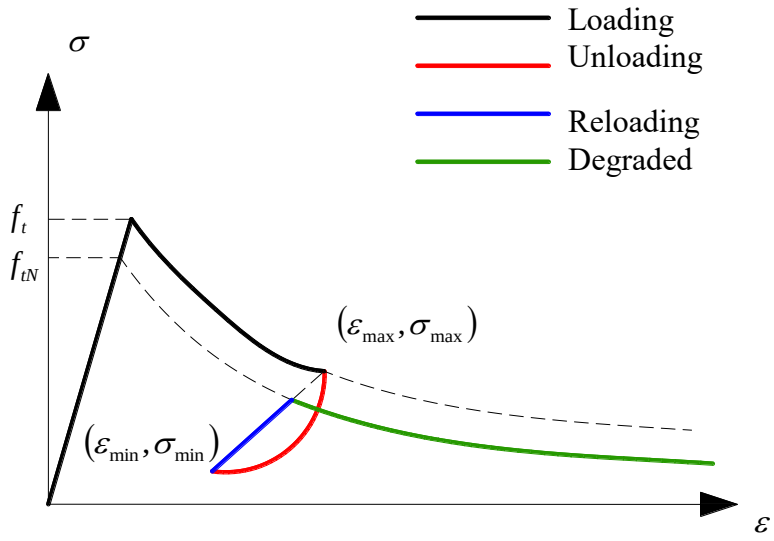

Fig. 2.6 Concrete behavior under cyclic loading

is indicated by red in **Fig. 2.6** following equation (2.21). The reloading curve is specified as the straight line connecting the point where reloading starts to the point of maximum stress–strain at further cycle ($\varepsilon_{N\max}$, $\sigma_{N\max}$). The reloading function is indicated by blue in **Fig. 2.6** following equation (2.22). The point of ($\varepsilon_{N\max}$, $\sigma_{N\max}$) is the deteriorated stress and strain at the number of cycles equaling *N* according to bridging stress degradation concept. Thus, the cracking behavior of concrete follows the deteriorated stress-strain relationship as shown in equation (2.23). These equations can be expressed as:

$$\sigma = \sigma_{\min} + (\sigma_{\max} - \sigma_{\min}) \cdot \left(\frac{\varepsilon}{\varepsilon_{\max}} \right)^2, \tag{2.21}$$

$$\sigma = \sigma_{\min} + \frac{\sigma_{\max} - \sigma_{\min}}{\varepsilon_{\max} - \varepsilon_{\min}} \cdot \varepsilon, \tag{2.22}$$

$$\sigma = f_{tN}\left(\frac{\varepsilon_t}{\varepsilon}\right)^{0.4}, \tag{2.23}$$

2.2.6 Concrete stiffness matrices

2.2.6.1 Uncracked concrete

The material stiffness matrix for the uncracked concrete has the form of an elastic matrix of the isotropic material. Its components can be expressed in terms of the elastic modulus, E_c, and Poisson's ratio, ν_c. It is written in the global coordinate system. The formulation is established in total form, in accordance with the following equations:

$$[\sigma] = [D] \cdot [\varepsilon], \tag{2.24}$$

$$[D] = \frac{E_c}{(1+\nu_c)(1-2\nu_c)} \begin{bmatrix} 1-\nu_c & \nu_c & \nu_c \\ \nu_c & 1-\nu_c & \nu_c \\ \nu_c & \nu_c & 1-\nu_c \end{bmatrix}, \tag{2.25}$$

where $[\sigma]$ is stress vector and $[\varepsilon]$ is strain vector.

2.2.6.2 Cracked concrete

For the cracked concrete, the matrix has the form of the elastic matrix for the orthotropic material. The matrix is formulated in a principal coordinate system in **Fig. 2.7**, which is coincident with the crack direction. The direction 1 is normal to the crack and the direction 2 is parallel with the crack. On each crack plane, there are one normal stress component, σ, and two shear stress components, τ. The relationships between stresses, σ, and strains, ε, on the crack plane are shown by the following equation. It is assumed that there is no dilatancy between normal and shear terms.

$$\begin{Bmatrix} \sigma_{11}^{cr} \\ \tau_{12}^{cr} \\ \tau_{13}^{cr} \end{Bmatrix} = \begin{bmatrix} d^{cr} & 0 & 0 \\ 0 & d_{\tau}^{cr} & 0 \\ 0 & 0 & d_{\tau}^{cr} \end{bmatrix} \cdot \begin{Bmatrix} \varepsilon_{11}^{cr} \\ \varepsilon_{12}^{cr} \\ \varepsilon_{13}^{cr} \end{Bmatrix}, \tag{2.26}$$

Herein d^{cr} is tangential slope of the normal stress–strain relationship after cracking and d_{τ}^{cr} is tangential slope of shear stress–strain relationship. The overall stress–strain relationship of the smeared cracked elements of concrete with respect to the global coordinate system can be written as follows [15].

$$\sigma = D^{cocr}\varepsilon, \tag{2.27}$$

$$D^{cocr} = \left[D^{co} - D^{co}N_t\left(D^{cr} + N_t^t D^{co} N\right)^{-1} N_t^t D^{co}\right], \tag{2.28}$$

where D^{cocr} = stiffness matrix of cracked concrete element formulated from the stiffness matrix of crack, D^{cr}, and stiffness matrix of concrete in elastic, D^{co}. N_t is a transformation matrix reflecting the orientation of the crack in **Fig. 2.2** (b). The off-diagonal terms of the crack stiffness matrix, D^{cr}, are negligible.

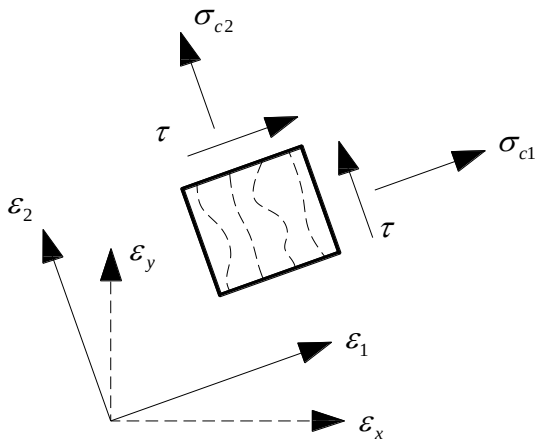

Fig. 2.7 Principal and global stress-strain directions

2.3 Reinforcing bar

Reinforcement can be modeled in two distinct forms: discrete and smeared. Discrete reinforcement is in form of reinforcing bars and is modeled by truss elements. The smeared reinforcement is a component of composite material and can be considered either as a single (only one-constituent) material in the element under consideration or as one of the more such constituents. The former case can be a special mesh element, while the later can be an element with concrete containing one or more reinforcements. In both cases the state of uniaxial stress is assumed and the same formulation of stress-strain law is used in all types of reinforcement. In this study, the reinforcement of RC slabs is modeled as a smeared rebar with its reinforcement ratio distributed in any desired direction as shown in **Fig. 2.8**. The total stress of RC elements can be calculated according to the following equations;

$$\sigma_{RC} = (1-\rho)\cdot\sigma_c + \rho\cdot\sigma_s, \tag{2.29}$$

$$\rho = \frac{A_s}{A_c}, \tag{2.30}$$

where σ_{RC}, σ_c and σ_s are numerical stress for reinforced concrete element, concrete and reinforcing bar. ρ is the reinforcement ratio equaling the ratio of reinforcing bar area, A_s, to concrete area, A_c.

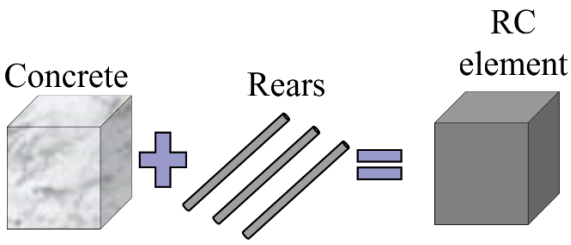

Fig. 2.8 Smeared reinforced concrete elements

2.3.1 Modified stress-strain relationship according to bond-slip effect

The stress-strain relationship of reinforcement is represented by a bilinear curve with explicit yield stress, f_y. For RC elements reinforced with plain bars, the bond effect between a plain reinforcing bar and its surrounding concrete is considered as the most influential factor to obtain a reliable simulation [16]. Therefore, it is important to consider the bond-slip effect during analysis. The modified steel bar model by Dehestani and Mousavi [17] is employed in this method to simulate the bond-slip effect on the stress-strain (σ-ε) relationship under a monotonic loading. This modification contains the addition of equivalent bond strain to reinforcing bar strain as shown in **Fig. 2.9**. This leads to a decrease in the effective stiffness of the rebar model and an increase in its deformations. To describe the assumption of this method, an RC element in bending is considered as shown in **Fig. 2.10**. There is no tensile stress in concrete at cracked section and the reinforcing bar transfers the tension force. However, the concrete between cracks participates in the tensile strength of the overall RC cross section. The concrete located between cracks can be divided to three main parts as shown in **Fig. 2.10**. In cracked section, there is no bond stress between the reinforcement and its surrounding concrete. The transmission length of bond stress, l_d, is located between the cracked section and the perfect bond zone. This method can be tailored for plain bars to obtain the effective stiffness, E_s^*, as follows.

$$E_s^* = \frac{f_y^*}{\varepsilon_y^*}, \tag{2.31}$$

$$f_y^* = f_y \cdot \left(0.93 - 2\frac{\left(f_{cr} / f_y \right)^{1.5}}{\rho} \right), \tag{2.32}$$

$$\varepsilon_y^* = \varepsilon_y + \frac{S_y}{l_d}, \tag{2.33}$$

$$S_y = 0.4\left(\frac{d_b}{4} \cdot \frac{f_y}{\sqrt{f_c'}} \cdot (2\alpha + 1) \right)^{1/\alpha} + 0.34, \tag{2.34}$$

$$l_d = \frac{d_b \cdot f_y}{4 \cdot \tau_b}, \tag{2.35}$$

where f_y^* is the effective yield stress [18], S_y is the slip displacement of a steel bar at yield point [19], d_b is the rebar diameter, f_c' is the concrete compressive strength, α is a tuning parameter used for adjusting the local bond stress-slip relationship = 0.5 for plain bar [20], τ_b is the average bond stress, ε_y and ε_y^* are the explicit and effective yield strain, respectively.

The effective stiffness degradation of plain bar due to a repetitive load is not taken into consideration in this study. Therefore, the reduction of rebar stiffness due to an applied load is the major effect on the RC element behaviors at first cycle. While, the bridging stress degradation in concrete plays the most important role in other cycles.

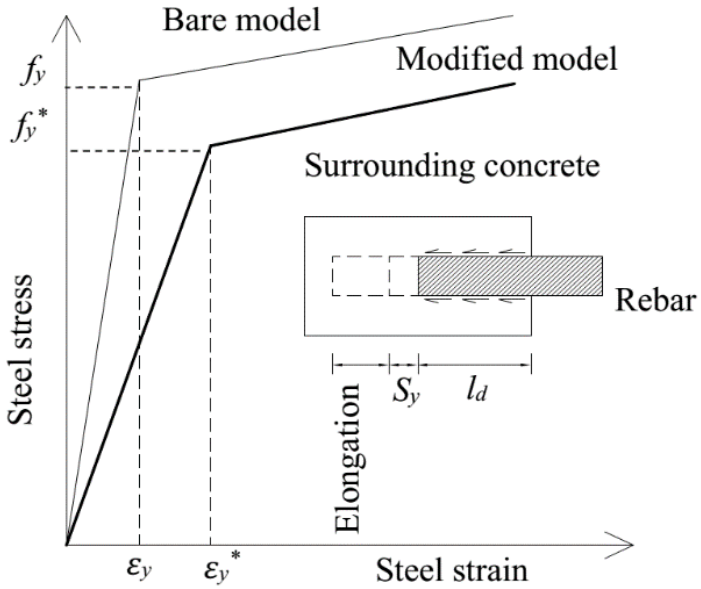

Fig. 2.9 Modified stress-strain relationship for reinforcing bar

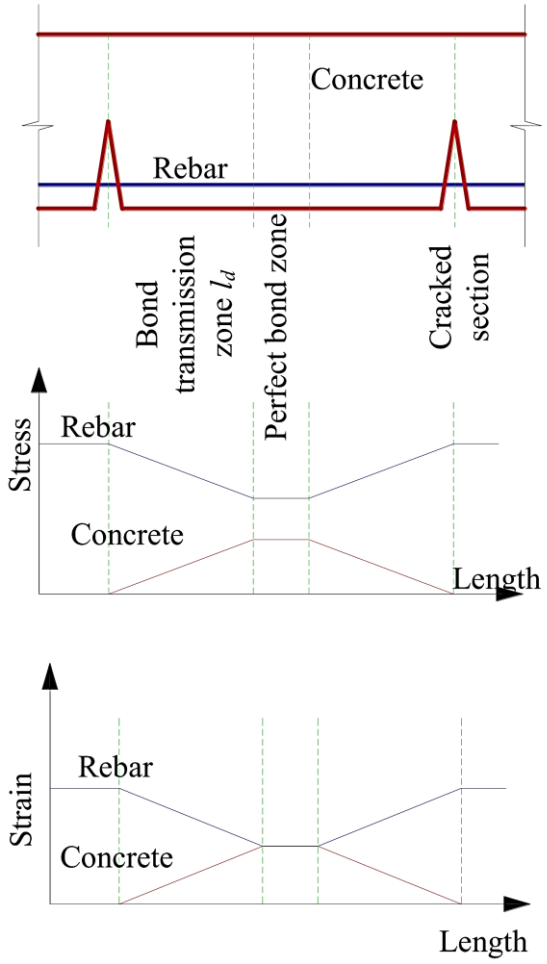

Fig. 2.10 Stress and strain distribution of a cracked RC element in bending

For RC elements reinforced with deformed bars, the bond between a non-yielded deformed bar and its surrounding concrete is assumed to be perfect. In other words, the slip displacement of a deformed bar at yielding is considered as zero ($S_y \approx 0$). Moreover, its bond degradation due to a repetitive load is not considered in this study. Since there is no report of RC slab failure due to fatigue rupture of reinforcing bar, this study focused on the concrete deterioration due to repetitive loading. For plain bar, the stiffness reduction at first cycle results in an increasing of concrete strain. According to equation **(2.20)**, this leads to a significant concrete degradation than that in deformed bar.

2.3.3 Cyclic behavior of reinforcing bar

The Giuffré-Menegotto-Pinto model [21] is employed to represent the hysteretic behavior of a rebar under repetitive load as following:

$$\frac{\sigma}{f_y^*} = H\frac{\varepsilon}{\varepsilon_y^*} + \frac{(1-H)\dfrac{\varepsilon}{\varepsilon_y^*}}{\left[1+\left(\dfrac{\varepsilon}{\varepsilon_y^*}\right)^R\right]^{1/R}}, \tag{2.36}$$

$$R = R_0 - \frac{a_1\xi_{\max}}{a_2 - \xi_{\max}}, \tag{2.37}$$

where H is the strain hardening parameter, R_0, and R are the transition parameter between elastic and hardening for the first and Nth cycle (R_0 =20), $\xi_{\max}$ is the maximum excursion in plastic range, a_1 and a_2 are the parameters for the change of R with repetitive load history, equal to 18.5 and 0.00015, respectively. Fig. 2.11 shows the cyclic behavior on the stress-strain relationship for reinforcing bar.

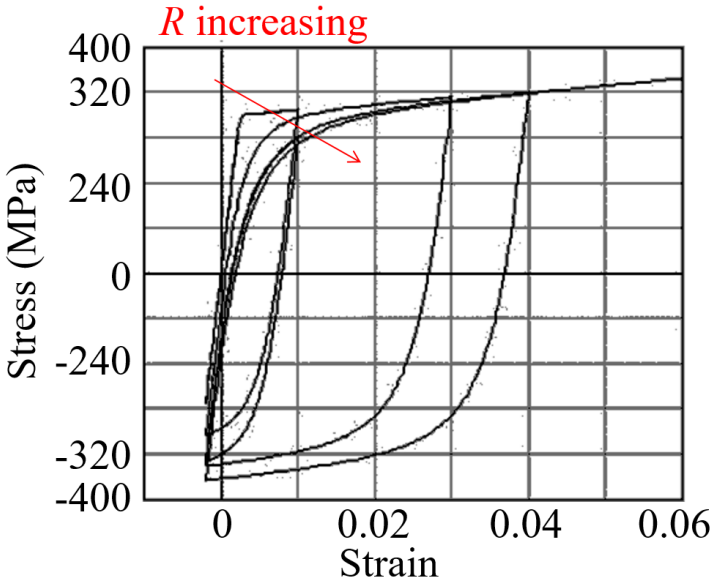

Fig. 2.11 Giuffre-Menegotto-Pinto model [21]

2.3.2 Smeared reinforcement stiffness matrix

The used stiffeness matrix of the i^{th} smeared reinforcement is;

$$D_{si} = \rho \cdot E_s^* \begin{bmatrix} \cos(\beta_i)^4 & \cos(\beta_i)^2 \sin(\beta_i)^2 & \cos(\beta_i)^3 \sin(\beta_i) \\ \cos(\beta_i)^2 \sin(\beta_i)^2 & \sin(\beta_i)^4 & \cos(\beta_i)\sin(\beta_i)^3 \\ \cos(\beta_i)^3 \sin(\beta_i) & \cos(\beta_i)\sin(\beta_i)^3 & \cos(\beta_i)^2 \sin(\beta_i)^2 \end{bmatrix}. \quad \textbf{(2.38)}$$

The angle β is between the global axis x and the i^{th} reinforcement direction, and E_s^* is the modified elastic modulus of reinforcement.

The total material stiffness of the reinforced concrete, D_t, is the sum of material stiffness of concrete and smeared reinforcement:

$$D_t = D_c + \sum_{i=1}^{n} D_{si} \, . \quad \textbf{(2.39)}$$

where D_c is the concrete stiffness. The summation is over n smeared reinforcing components in global directions.

2.4 FRP and interfacial bond element

Fiber-reinforced polymer (FRP) have been extensively used for external strengthening of RC structures as shown in **Fig. 2.12 (a)**. The effectiveness of this strengthening technique is intrinsically dependent on the bond performance between FRP and the concrete surface. Epoxy resin adhesive was used to bond these sheets with the bottom surface of RC slab as shown in **Fig. 2.12 (b)**. The bond mechanism is considered as a key for transferring the stresses from structural elements to the composite material. Therefore, its failure results in deterioration of the premature debonding. The mechanical behavior for FRP sheets and interfacial bond element will be presented in this section. The components of this composite structures are shown in **Fig. 2.13**.

(a)

(b)

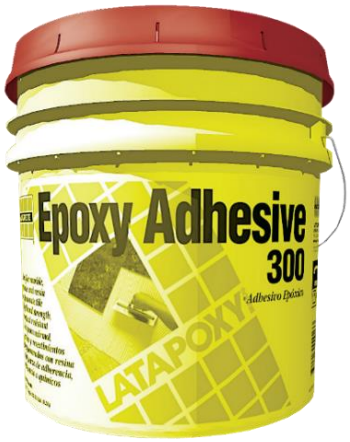

Fig. 2.12 (a) FRP sheets and **(b)** Epoxy resin adhesive

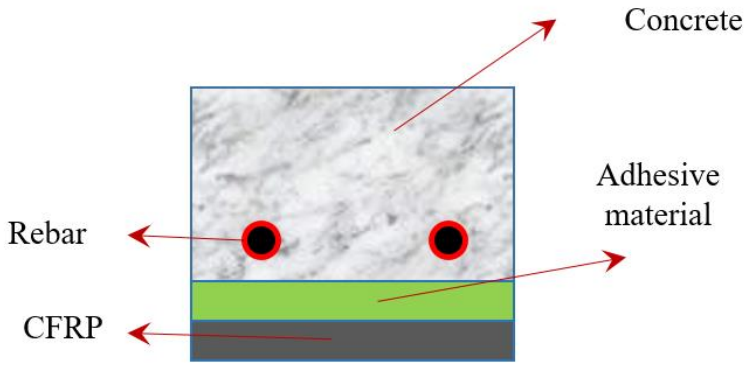

Fig. 2.13 FRP installation

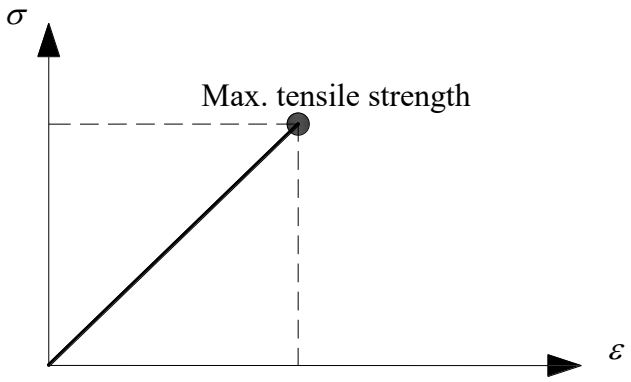

Fig. 2.14 Stress-strain relationship for FRP

2.4.1 FRP

A linear elastic constitutive relation is assumed for the FRP composites as shown in **Fig. 2.14**. The elastic modulus is assumed to be E_{frp}. The maximum tensile strength of the FRP is much larger than other materials. Therefore, reaching to this limit is assumed to be very difficult. According to this, the assumption of linear elastic relation is good enough to simulate FRP behavior. Moreover, the authors assumed that there is no strength degradation due to fatigue loading.

2.4.2 Interfacial bond element

Strengthening two-way slabs by using fiber-reinforced polymer (FRP) under moving load is numerically evaluated in Chapter 5 as shown in **Fig. 2.15**. Adhesive material such as epoxy resin was used to bond these sheets with the bottom surface of RC slab. Therefore, the bond mechanism between FRP sheets and concrete surface is important to obtain an accurate numerical simulation.

Significant progress has been achieved in the last years in the development of refined computational approaches to investigate the debonding mechanism and damage in FRP-strengthened concrete elements or analysis of full-scale strengthened structures. Numerical

Fig. 2.15 Strengthened RC slab

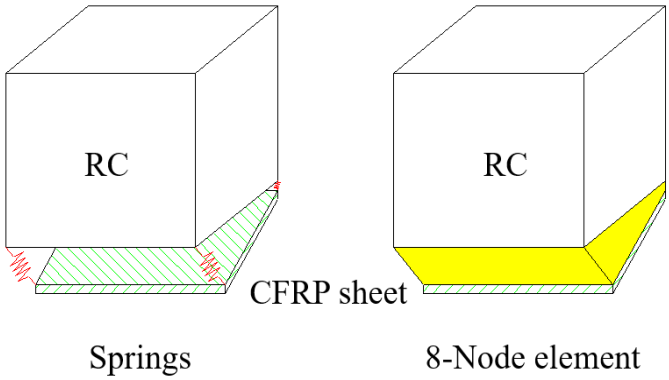

Fig. 2.16 Comparison between springs and 8-node interfacial element approaches

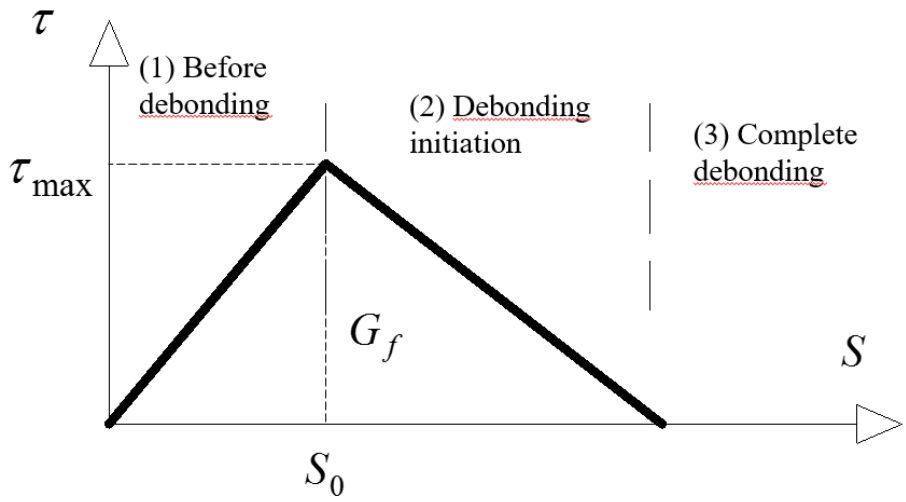

Fig. 2.17 Interfacial bond-slip model

models usually follow two main approaches. In the first approach, the bond behavior is modeled using a horizontal spring elements at all connected nodes between concrete and FRP elements as shown in **Fig. 2.16**. The constative law of these springs represents the interfacial bond-slip displacement relation.

The second approach, adopted in the following, involves a very thin layer of elements specially designed for large shear deformation. This layer can be modeled by 8-nodes continuous interface element. This type can simulate the vertical and horizontal deformations as opening and sliding between composite material. Moreover, this approach is recommended for simulating interfaces under large shear deformations.

According to previous description, 8-node interfacial element approach is suitable in this study. The reason is that interfacial bond element subjected to repetitive loading leads to large deformations in horizontal direction. Therefore, this approach can be employed for simulating interfacial bond in horizontal direction and adhesive material in vertical direction.

The mechanical behavior of the interfacial bond element is modeled by can be simulated as a relationship between the local shear stress, τ, and the relative slip displacement, S, between the FRP laminate and the concrete. The area under the $\tau - S$ curve represents the interfacial fracture energy, G_f, which corresponds to the energy per unit bond area required for complete debonding. A bilinear bond-slip relation proposed by Lu et al. [22, 23] is employed in the present study as shown in **Fig. 2.17**. This relationship can be divided to three parts; (1) before debonding, continuum, (2) debonding initiation, and (3) complete debonding.

The maximum bond strength, τ_{max}, the corresponding slip, S_0, and the total fracture energy, G_f, are governed by the tensile strength of the concrete, f_t, and a width ratio parameter, β, as follows;

$$\tau_{\max} = 1.5 \cdot \beta \cdot f_t, \quad \textbf{(2.40)}$$

$$S_0 = 0.0195 \cdot \beta \cdot f_t, \quad \textbf{(2.41)}$$

$$G_f = 0.308 \cdot \beta^2 \cdot \sqrt{f_t}, \quad \textbf{(2.42)}$$

$$\beta = \sqrt{\frac{2.25 - b_f / b_c}{1.25 + b_f / b_c}}, \quad \textbf{(2.43)}$$

where b_f / b_c is the ratio of total FRP laminate width, b_f, to the total slab width, b_c.

The total fracture energy, G_f, corresponds the area under the $\tau - S$ curve. Therefore, the maximum slip displacement, S_u, can be calculated by the following equation;

$$S_u = \frac{2G_f}{\tau_{\max}}. \quad \textbf{(2.44)}$$

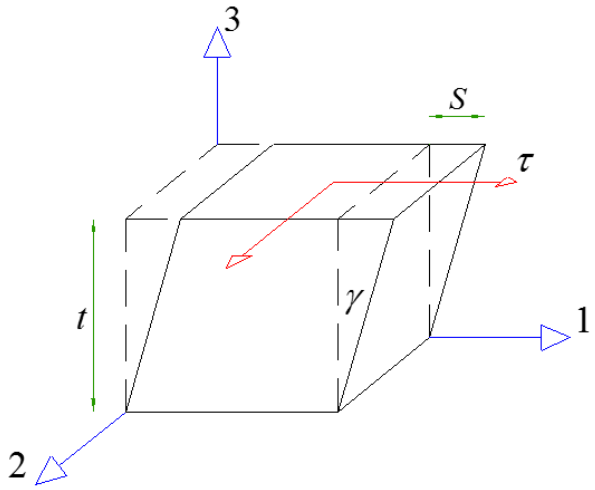

Fig. 2.18 8-ndoe interface element

To simulate the interfacial bond element, 8-node orthotropic element is employed as shown in **Fig. 2.18**. In this element, the upper and bottom faces are connected to slab surface and FRP laminate, respectively. Therefore, the vertical displacement in local axis 3 is influenced by the normal stress of adhesive material. The horizontal displacement in local axes 2 and 3 are influenced by the interfacial bond stress.

The following assumptions are considered in the numerical analysis.

- Young's modulus of adhesive material is used in all directions.
- Element thickness, t, is assumed as the same as CFRP sheet thickness.
- Shear modulus, G_{31} and G_{23}, are enrolled to simulate interfacial bond stiffness, E_b, and can be calculated by the following equations.

$$G_{31} = G_{23} = \frac{\tau}{\gamma} = \frac{\tau_{\max}}{S_0/t} = \frac{E_b}{t}, \tag{2.45}$$

where γ is the shear strain due to relative bond displacement, S. E_b is the ratio of bond stress to corresponding slip displacement in continuum stage as shown in **Fig. 2.17**.

2.4.3 Interfacial bond behavior under cyclic loading.

According to previous studies, the material bond strength was obtained from single shear or double-shear bond tests by Dai et al. and Yun et al. [24, 25]. In the case of cyclic fatigue loading, the average bond stress, τ_{ave}, versus slip, S, relationships reported by Dai et al. [24] in their FRP-to-concrete lap joint tests shows a decreasing of interfacial bond stiffness and an increasing of the slip displacement as shown in **Fig. 2.19**. This relationship is similar to that developed by Holmen et al. [26].

According to these studies, the model by Loo et al. [27] is employed in this study by reducing of the interfacial bond stiffness according to the following equation. **Fig. 2.20** shows the degradation of interfacial bond stiffness due to cyclic loading.

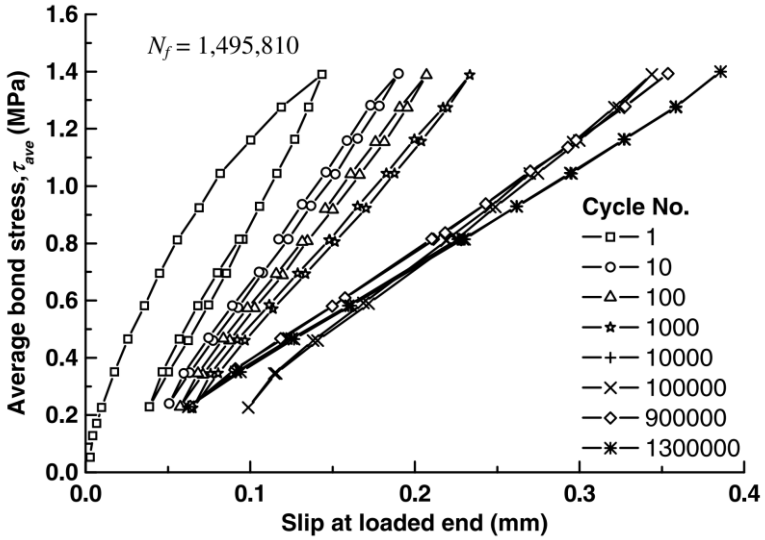

Fig. 2. 19 Bond stress versus slip displacement relationships under cyclic loading for Specimen S1-3 of Dai et al. [24]

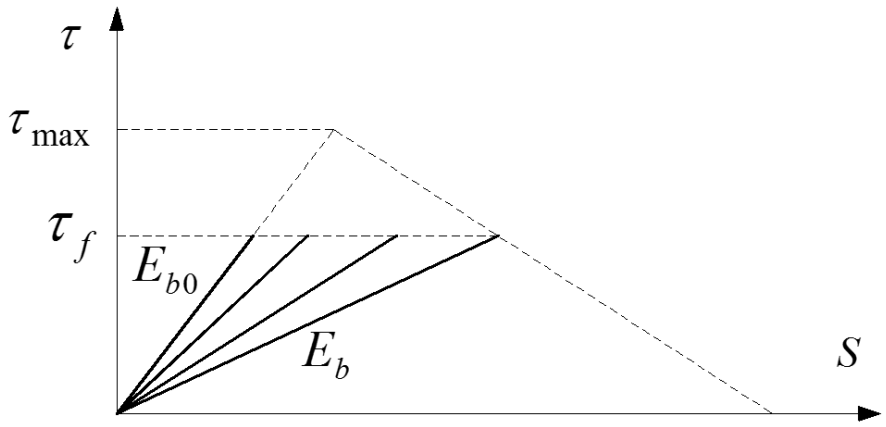

Fig. 2.20 The degradation of interfacial bond stiffness due to cyclic loading

$$E_b = E_{b0}\left[1+\alpha(\log N)^{\beta}\cdot\left(\frac{\Delta\tau}{\tau_f}\right)^{\gamma}\right], \qquad \textbf{(2.46)}$$

where E_b is the interfacial bond stiffness at cycle N, E_{b0} is the interfacial bond stiffness at the first cycle; N_f = number of cycles at failure; $\Delta\tau$ is the bond stress range, τ_f is the bond stress at failure, and the constants α, β and γ are parameters to fit the experimental data. For verification, this equation are compared with the limited available test data of Dai et al. and Yun et al. [24, 25]. α, β and γ equal to -190.3, 0.990 and 8,797, respectively.

For simplicity, uniform interfacial bond stiffness, E_b, is used for all bond elements according to the biggest average bond stress rang, $\Delta\tau$.

CHAPTER 3

FATIGUE ANALYSIS OF PLAIN AND REINFORCED CONCRETE BEAMS

3.1 Introduction

To examine the applicability of the numerical method explained in the previous chapter, fatigue analysis of plain and reinforced concrete beams under pulsating and moving load is conducted in this chapter. According to previous studies [5, 12, 28], researchers have succeeded in providing a good conception of fatigue failure mechanism. But, dealing with the large structural elements requires the use of a numerical computational method such as finite element method. Therefore, it is the time to improve a well-established numerical method that will be used for predicting fatigue behaviors.

In the present chapter, a proposed numerical method is used to simulate the fatigue behaviors of plain and reinforced concrete beams under pulsating and moving load regarding distributed cracks, and their bridging stress degradation characteristics. Fatigue life, crack propagation characteristics, and failure mechanism of these beam under fixed pulsating and moving load will be numerically obtained by this method and will be compared by the experimental results. Furthermore, the effect of cyclic, i.e. pulsating and moving loading type on the deformation and fatigue behavior is studied.

3.2 Plain concrete beam

3-point bending static and fatigue analysis of plain concrete beams are carried out for the dimensions of 100 x 100 x 420 mm and the span of 400 mm to compare with experimental results by Zhang et al. [11] (**Fig. 3.1**). For fatigue analysis, these beams are subjected to constant amplitude between maximum and minimum load levels. Maximum load level is changed to obtain S-N relationship. The concrete properties of these beams are the same as those used in the experimental study. The tensile strength, f_t, compressive strength, f_c, and modulus of elasticity, E_c, of used concrete are 5.20 N/mm^2, 53.22 N/mm^2 and 30000 N/mm^2, respectively.

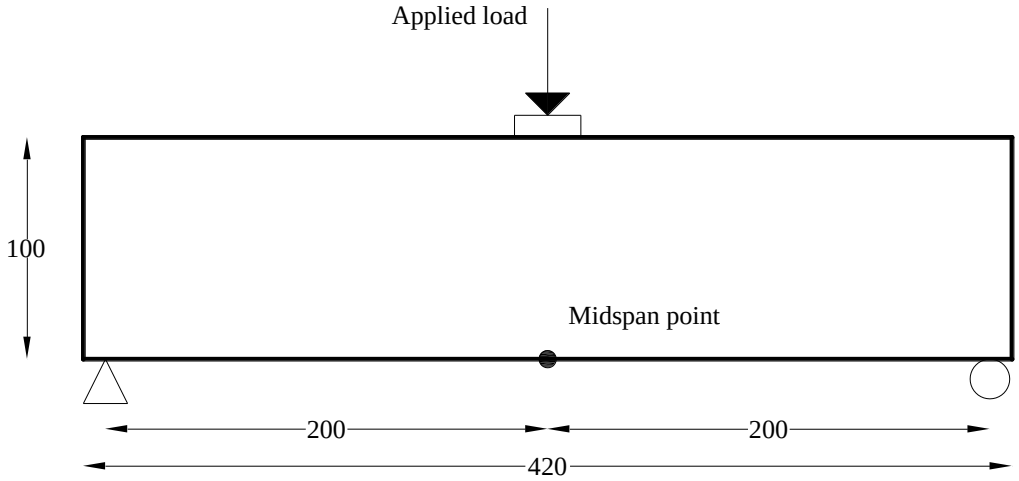

Fig. 3.1 Three-point bending beam (all dimensions in mm)

3.2.1 Static analysis of plain concrete beam

Fig. 3.2 shows the load-midspan displacement relationships for numerical result and hand calculation. This figure shows the almost same initial stiffness. The numerical result shows an acceptable agreement with the ultimate load level by Zhang et al. [11]. For hand calculation, a short segment of a simply supported rectangular beam is considered width, b, depth, t, and span, L, and external load, P, at the middle. Flexural stress, σ, and midspan displacement, δ, are calculated according to simple beam theory given by the following equations.

$$\sigma = \frac{1.5PL}{bt^2} \tag{3.1}$$

$$\delta = \frac{P}{4E_c b}\left(\frac{l}{t}\right)^3 \tag{3.2}$$

Beam theory shows the smallest strength value because it was not taken into the account the bridging stress for cracked concrete.

Fig. 3.3 shows stress and strain distributions along beam section at midspan for different loading points (A: pre-peak loading, B: peak loading, and C: post-peak loading). This figure shows that the crack tip is gradually extended up with increasing of static loading. The stress and strain distribution of the loading point (A) shows a linear relationship and significant agreement with the hand calculation. Increasing load to a point (B) leads to an increasing of tensile stress and generating the crack that expands from the lower-center of the beam to crack tip. While, the crack tip located when the tensile strain is just larger than cracking strain, ε_t, to show a bilinear strain and bridging stress distributions along the crack length. According to this procedure, for loading point (C), the crack propagation leads to generate of new fracture zone that showing larger strain value and smaller bridging stress at its crack mouth.

As shown in **Fig. 3.4**, the cracking pattern of the numerical result at maximum load (Point B) shows that vertical crack formed in the maximum moment region.

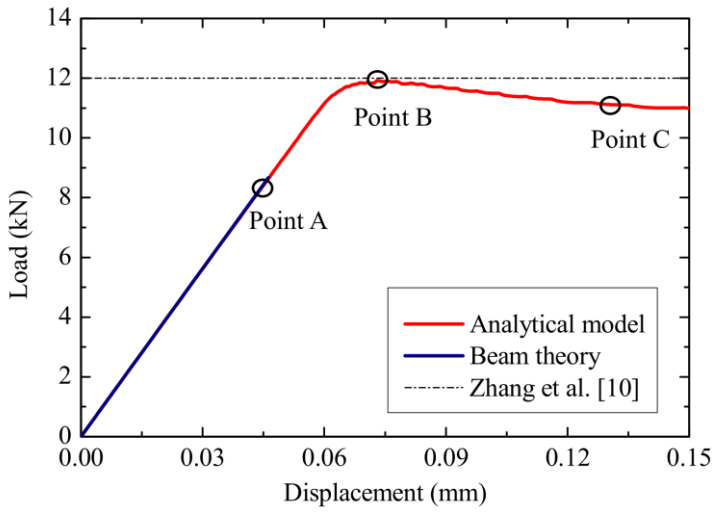

Fig. 3.2 Load-midspan displacement relationships

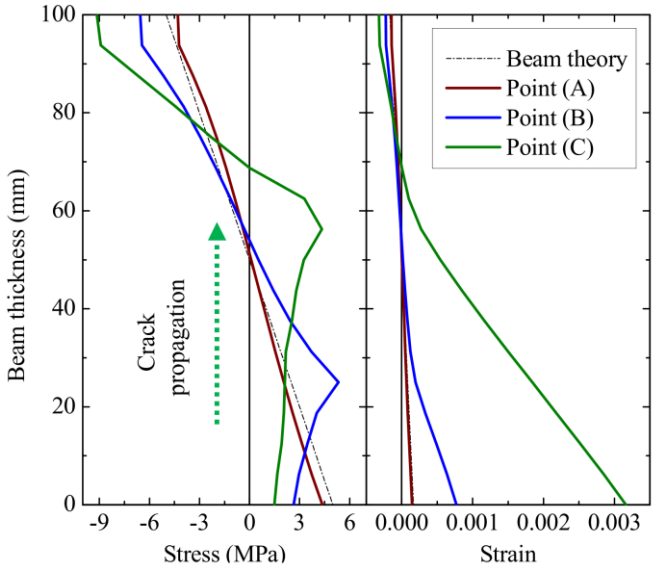

Fig. 3.3 Stress and strain distributions at midspan section

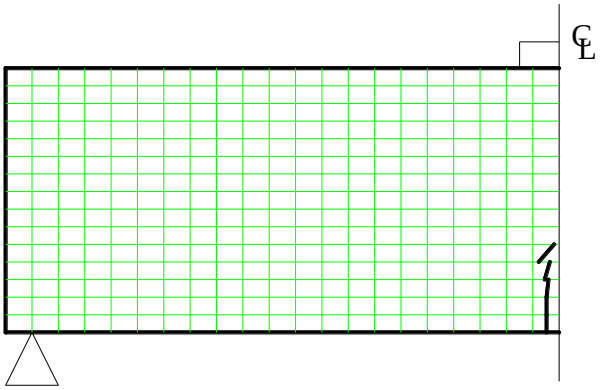

Fig. 3.4 Cracking pattern at maximum load (point B)

3.2.2 Fatigue analysis of plain concrete beam

Fatigue strength is generally defined as a friction of the static strength that can be supported repeatedly for a given number of cycles. The beams were tested under different maximum loads. Every beam has a constant amplitude fatigue loading between maximum and minimum load levels.

As an example, a specific fatigue loading procedure with maximum load equal to 8.98 kN leads to generate a cracked zone at first cycle as shown in **Fig. 3.5** (N=1). The bridging formula without stress degradation was used in this area. By increasing number of cycles, the fatigue crack bridging degradation will occur in the cracked zone because it is subjected to crack closing and opening processes. The load capacity cannot reach the maximum load level with this already formed cracked area. Therefore, a new cracked area is needed, in order to reach the maximum load level as shown in **Fig. 3.5** (N=100). The bridging formula with different cycle numbers will be used in the old fracture zones (N=2, 3~N_i) and the newly developed fracture zone (N=1). This progressive crack propagation proceeds until the final failure occurs as shown

in **Fig. 3.5** (N=10,000). The explanation of bridging-stress degradation procedure along midspan section for different number of cycles under a constant maximum load equaling 8.98 kN are shown in **Fig. 3.6**. This figure shows the crack bridging stress tip gradually extended up with increasing of number of cycles. Moreover, increasing number of cycles leads to decrease the bridging stress in the cracked zone. This leads to the loss of sectional moment balance in the end. Hence, its overall stiffness gradually decreases resulting to a fatigue failure.

By applying this procedure for different maximum load levels, the fatigue life is predictable. The numerical result of the relationship between fatigue life and maximum load level compared to experimental results of Zhang et al. [11] is shown in **Fig. 3.7** Increasing maximum fatigue load level leads to a decreasing of the fatigue life. The numerical results show satisfactory agreement compared with the experimental results by Zhang et al. [11]. One of the benefits of this developed numerical model simulation is that it can capture much more crack in the material elements compared with the theoretical proposal of Zhang et al. [11] which considers only single crack at midspan.

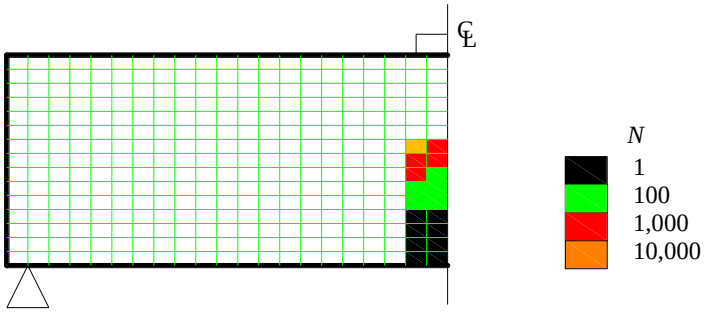

Fig. 3.5 Cracked elements propagation

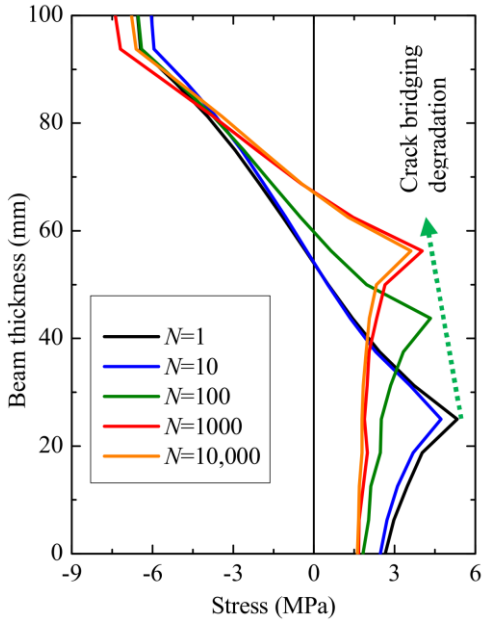

Fig. 3.6 Stress distributions at midspan of the beam at different number of cycles

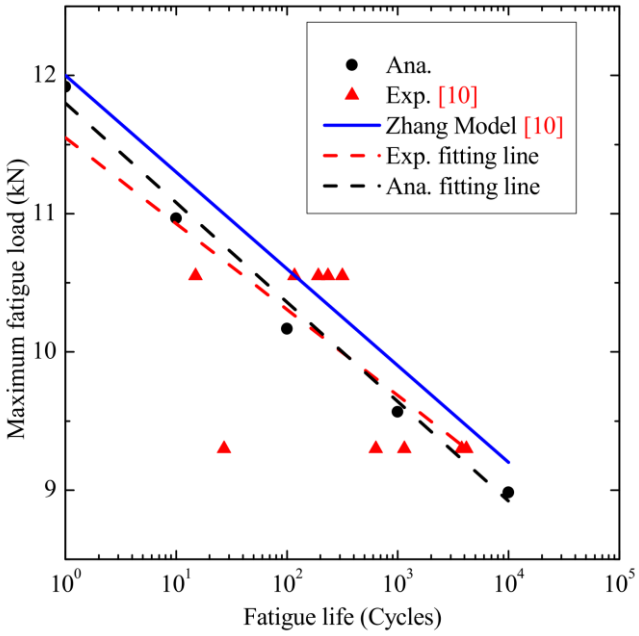

Fig. 3.7 Relationships of maximum load level and fatigue life for numerical and experimental results

3.3 Reinforced concrete beam

In this section, 3-point and 4-point bending static and fatigue analysis of the RC beams were carried out for a beam dimension of 150×300×3000 mm and their span is 2850 mm to compare with experimental results of P. J. Heffernan and M. A. Erki [29]. **Fig. 3.8 (a)** and **(b)** show the tested beam with reinforcement details and the analytical model with boundary conditions and dimensions, respectively. The concrete and steel reinforcement properties of these beams are the same as those used in the experimental study. The concrete and main reinforcement properties used in the analytical model are shown in **Table 3.1**.

Static and fatigue analysis of 4-point bending beams (**Fig. 3.8 (a)**) have been used to verify the proposed numerical method. In order to study the effect of cyclic loading type (fixed pulsating and moving loads) on fatigue behavior, the 3-point bending beam analysis are used as shown in **Fig. 3.8 (b)**.

Table 3.1 Material properties [29]

	Concrete	Reinforcement (Deformed)
Elasticity (GPa)	27	200
Poisson's ratio	0.2	0.3
Strength (MPa)	32 (Compression) / 3 (Tension)	512 (Yield)

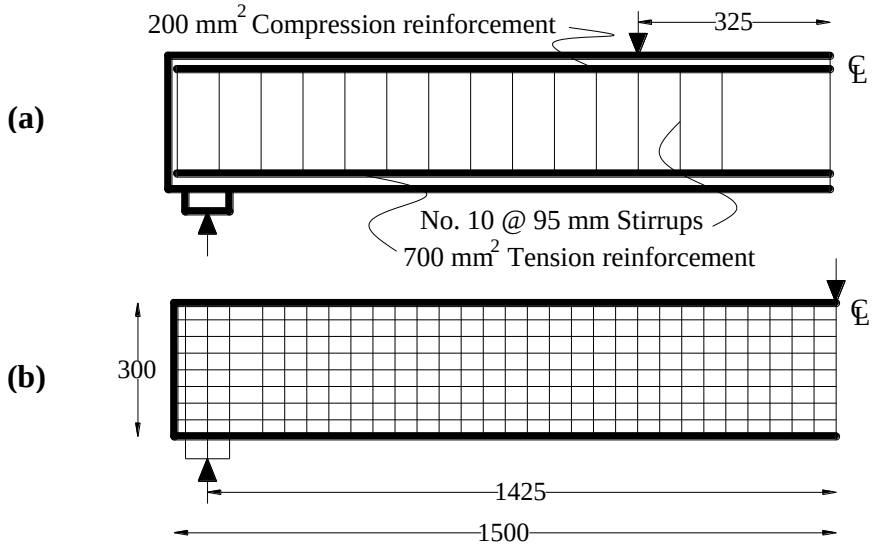

Fig. 3.8 Beam details and numerical model

3.3.1 Static analysis of RC beam

The experimental results of the 4-point bending beam by P. J. Heffernan and M. A. Erki [29] are compared to numerical model results. As shown in **Fig. 3.9**, load-midspan displacement relationships of numerical results (the 3-point and 4-point bending beam) and the experimental results almost show the same initial stiffness. The 4-point bending numerical model shows an acceptable agreement with the experiment [29], and it continued to resist an increasing load as the main reinforcement carried increasing tensile load to yielding of steel. Finally, these beams are failed by a bending failure mode. The 3-point bending beam shows a smaller strength value than the 4-point bending beam because it causes larger bending moment.

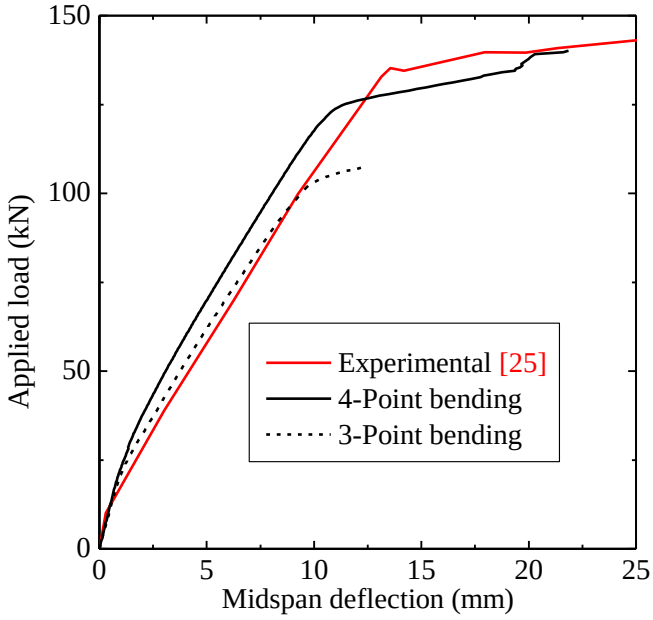

Fig. 3.9 Load-midspan displacement relationships for numerical and experimental results

3.3.2 Fatigue analysis of RC beam

The 4-point bending beam was analyzed under a constant amplitude fatigue loading between maximum and minimum load level, where maximum and minimum loads are equal to 80% and 20% of the ultimate static load, respectively. Two same beams were tested by P. J. Heffernan and M. A. Erki [29] under the previously fatigue loading scheme to verify the numerical method.

As shown in **Fig. 3.10**, a fatigue loading procedure with a maximum load equal to 112 kN (80% of the ultimate load) leads to generate a cracked zone at the first cycle (N=1). Increasing number of cycles leads to a degradation of the cracked elements according to the bridging stress degradation concept. This leads to propagate new cracked elements to exceed the maximum load level. This progressive cracks propagation would be proceeded until the final failure occurs. There are no experimental crack pattern data [29] to compare with the numerical cracked element propagation. But, experimental results of midspan displacement evolution can be used for verification.

Fig. 3.11 shows strain and stress distribution along beam section at midspan, from the bottom to 200 mm height, at midspan for different cycle numbers. According to the previously described fatigue procedure, increasing number of cycles leads to a degradation of concrete bridging stress and an increasing of its strain. This observation is significant from cracking tip to non-reinforced part. For reinforced part, increasing of strain at crack mouse leads to an increasing of the RC stress due to increasing of reinforcing bar force. This numerical method assumed that there is no degradation of deformed reinforcing bar due to fatigue loading.

The numerical and experimental midspan displacement evolution for RC beam under fixed pulsating load equaling 80% of ultimate static load is shown in **Fig. 3.12**. This figure shows a slightly increasing of maximum and minimum midspan displacement with increasing of the number of cycles, until the midspan displacement began to increase rapidly at the imminent failure. One of the reasons is that the reinforcement can propagate small cracks beside the main crack in the maximum moment region. For an imminent failure stage, the accelerated reduction in stress transfer was attended by further extension of the main crack according to the stress distributions in **Fig. 3.11**.

3.3.3 Comparison between fixed pulsating and moving load

Two reinforced concrete beams were analyzed under fixed pulsating and moving load. These beams were analyzed to provide a comparison between the fatigue behavior of both RC beams subjected to fixed pulsating and moving load. The same steel reinforcement arrangement and material properties were used for two previously described beams. The first beam was cycled under a fixed pulsating loading at midspan, 3-point bending loading, between a minimum, P_{min}, and maximum, P_{max}, load level equaling 33% and 63% of the ultimate load, P_{ult}, which was obtained by the 3-point bending static analysis, respectively. These load percentages were adopted based on the safety factors proposed by AASHTO [30] which were simulated common service conditions.

The second beam was subjected to a constant moving load, P_{mov}, equal to 63% of the ultimate load. For each analysis cycle, this moving load was simulated by moving the applied load from midspan, point 1, to several points, 2, 3, and 1 again, along the longitudinal direction of the beam as shown in **Fig. 3.13**. In order to provide accurate comparison, this moving path was chosen to decrease the shear effect by keeping shear span-to-depth ratio more than 2.58.

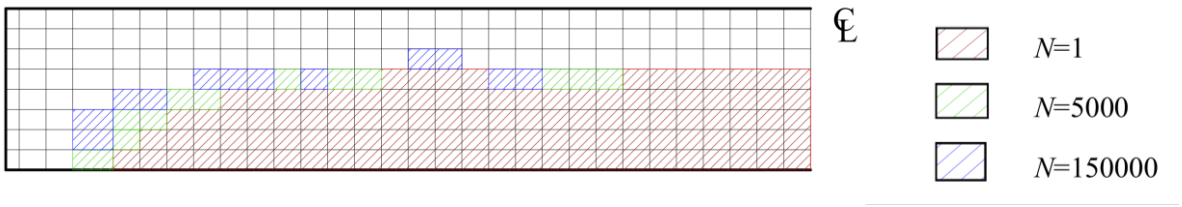

Fig. 3.10 Propagation of cracked elements due to fixed pulsating load equaling 80%

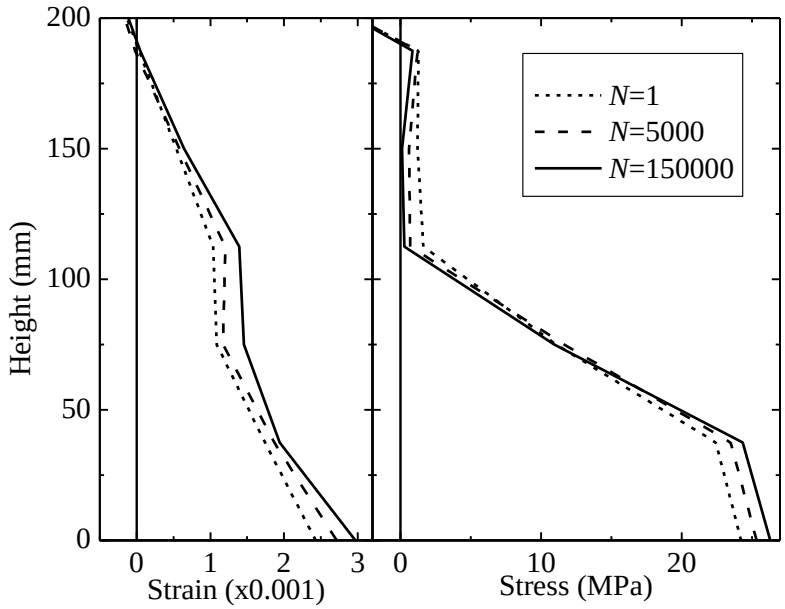

Fig. 3.11 Strain and stress distribution curves along the beam section at midspan (0~200 mm)

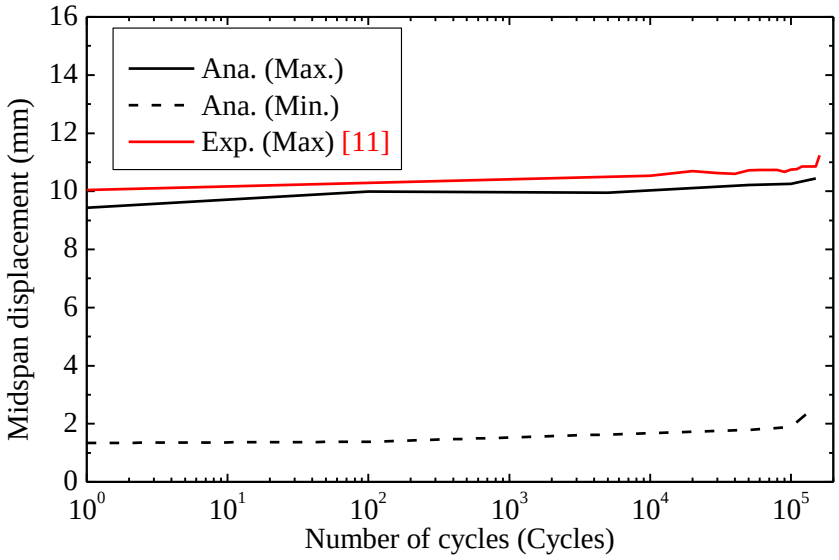

Fig. 3.12 Midspan displacement evolution of RC beam under fixed pulsating load equaling 80%

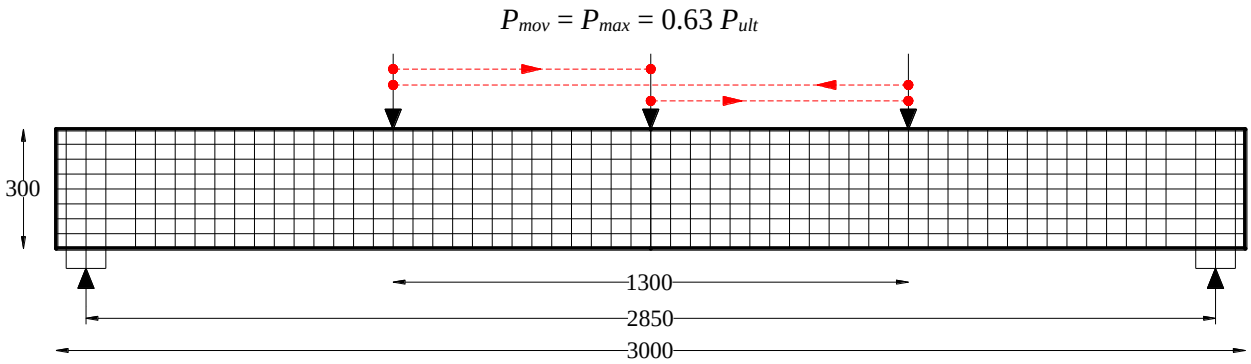

Fig. 3.13 Schematic moving load path on numerical model

The propagation of the cracked elements at a different number of cycles of the RC beam under fixed pulsating and that under the moving load is shown in **Fig. 3.14**, and it is considered in comparison. The cracked zone at the first cycle, N=1, of the RC beam under the fixed pulsating load case is smaller than that under moving load. The RC beam under fixed pulsating shows the cracked area that distributed from the loading point at midspan. On the other hand, the RC beam under moving load shows the cracked area that expands all over the tension side due to the effect of load movement. Increasing number of cycles leads to an increasing of the cracked zone for RC beam under fixed pulsating load and that under moving load. In the case of fixed pulsating load, the propagated cracked elements are extended from loading point resulting a trapezoidal shape after million cycles. In the case of moving load, the new cracked elements are propagated with increasing number of cycles resulting a rectangular shape.

According to **Table 3.2**, the percentage of cracked elements volume for RC beam under fixed pulsating load is smaller than that under moving load at 1st cycle and million cycles. This table shows the average degradation ratio for both beams. This ratio can be defined by the ratio of the difference between the cracked elements volume after million cycles and 1st cycle by mm^3 to the number of cycles. RC beam under fixed pulsating load leads to higher degradation ratio than that under moving load.

The maximum and minimum midspan displacement evolutions of the RC beam under fixed pulsating load compared with that under the moving load are shown in **Fig. 3.15**. According to previously described part of the propagation of cracked elements, RC beam under moving load shows higher maximum midspan displacement than that under fixed moving load due to its

Table 3.2 Percentages of cracked element volume and average degradation ratio

Loading type	The cracked elements volume%		Average degradation ratio (mm^3/Cycle)
	1st cycle	10^6 cycles	
Fixed pulsating	34.17%	48.33%	7.31
Moving load	45%	53.75%	3.66

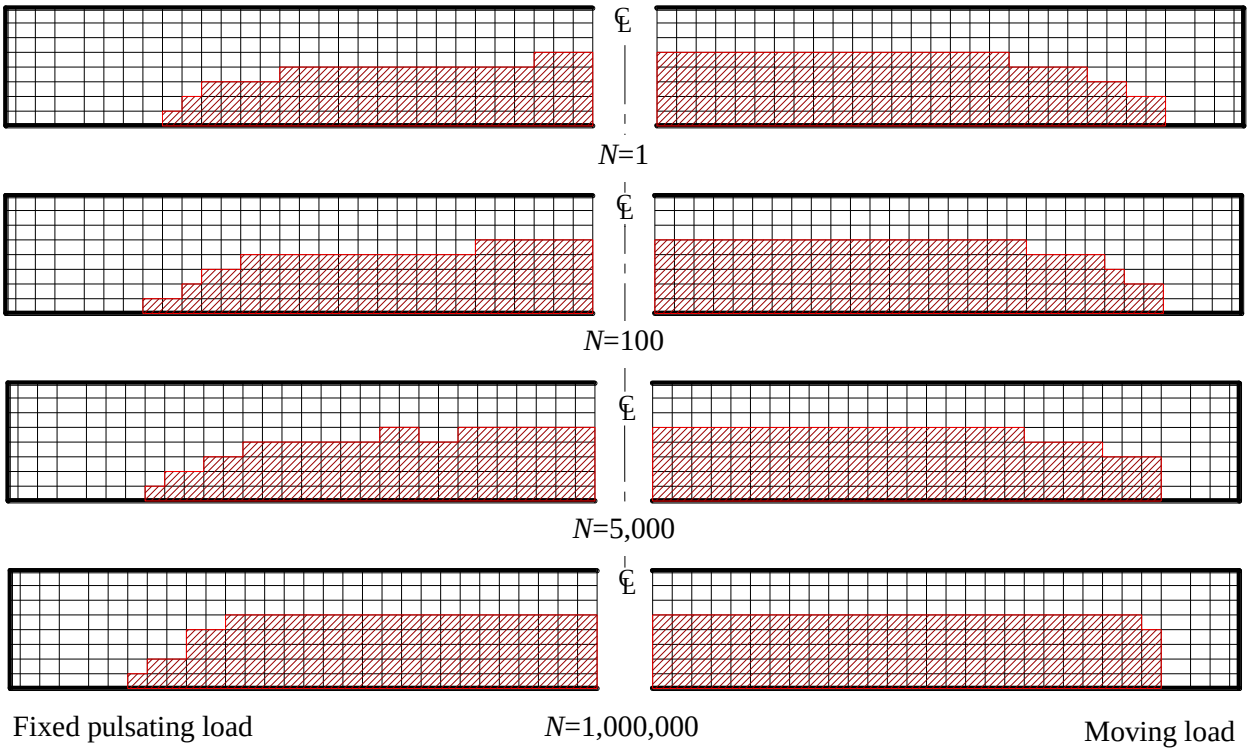

Fig. 3. 14 Comparison between the propagation of cracked elements for RC beam under fixed pulsating load and that under the moving load

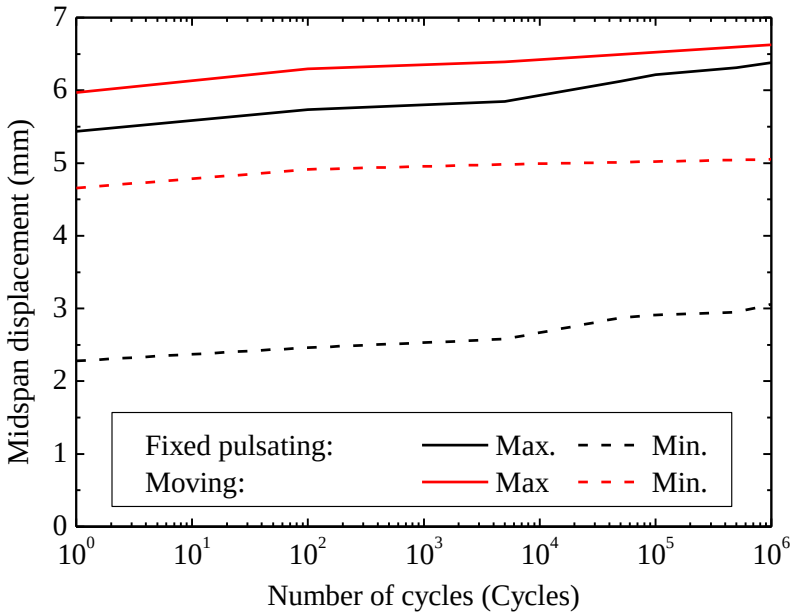

Fig. 3.15 Maximum and minimum midspan displacement evolution for RC beam under fixed pulsating load and that under moving load

wide propagation of cracked elements. This wide propagation leads to a significant decreasing of the beam stiffness resulting a higher deformation. The minimum midspan displacement of the RC beam under fixed pulsating load and that under the moving load correspond to the minimum fatigue load level, P_{min}, at midspan and the moving load, P_{mov}, which locating at 650 mm from midspan respectively. It is noticed that, the minimum midspan displacement of the RC beam under moving load is larger than that under the fixed pulsating load. The reason is that the moving load is more than the minimum load level of RC beam under fixed pulsating load. Maximum displacement evolution of RC beam under fixed pulsating load shows as slightly higher slope than that under moving load due to its higher average degradation ratio as shown in **Table 3.2**.

In this chapter, the amplitude of the midspan displacement of RC beams is regarded as an indicator for the progress of damage. According to the mentioned results, the RC beam under moving load shows a larger midspan displacement and wide propagation of cracked elements than that under fixed pulsating load. Therefore, RC beam under moving load shows a significant damage than that under fixed pulsating load. There is no fatigue failure for both beam during one million cycles. But, according to previous results discussions, the fatigue life of RC beam under moving load will be predicted to be shorter than that under fixed pulsating load.

3.4 Deciding a reinforcing model technique

In this section, RC beam subjected to static loading under 4-points bending was selected for verification and deciding analysis techniques of reinforcing bar modeling. This analysis is conducted using three techniques of modeling steel reinforcement in finite element models for reinforced concrete; the discrete model, the embedded model, and the smeared model [31] to compare with experimental data. **Fig. 3.16** shows the numerical technique for modeling of reinforcement.

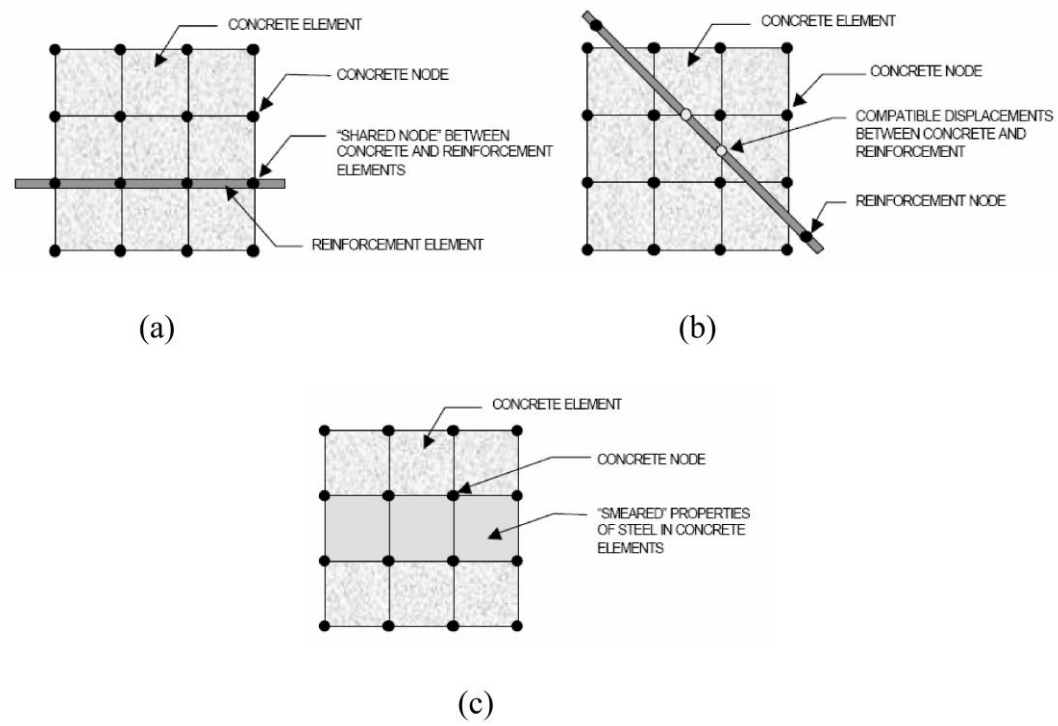

Fig. 3. 16 Models for Reinforcement: (a) discrete; (b) embedded; and (c) smeared [31]

For the discrete reinforcement model in **Fig. 2.16 (a)**, link bars or beam elements are connected to concrete mesh nodes. Therefore, the reinforcement and concrete mesh use the same nodes. This leads to assuming a perfect bond between concrete and reinforcement. Moreover, the concrete elements are restricted by the location of the reinforcement and bar meshing nodes.

In the embedded model in **Fig. 2.16 (b)**, the reinforcement overcomes the concrete mesh restrictions because the stiffens of the reinforcing bar is evaluated separately from the concrete elements. This model keeps the displacements of reinforcing bars compatible with the surrounding concrete elements. This model leads to increasing of the number of nodes and degree of freedom in the composite. Therefore, using this model leads to an increasing of the run time and computational cost.

In **Fig. 2.16 (c)**, the smeared model assumes that the reinforcement is uniformly distributed in the concrete element. The reinforcement and concrete will be combined to generate RC element according to the reinforcement ratio in concrete element. Therefore, there are no generated nodes for reinforcement. This model is suitable for large-scale models and uniformly reinforcing bars distributions such as RC slabs and shear walls.

3.4.1 Analytical model of the tested RC beam

Buckhouse et al. [32] studied a strengthening RC beam for flexure using external structural steel channels. This study included experimental testing of control beam without strengthening. This beam can be used for calibration of the different finite element model types. The width and height of the tested beams were 254 mm and 457.2 mm, respectively. As shown in **Fig. 2.17**, the length of the beam was 4724.4 mm with supports located 76.2 mm from each end of the beam allowing a simply supported span of 4572 mm. The main reinforcements used were 16 mm diameter bars and shear reinforcements included 10 mm bars U-stirrups. The layout of the reinforcements is detailed in **Fig. 2.17**. The properties of steel reinforcements and concrete are included in **Table 1**.

Anthony et al. [33] studied a flexural behavior of reinforced and prestressed concrete beams using finite element analysis. This study included a numerical result which obtaining from analysis of the previous experimental beam using ANSYS. A quarter of the beam was analyzed due to symmetry. This analysis used a discrete reinforcement model approach. The beam, plates, and supports were modeled as volumes. Link8 elements were used to create the flexural and shear reinforcement as shown in **Fig. 2.18**, which illustrates that the rebar shares the same nodes at the points that it intersects the shear stirrups and divided nodes of concrete volume.

Table 3.3 materials properties of tested beam [32]

	Concrete	Reinforcement
Elasticity (GPa)	27.23	200
Poisson's ratio	0.2	0.3
Strength (MPa)	32.73 (Compression) 2.73 (Tension)	320 (Yield)

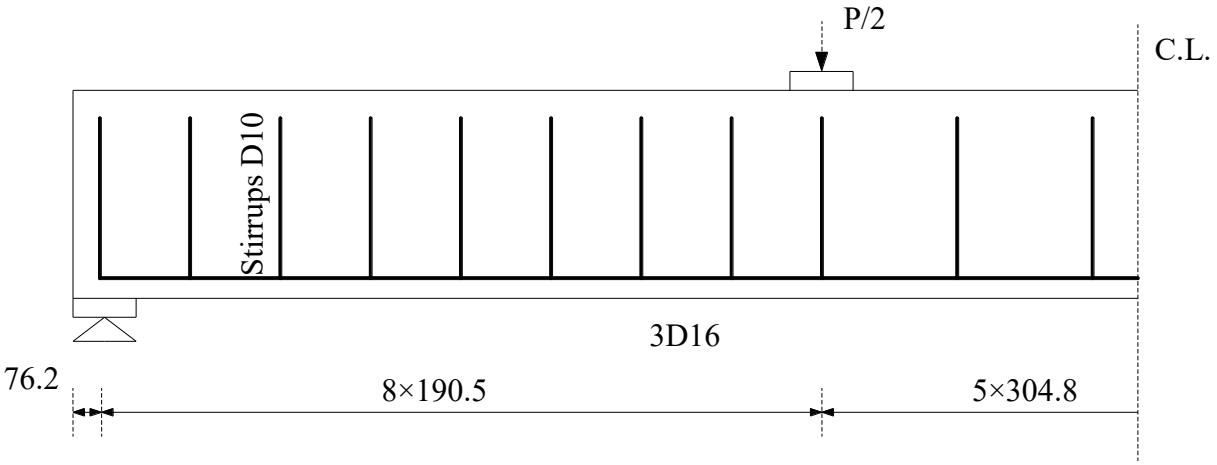

Fig. 3.17 detail for control beam reinforcement (all dimensions in mm) [32]

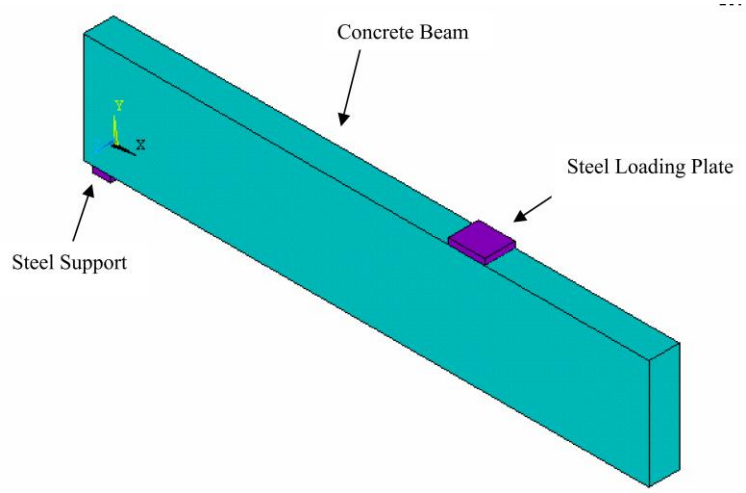

(a)

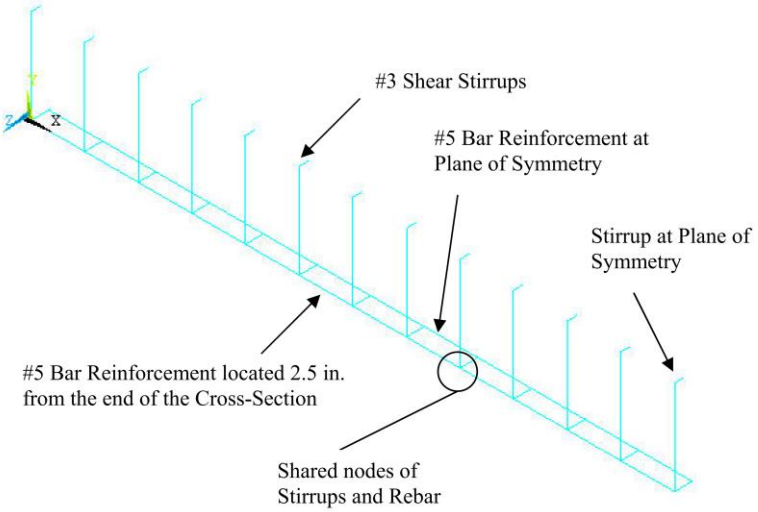

(b)

Fig. 3.18 (a) Volumes created in ANSYS; **(b)** Reinforcement configuration [33]

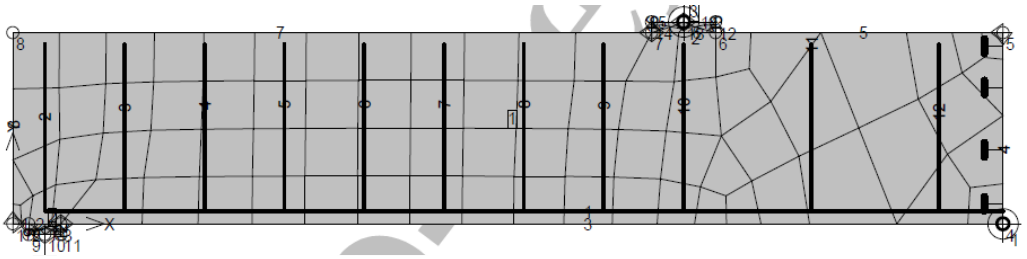

Fig. 3.19 Finite element meshing of a beam in embedded model by ATENA

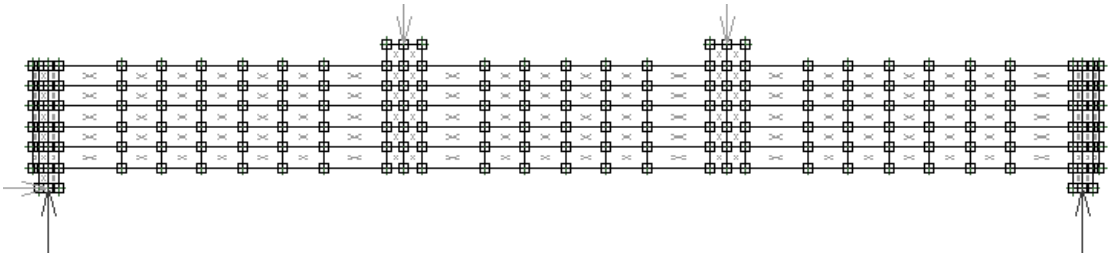

Fig. 3.20 Numerical model using smeared reinforcement approach

In the embedded reinforcement model, ATENA 2D software was used to analyze this beam. SBETA was chosen to simulate concrete element. To take advantage of the symmetry of the beam and saving processing time, only one half of the model was conducted and the horizontal freedom degree of the nodes in the beam medium center line was restricted by applying horizontal roller support. In order to reduce some stress concentration due to concentrated loads and avoiding a local failure in the elements near the loading point, linear elastic steel plates were added at loading and supporting points. The concrete of the beam was meshed as shown in **Fig. 2.19**.

Fig. 2.20 shows the model of smeared reinforcement with the boundary conditions. The reinforcement can be modeled in smeared rebar according to the dimensions of reinforced elements and the reinforcement ratio. Smeared rebar may be placed in each element based on a reinforcement ratio in any direction desired., MSC Marc-Mentat was employed for mesh generation, graphics, and post processing only. 8-Nodes 3D solid elements were utilized for reinforced concrete. 254 mm thickness steel plates were used at the supports and load application location. A vertical constraint was applied at the bottom of the support plate along its center line. Applied load was distributed to central line nodes on the top of the loading plate as shown in **Fig. 2.20**.

3.4.2 Results and discussions

This section presents the results of RC beam obtained from the finite element analysis and the comparison between the experiment and the analysis.

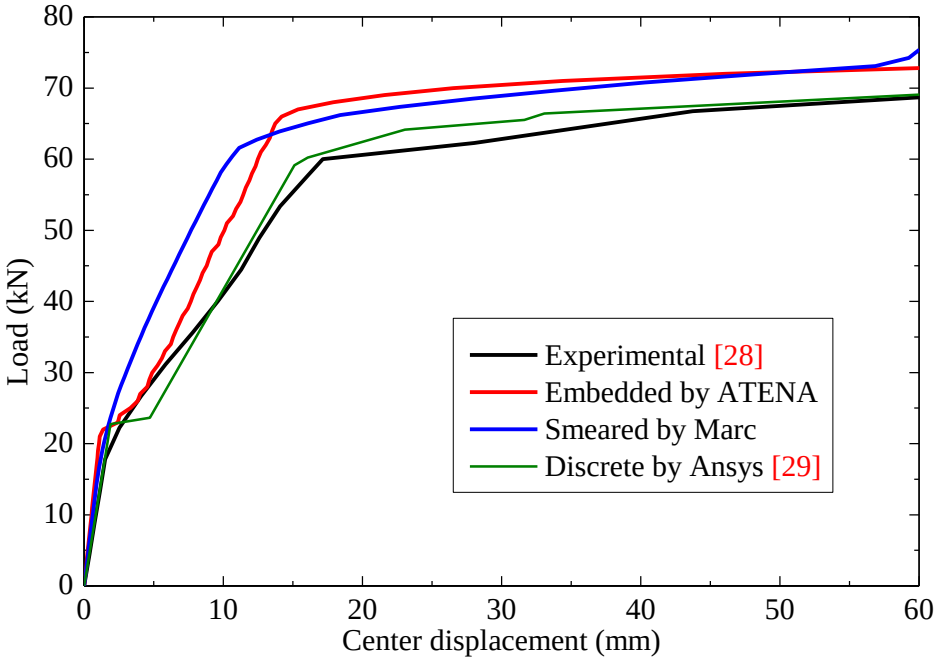

Fig. 3.21 Load-displacement relationships for analyzed beam

Table 3.4 Cracking load and displacement for analyzed beam

Calculation method	Cracking load (kN)	Displacement (mm)
Experimental [32]	20	1.65
Hand calculation	22.77	1.34
Discrete model [33] (ANSYS)	23.2	1.36
Embedded model (ATENA)	20	1.07
Smeared model (Marc)	19	1.31

Fig. 3.21 shows the load-displacement relationships for experimental and numerical results. Generally, all numerical results show a good agreement with the experiment. This figure shows that the best modeling strategy is the discrete reinforcement model (which analyzed by ANSYS). The reason is that the smeared model assumes that reinforcement is uniformly spread throughout the concrete elements in a defined region of the FE mesh. In RC beams, the reinforcing bars are not uniformly distributed in all concrete elements. But, there are two advantages in the smeared reinforcement model. First one is decreasing of processing cost due to a decreasing of used elements comparing with other models, discrete and embedded

reinforcement model. Second one is applicability for modelling bond-slip effect between reinforcing bar and its surrounding concrete without modeling additional springs.

The initial cracking load in the analyzed beam can be defined as that a load causes stress just larger than the rupture strength of concrete. In all analyzed beams, the first crack occurs in the constant moment region. These cracks are flexural cracks in every analyzed beam. The cracking load and corresponding displacement for all results are listed in **Table 3.4**. The cracking load of smeared reinforcement model shows a smaller value than those in the discrete and embedded reinforcement models. The reason is that the smeared reinforcement model leads to distribute the contribution of the reinforcing bar in the concrete element. This results in a faster cracking load. In the case of the smeared reinforcement model, the reinforcing bar restricts the concrete deformations and crack opening. Therefore, its cracking load is larger. Smeared reinforcement model shows a best agreement for cracking load comparing with the experimental results than those in the discrete and embedded reinforcement models. Therefore, the smeared reinforcement model successfully simulates the cracking behaviors of the reinforced concrete elements.

3.5 Summary and conclusions

The fatigue life and fatigue behaviors of the plain and reinforced concrete beam under fixed pulsating and moving load can be simulated through this numerical method by knowing the relation of bridging stress degradation of concrete.

Applying fatigue load results in a propagating of the cracked element due to the degradation of their bridging stress. This leads to a significant decreasing of beam stiffness and an increasing of its deformations.

RC beam under moving load leads to a higher midspan displacement evolution and wide propagation of cracked elements than that under fixed pulsating load due to the effect of load movement.

Increasing number of cycles results in an increasing of strain distribution and decreasing of bridging stress distribution at critical section for plain concrete beam. In the case of RC beam, increasing or strain distribution leads to an increasing of stress distribution in the reinforced zone.

Generally, RC beam shows a longer fatigue life and wide propagation of cracked elements than plain concrete beam. One of the reason is that the participation of bridging stress in concrete is very small in the resistance bending moment comparing with the effect of reinforcing bars. Moreover, the plain concrete beam under fatigue loading leads to a localized crack zone at critical section.

The numerical results show some agreement with the experimental results for plain and reinforced concrete beams.

This Chapter focused on the flexural fatigue analysis for plain and reinforced concrete. Many beams are suffering from the shear failure mode at fatigue failure. Therefore, it is recommended to examine the fatigue behaviors of theses beams. This failure mode is mainly affected with concrete properties than reinforcing bar. Therefore, considering the bridging stress degradation in concrete is very important.

For perfect verification, many experimental data are required to compare with the numerical results such as cracking pattern, reinforcing bar strain, displacement distribution and S-N relationship.

The discrete reinforcement model shows a good agreement with experimental for RC beams than smeared model. The smeared reinforcement model is suitable for uniformly reinforcing bars distributions such as RC slabs. Moreover, the smeared reinforcement model can simulate the bond-slip effect between reinforcing bar and its surrounding concrete without modeling additional springs.

CHAPTER 4

FATIGUE ANALYSIS OF RC SLABS REINFORCED WITH PLAIN BARS

4.1 Introduction

In Chapter 2, the bridging stress degradation concept is employed in the finite element method to predict fatigue behaviors. The modified reinforcing bar stress-strain relation based on the bond-slip effect between plain reinforcing bar and its surrounding concrete was proposed in this numerical method. The previous chapter extended the validation of this method for the case of plain and reinforced concrete beams and it discussed the cracked element propagation due to fixed pulsating and moving load.

The main challenge of this study is prediction of the fatigue behavior of RC slabs reinforced with plain bars. According to the previous studies as mentioned in Chapter 1, RC slab under moving load leads to a shorter fatigue life and widely cracking pattern than that under fixed pulsating load. Therefore, the case of RC slab under moving load is chosen. In order to verify the proposed numerical method explained in Chapter 2, the fatigue analysis of the RC slabs reinforced with plain bars under a moving load is conducted.

In this chapter, four RC slabs under moving load and one RC slab under static load are analyzed. Slab geometry and materials properties are the same as those used in the experimental study by Shakushiro et al. [7]. This study is used to verify the analytical results in static [34] and fatigue loading. The analytical producers of fatigue analysis were introduced. Furthermore, propagation of cracked elements, fatigue life, slab center displacement evolution and rebar strain are shown in this study. The comparison of fatigue behaviors between RC slab reinforced with plain bars and that reinforced with deformed bars is also provided.

4.2 RC slab modeling and analytical procedure

An RC slab model of smeared crack elements is analyzed using the method explained in the chapter 2. The loading pattern and load levels are the same as those used in the experiments [7, 34]. All slabs were supported by steel I-beams and hinged supports along its longitudinal and transverse directions, respectively. The concrete and reinforcement properties of these slabs are the same as those used in the experimental study. The details of these tested slabs are shown in **Table 4.1** [7, 34].

For static analysis, RC slab is analyzed with dimensions of 2650 × 4000 × 160 mm. A distributed load with a size of 120 × 300 mm is applied at 780 mm from the slab center to check the punching shear behavior as shown in **Fig. 4.1 (a)**. For fatigue analysis, the dimensions of the analyzed slabs are 2650 × 3300 × 160 mm. A moving load was simulated by moving a constant load level along the longitudinal direction with a distributed size of 125 × 300 mm as shown in **Fig. 4.1 (b)**. This figure shows the upper and lower reinforcing layer arrangement.

The fatigue analysis was conducted as shown in **Fig. 4.2**. Firstly, a moving load is applied at the center of the slab elements. Then, these elements are unloaded, while other elements, adjacent to the right side of the loaded elements, are loaded simultaneously with equal increments. In this technique, a constant load is made to move along longitudinal directions. Due to the geometrical symmetry at longitudinal direction, only half of the model is analyzed. This loading leads to the propagation of cracked elements in the first cycle as shown in **Fig. 4.2.**

(b). By increasing the number of cycles, the constitutive laws of cracked elements are modified according to the bridging stress degradation concept. This leads to the loss of tensile stress in these cracked elements resulting a stress concentration at crack tip. Therefore, new cracked elements are propagated around this stress concentration as shown in **Fig. 4.2 (c)**. According to this propagation and the bridging stress degradation of these cracked elements, the overall RC slab stiffness decreases with an increasing number of cycles. At different moving load locations, the output-cracked elements were stored to be used in updating the numerical model for the next cycle step. This procedure is repeated in each cycle until fatigue failure occurs, while the numerical results are recorded in each cycle.

According to this technique, a repetition of moving load leads to the loss of sectional moment balance. The fatigue failure occurs when the equilibrium cannot be exceeded with the deteriorated cracked elements. Hence, the cracked elements are propagated rapidly resulting a significant decreasing of slab stiffness. This leads to an accelerated increasing of slab displacement indicating to a fatigue failure.

4.3 Static analysis results

To verify the bond effect between a plain reinforcing bar and its surrounding concrete on its stress-strain relation, static analysis was conducted on the full-scale RC slab to compare with the experimental results in Shakushiro et al. [34] as follows.

4.3.1 Load-maximum displacement relation due to static loading

The load-maximum displacement relationship of an RC slab under static load for experimental and numerical results is shown in **Fig. 4.3**. This slab was analyzed with and without considering the bond-slip effect. The displacement was measured at the loading point. The analyzed RC slab with considering the bond-slip effect shows a good agreement with the experimental one. At a load more than 75 kN, RC slab stiffness decreased gradually due to the propagation of cracks. After the cracking load, the bond-slip effect of plain bar is significant due to a rebar slip displacement in between cracks. Finally, the experimentally and numerically static ultimate load of this slab equals to 311 and 309 kN, respectively.

Table 4.1 RC slabs details

Slab ID	Loading type (kN)	Concrete properties (MPa)		Yield strength of Reinforcement (MPa)
		Strength	Stiffness	
S	Static	39.9	24300	235 (Plain)
P110	Moving (110)	43	25900	
P150	Moving (150)	41.7	25400	
P190	Moving (190)	36.6	26000	
D150	Moving (150)	38.6	23900	345 (Deformed)

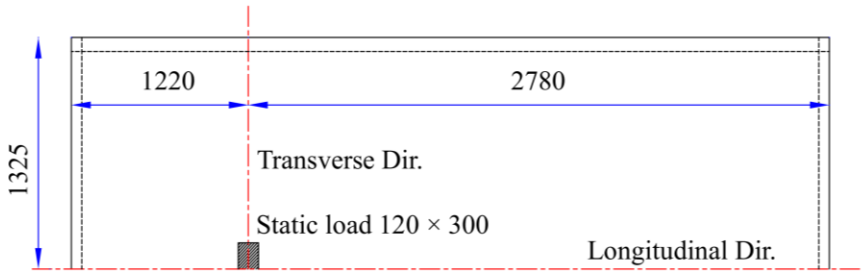

(a) RC slab under static load

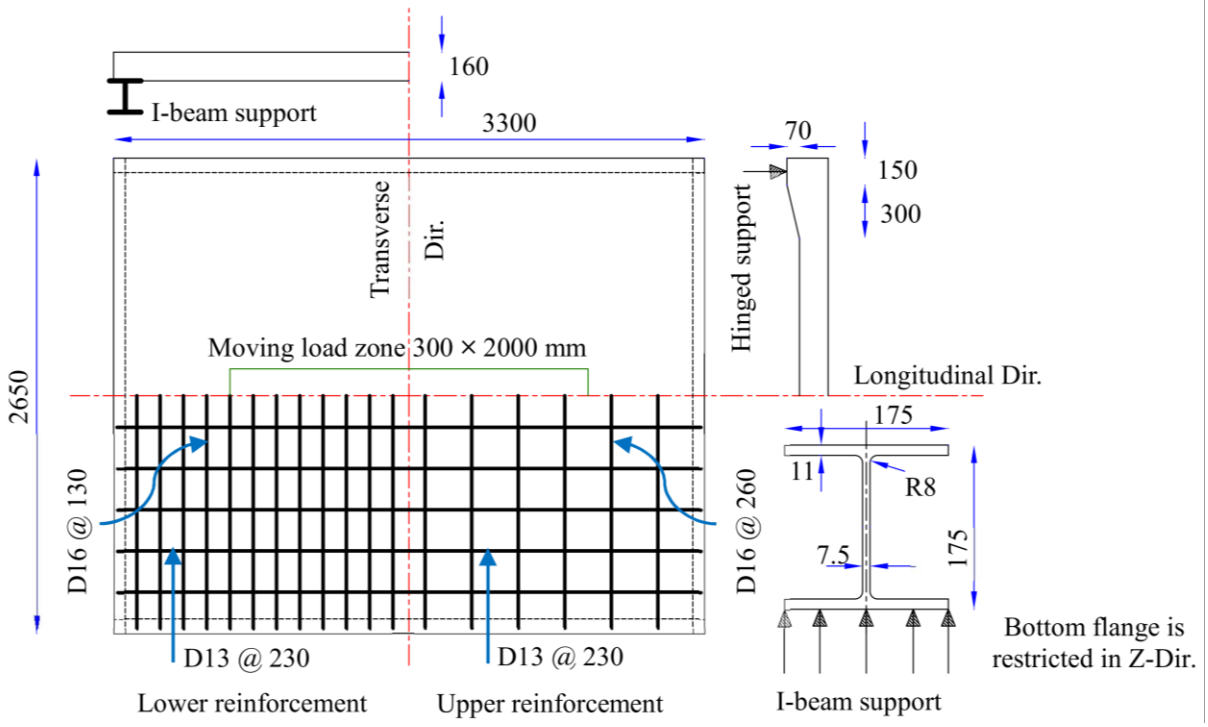

(b) RC slab under moving load

Fig. 4.1 RC slab geometery and reinforcement arrengment

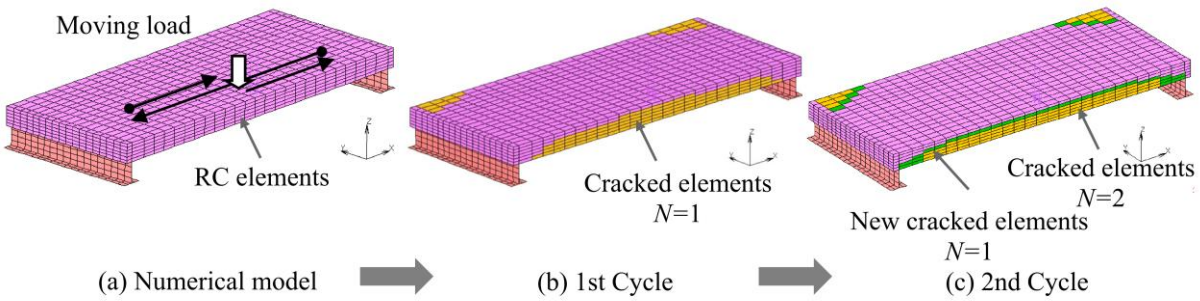

Fig. 4.2 Analytical procudure for fatigue analysis

4.3.2 Maximum principle tensile strain distribution

The distribution of maximum principal tensile strain on the bottom of the RC slab at failure is shown in **Fig. 4.4**. This figure presents only half of the slab due to symmetry in longitudinal direction. This figure shows the strain concentration under the loading point indicating that the cracks are localized at this point. This observation can be considered as an indication of punching shear failure. This agrees with the experimental results of the RC slabs under static loading.

4.3.3 Longitudinal and transverse displacement distribution

At different load levels, the displacements of various points were experimentally measured by Shakushiro [34]. The comparison of displacement distributions along the longitudinal and transverse directions between the experiment and the numerical model at different applied load levels is shown in **Fig. 4.5**. This comparison represents an acceptable agreement between them. As shown in this figure, the maximum displacement of the numerical model is located under the loading point.

4.4 Fatigue analysis results

Four full scale RC slabs under moving load were analyzed to verify the numerical method. The obtained numerical results are compared with the experimental results in Shakushiro et al. [7].

4.3.1 Propagation of cracked elements

This numerical method considers the fundamental factor that the propagation and degradation of cracked elements are the main causes of fatigue failure. Therefore, it is important to describe the propagation of cracked elements. The propagation of cracked elements of the RC slabs under a moving load at different numbers of cycles is shown in **Fig. 4.6**. The one fourth of a slab model is shown due to the symmetry in both directions. As shown in this figure, uncolored elements point to a non-cracked zone. The cracked zone caused by the first cycle of the moving load is indicated in blue, while the cracked zones caused by further cycles are indicated by other colored elements. In all slabs, the transverse direction (T.D.) shows the propagation of cracked elements that extend from the center of the loading area, whereas the longitudinal direction (L.D.) shows the cracked elements that distribute all over the movement zone. In other words, the cracked zone in the longitudinal direction is larger than that in the transverse direction. The reason is that the movement effect of load was transmitted along the longitudinal direction.

To explicate the propagation effect of these cracked elements on fatigue life, the size of the cracked zone after the first cycle (blue color elements) is considered as an indication of the fatigue life of these slabs. For example, the cracked zone at the first cycle of P110 is smaller than that of other slabs. Therefore, this slab needs more cycles to propagate additional cracked zones until fatigue failure occurs compared with the other slabs. Moreover, cracked elements at the first cycle were subjected to crack closing and opening processes more than those at the additional cycles. According to the bridging stress degradation equation, these cracked elements deteriorated more than the cracked elements at later cycles with an increasing number of cycles. Therefore, P190, which shows the largest cracked zone at the first cycle, deteriorated more quickly than the other slabs.

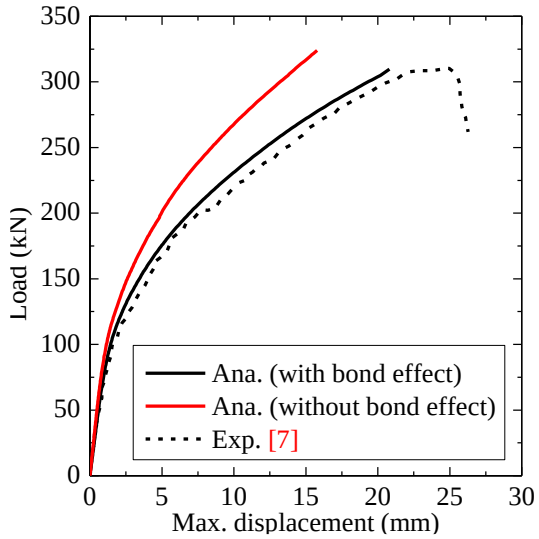

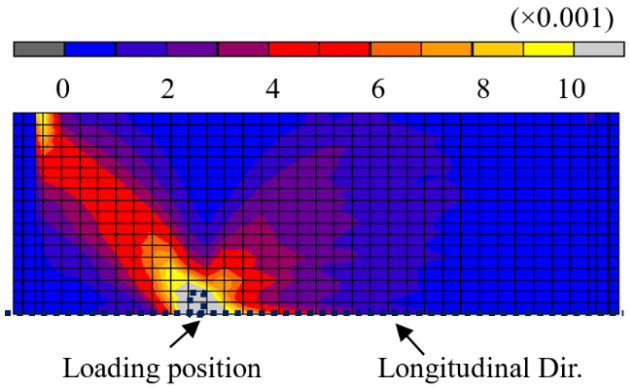

Fig. 4.3 Maximum principal tensile strain on slab bottom surface at load equaling 309 kN

Fig. 4.4 Load-maximum displacement curves

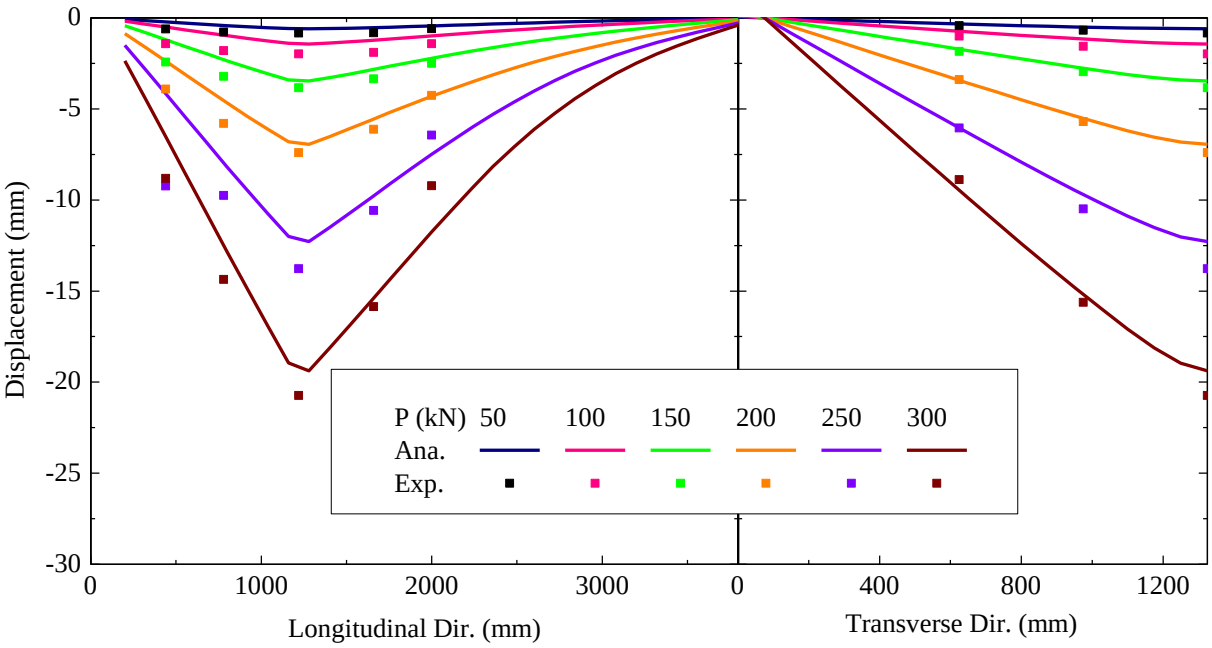

Fig. 4.5 Displacement distribution for longitudinal and transverse direction

According to the percentages of cracked elements volume in **Table 4.2**, the propagation of the cracked elements observed in D150 and P150 show that D150, which was reinforced with deformed bars, resulted in a slightly smaller cracked zone at the first cycle than P150, which was reinforced with plain bars. However, this observation is significant at the fatigue failure indicating a higher average degradation ratio for P150 than that of D150. The average degradation ratio is the ratio of the difference between the cracked elements volume at fatigue failure and 1st cycle by mm^3 to the fatigue life by cycles. The reason is that the bond effect between a plain bar and its surrounding concrete leads to larger slab deformations than that

between a deformed bar and its surrounding concrete. This leads to a higher maximum tensile strain, ε_{tmax}, for P150 than that of D150. According to the bridging stress degradation equation, the concrete bridging stress of P150 deteriorated more than that of D150 causing a larger cracked zone and a smaller fatigue life for P150. Shakushiro et al. [7] used the damaged area of the bottom slab surface to evaluate the fatigue failure. However, the cracked elements propagation in the thickness direction is consider as a primary factor for fatigue failure. Therefore, this study considers the percentage of cracked elements volume as a suitable comparison tool for these slabs.

For all slabs, the cracked elements are vertically propagated with an increasing number of cycles. At fatigue failure, the non-cracked zones are located at the top of the slab, until one-sixth of slab thickness. Therefore, a repetition of moving load leads to a decreasing of a compression zone. This approaches to an unequal sectional stress distribution resulting a fatigue failure.

4.3.2 Center displacement evolution

According to the previous section, the propagation of cracked elements and its degradation indicate that the RC slab stiffness decreases and slab center displacement increases as the number of cycles increases. The center displacement evolution versus the number of cycles for all slabs is compared with the experimental results in **Fig. 4.7**. The slab under a higher moving load level shows a larger slab center displacement than that under a lower moving load level due to the initial displacement at first cycle. In addition, at a higher moving load level, the center displacement evolution shows a larger slope than that at a lower moving load level. The reason is that the slab under a higher moving load level deteriorated more quickly than that at lower moving load level according to the average degradation ratio in **Table 4.2**. According to reinforcing bars modeling, the center displacement evolution of RC slab reinforced with deformed bars, D150, is smaller than that reinforced with plain bars, P150.

This figure shows the comparison of center displacement evolutions between the experimental and analytical results at different moving load levels. It reveals similar values for fatigue life and center displacement, indicating an acceptable agreement between them.

4.3.3 Fatigue life and S-N relationship

The fatigue life of RC slabs is described as a relationship between fatigue load ratio and the number of cycles to failure. The ratio of an applied moving load to the ultimate static load is considered as the fatigue load ratio, *S*. The S-N relationship of RC slabs under a moving load is plotted with the experimental results for verification as shown in **Fig. 4.8**. It suggests a good agreement between the analytical results of RC slabs and the fatigue life of those slabs from the experiment. Due to the propagation of cracked elements, the RC slab subjected to a higher fatigue load ratio shows a shorter fatigue life than that at a lower fatigue load ratio. The fatigue life of theses slabs is listed in **Table 4.3**.

4.3.4 Cracking patterns

To examine the crack locations in the numerical model, the cracking pattern on bottom surface of RC slabs under a moving load at fatigue failure is compared with the experimental results as shown in **Fig. 4.9**. For all slabs, the main crack started at its center, the first location of the moving load, thereafter extending to the supporting corners. As the load began to move, diagonal cracks formed between the locations of the moving load in the longitudinal direction

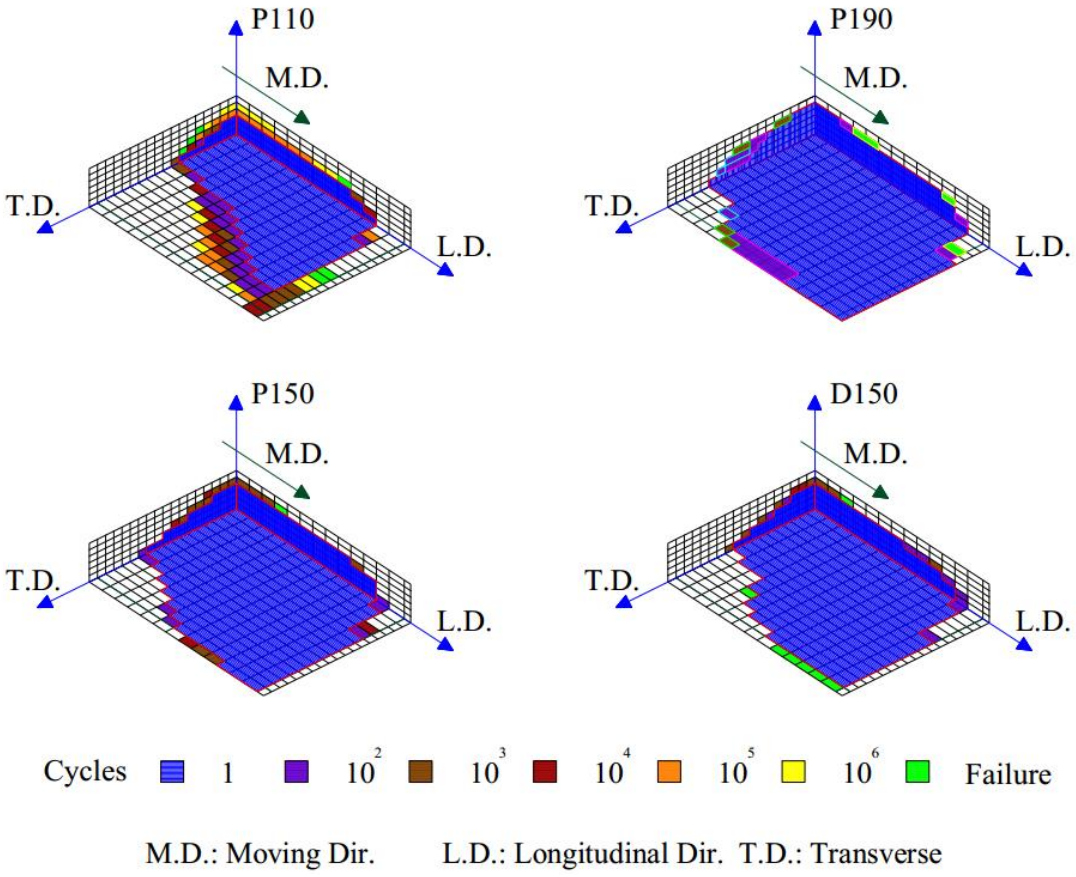

Fig. 4.6 Propagation of cracked elements

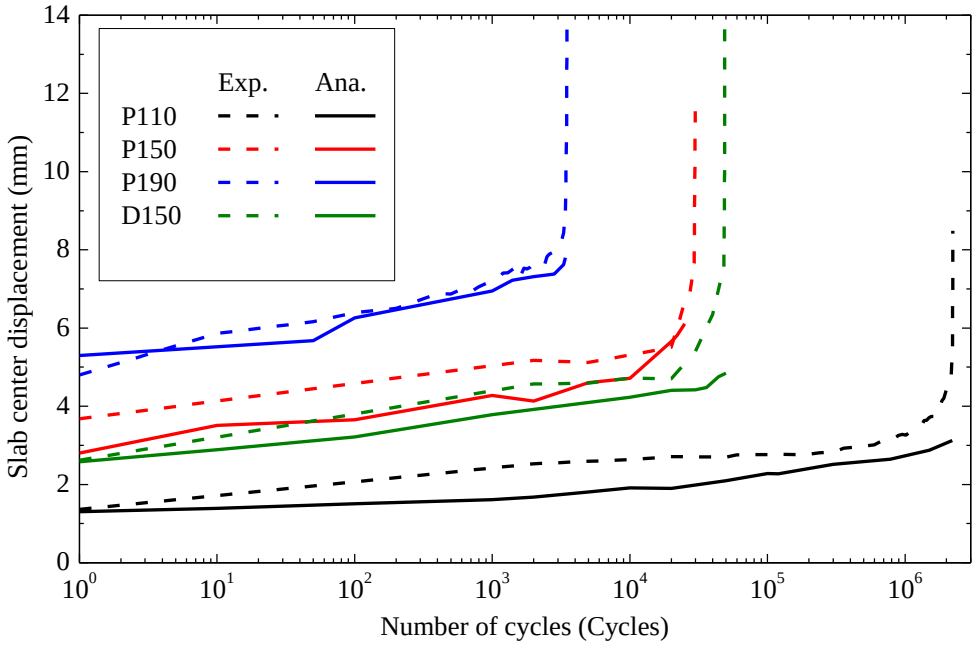

Fig. 4.7 Center displacement evolutions

Table 4.2 The percentage of the cracked elements volume

Slab ID	The cracked elements volume%		Average degradation ratio (mm^3/Cycle)
	1st cycle	Failure	
P110	12%	40.8%	91
P150	33.4%	59.1%	7070
P190	57.2%	68.6%	23456
D150	32.6%	51%	2575

Table 4.3 Fatigue life of RC slabs

Slab ID	Fatigue life (Cycles)	
	Numerical	Experimental [7]
P110	2,200,000	2,160,000
P150	25,500	29,350
P190	3,400	3,400
D150	50,000	48,916

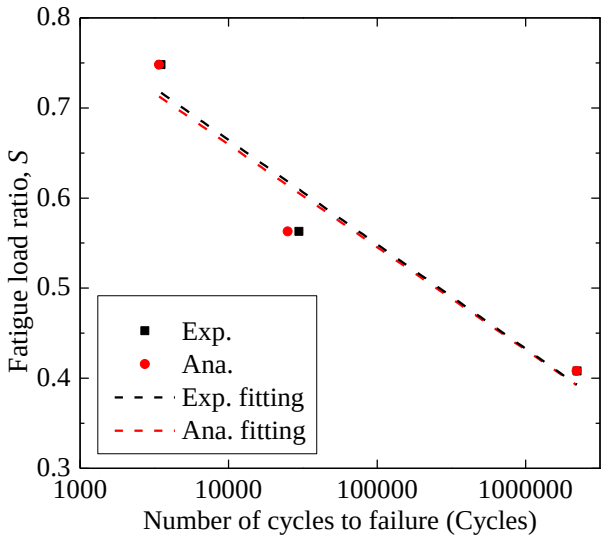

Fig. 4.8 S-N relationships for RC slabs reinforced with plain bars

and the supporting corner, making the first crack set. At the same time, other cracks formed perpendicular to the existing cracks as the second and third crack sets, surrounding the moving load zone to create an ellipse shape. An increase in the number of cycles resulted in much more extensive cracking.

As shown in **Fig. 4.9**, the effect of increasing the moving load level on the cracking pattern appears to be wide-ranging. The cracking pattern at fatigue failure contains an initial damage at the first cycle and accumulated damage by moving loading. The initial damage at the first cycle is influenced by moving load value. Moreover, applying higher moving load level leads to an increasing of maximum tensile strain, $\varepsilon_{t\max}$, in the bridging stress degradation equation. By increasing number of cycles, this leads to a significant bridging stress degradation and an increasing in degradation ratio as shown in **Table 4.2** resulting a wide-ranging in cracking pattern. An observation of the cracking patterns for P150 and D150 shows that the RC slab reinforced with plain bars suffered more broad-distribution cracking than that reinforced with deformed bars. The reason is that the bond effect between a plain bar and its surrounding concrete leads to a greater principal strain than that reinforced with deformed bars. However, the experimental cracking pattern for the RC slab reinforced with deformed bars shows an extensive cracking than that reinforced with plain bars. The reason is that the crack spacing of the RC slab reinforced with deformed bars is smaller than that reinforced with plain bars due to its shorter bond-deterioration length. On the other hand, the numerical crack spacing is controlled by the element size. Therefore, this observation cannot be detected in the numerical results. All cracking patterns and cracked elements distribution in the transverse direction suggest that these slabs failed with the punching shear mode around the moving area. This failure mode can be observed in the experiments. According to this observation, numerical cracking patterns show a good agreement with the experiments.

4.3.5 Fatigue failure mechanism

To demonstrate the fatigue failure mechanism, the maximum principal strain distribution on bottom surface and inner cracking pattern at fatigue failure in transverse direction are shown in **Fig. 4.10**. The reason of choosing transverse direction is that the strain concentration can be clearly observed in this direction than that in longitudinal direction due to the effect of moving load direction. In this figure, the maximum principal strain can be considered as an indication of the crack opening. For all slabs, a repetition of moving load leads to an increase of tensile strain. This increasing is significant at the punching zone as shown in **Fig. 4.10**. The punching zone on bottom surface is assumed to be as a linear extension of loading zone with a slope equaling 45º. In other words, applying moving load leads to a significant increasing of crack opening in this zone. Therefore, the cracks are localized in the punching zone at fatigue failure. Moreover, the inner cracking pattern shows that the orientation of the distributed cracks in this zone almost equals to 45º. According to these observations, all slabs are failed as a punching shear failure. This agrees with the experimental results of the RC slabs under moving loading in Shakushiro et al. [7]. There are two reasons for strain concentration in the punching zone at fatigue failure. Firstly, the maximum tensile strain, $\varepsilon_{t\max}$, for the cracked elements in this zone at 1st cycle is larger than that in other elements. Secondly, the cracked elements in this zone suffered from a larger number of crack opening and closing process than other cracked elements. According to the bridging stress degradation equation, these two factors lead to a significant concrete bridging degradation in this zone.

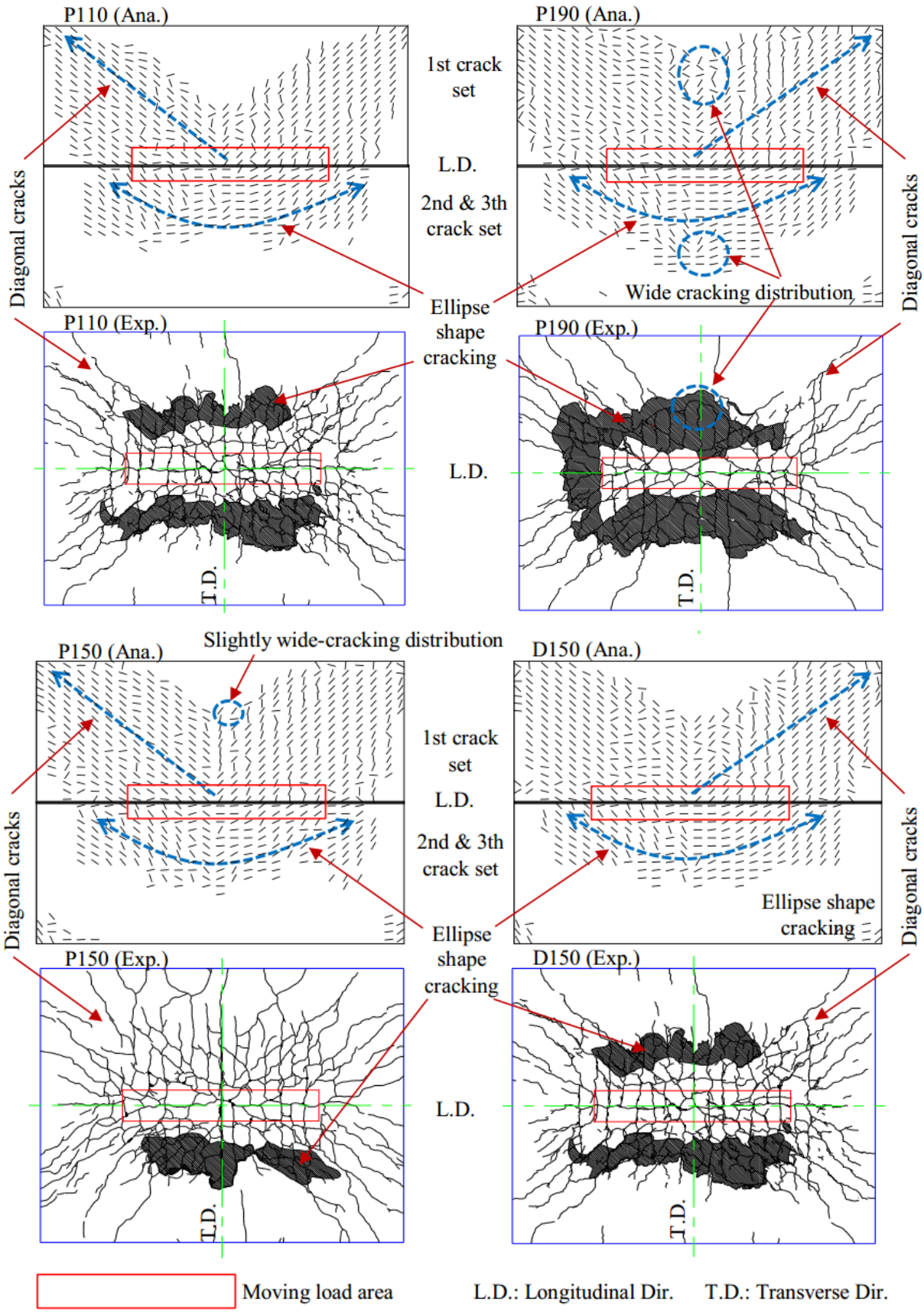

Fig. 4.9 Cracking patterns on bottom surface for analytical and experimental RC slabs at fatigue failure

4.3.6 Reinforcing bar strain

It is important to examine the behavior of plain bars under a moving load. To evaluate this numerical method, the strain evolutions of longitudinal and transverse lower rebar at slab center are compared with the experimental evolutions in **Fig. 4.11**. In all slabs, increasing number of cycles leads to an increasing of a rebar strain relatively. The reason is that the degradation of bridging stress of cracked elements with increasing number of cycles leads to an increasing of RC elements strain as shown in the bridging stress degradation equation. This numerical procedure simulates the cracks opening due to a repetitive of the moving load. This increasing of rebar strain is significantly observed in the RC slab under a higher moving load level due to its rapid propagation of the cracked elements comparing with that under a lower moving load level. For P150 and P190, the reduction in rebar stiffness in the plastic range, characterized by pinched hysteretic loops, occurred with an increasing number of cycles based on the transition parameter, *R*, according to the equations **(2.36)** and **(2.37)**. This process leads to an additional increasing of rebar strain accordingly. Therefore, the transverse rebar strain of these slabs rises to the yield strain at the fatigue failure. According to the reinforcing bars arrangement and slab geometry in **Fig. 4.1 (b)**, the reinforcement ratio in transverse direction (shorter length) is larger than that in longitudinal direction. Therefore, the load is distributed more along the transverse direction than in the longitudinal direction due to a higher stiffness in the transverse direction. This leads to an increasing of the rebar strain in the transverse direction than that in the longitudinal direction at the same number of cycles.

For RC slabs reinforced with plain bars, the rebar strain is calculated by the multiplying numerical strain by the explicit, ε_y, to effective, ε_y^*, yield strain ratio as shown in **Fig. 2.11**. This reduction of the rebar strain simulates the slipping action between the plain bar and its surrounding concrete. According to the assumptions of rebar modeling in chapter 2, the explicit, ε_y, and effective, ε_y^*, yield strain of deformed bar are with the similar value. Therefore, there is no reduction of the deformed bar strain. This explanation proves the increasing of rebar strain of RC slab reinforced with deformed bars, D150, than that reinforced with plain bars, P150, at first cycle, even though these slabs show insignificant difference in their center displacement at first cycle. By increasing the number of cycles, P150 shows a quick increasing of its rebar strain than D150 in the longitudinal and transverse directions. The reason is that the cracked elements of P150 are rapidly propagated than D150 with an increasing number of cycles as shown in **Table 4.2**.

For P110 and D150, the numerical results show an agreement with the experimental ones. For other slabs, there is a difference between the numerical and experimental results. Numerical rebar strain increases with an increasing number of cycles. However, experimental rebar strain decreases with an increasing of number of cycles. The possible reason is that the experimental measurement of a rebar strain is influenced by crack locations. Moreover, at a higher fatigue load level, the widening of the main crack causes the shrinkage in the other cracks. This leads to the decreasing of rebar strain in the experiments.

Fig. 4.12 shows the comparison of longitudinal and transverse sectional strain distributions with the experimental distributions for P110, P150, P190 and D150 at a selected number of cycles, *N*, to the number of cycles to fatigue failure, N_f, giving the ratio 0.946, 0.985, 0.97 and 0.991, respectively. These ratios are chosen to avoid the overestimated strain values in the fatigue failure. This comparison shows a difference between the numerical and experimental strain distribution for P150 and P190. Other slabs shows some agreements for numerical results. The transverse direction shows a larger strain distribution than that in the longitudinal direction. In the longitudinal and transverse directions, the strain distribution of RC slab reinforced with

plain bars, P150, is a larger than that reinforced with deformed bars, D150, because this slab is degraded rapidly until the fatigue failure.

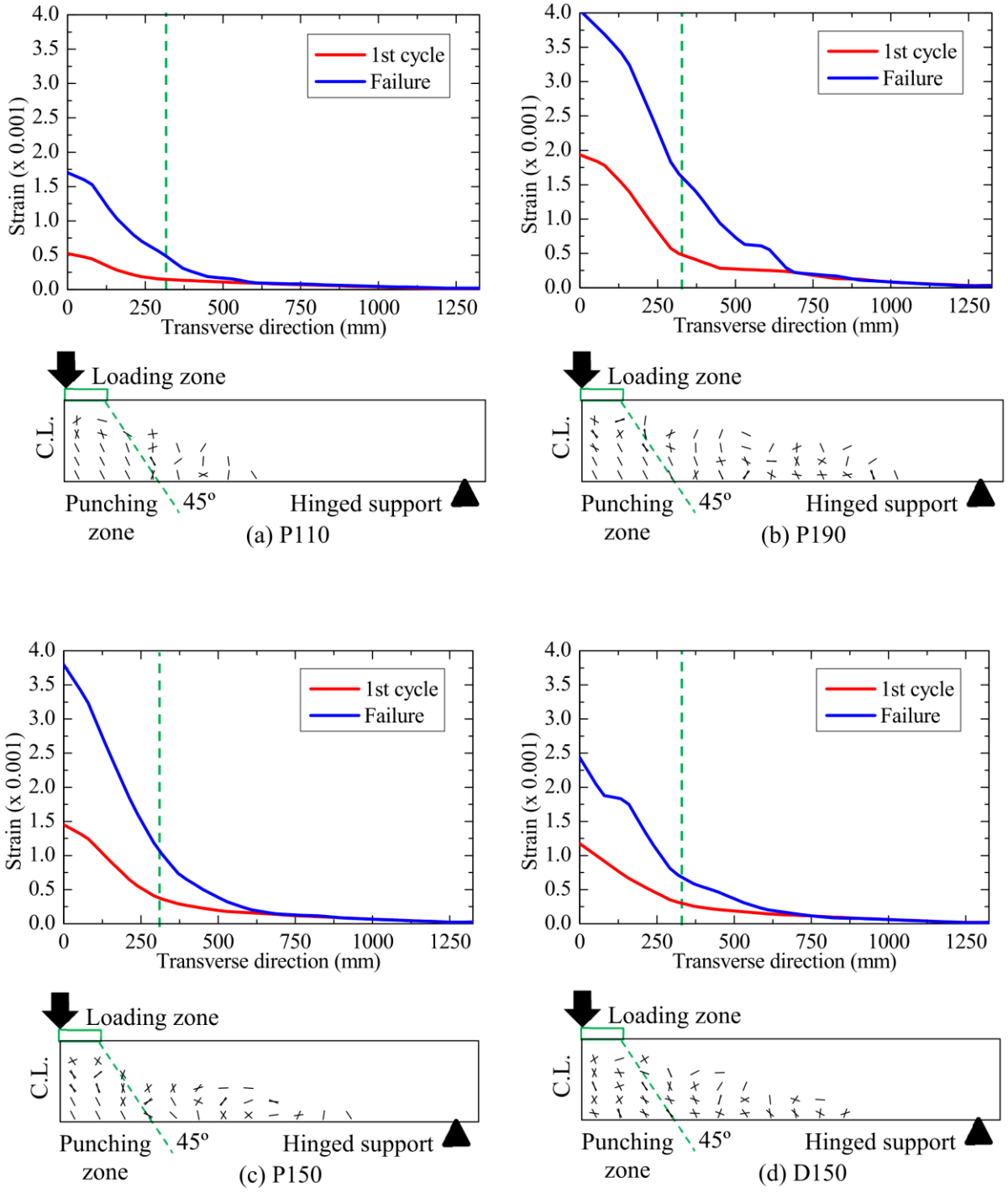

Fig. 4.10 Maximum principal strain distribution on bottom surface and inner cracking pattern at fatigue failure in transverse direction for RC slabs under moving load

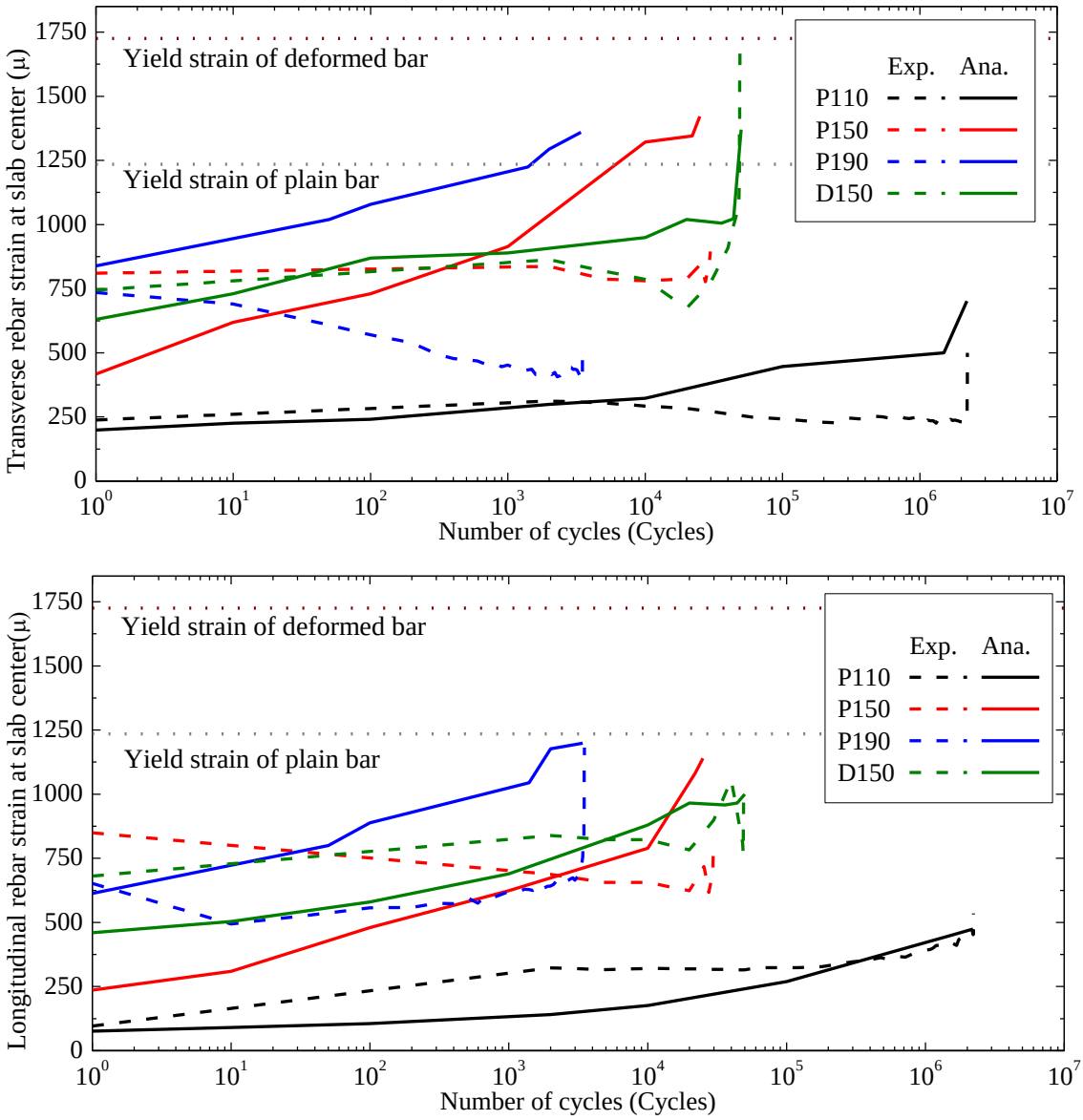

Fig. 4.11 Lower rebar strain evolution at the slab center

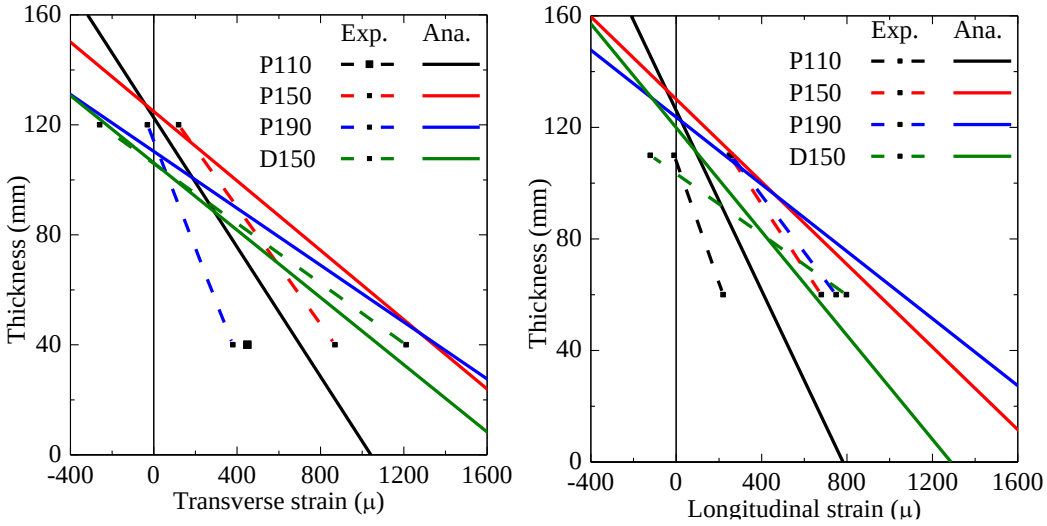

Fig. 4.12 Strain distribution at slab center

4.5 Summary and conclusions

This chapter showed a numerical analysis of RC slabs reinforced with plain bars under static and moving load to verify the proposed numerical method and predict the fatigue behaviors of these slabs.

For static analysis, RC slab reinforced with plain bars was analyzed to compare its numerical results with the experimental results by Shakushiro [34]. The modified reinforcing bar model according to the bond-slip effect between plain reinforcing bar and its surrounding concrete was incorporated in this numerical method. This effect can be briefly accounted for by adding equivalent bond strain to plain bar strain in smeared reinforced concrete elements.

The numerical results confirm that this effect leads to decrease the overall slab stiffens and increase its deformations. This observation is noticeable after the beginning of the cracking load. This proposed method presented an excellent agreement between the numerical and experimental results for the longitudinal and transverse displacement distributions and the load-maximum displacement relation.

For fatigue analysis, a numerical method based on the concrete bridging stress degradation concept was employed to cause the propagation of the cracked elements during increasing the number of cycles. Three RC slabs reinforced with plain bars were analyzed with the modified numerical method based on the bond-slip effect between plain reinforcing bar and its surrounding concrete under different moving load levels. One RC slab reinforced with deformed bars was analyzed with the prefect bond assumption between the reinforcing bar and its surrounding concrete. These slabs were compared with the experimental results of Shakushiro et al. [7] to verify this method.

According to the basis of this method, the propagation of cracked elements due to its bridging stress degradation is considered as the primary cause of fatigue failure. By increasing the number of cycles, the bridging stress degradation of these cracked elements leads to a decrease in slab stiffness and an increase in slab deformations. This degradation is significant in the punching zone indicating to a crack localization in this zone. This reveals that all analyzed RC slabs are failed with the punching shear mode.

Applying higher moving load level leads to a larger cracked zone and a higher degradation ratio. This results in a higher slab deformation and a shorter fatigue life.

The longitudinal and transverse reinforcing bar strain evolutions at slab center show that RC slab under higher moving load level leads to a higher strain with a higher curve slope due to its higher degradation ratio. There is a difference between these results and experimental ones. The possible reason is that the experimental measurement of reinforcing bar strain may be influenced by the location of the surrounded cracks.

To study the bond-slip effect of plain reinforcing bar and its surrounding concrete on the fatigue behaviors, the numerical comparison between RC slabs reinforced with plain and deformed bars was conducted in this chapter. RC slab reinforced with plain bars showed a higher average degradation ratio than that reinforced with deformed bars resulting a higher center displacement with a higher curve slope by increasing number of cycles. The proposed model of the bond-slip effect between plain reinforcing bar and its surrounding concrete leads to a significant increasing of cracks opening at the punching zone. This results in shorter fatigue life and higher strain for longitudinal and transverse reinforcing bar at slab center.

This numerical method was verified in this chapter by using the experimental results. The numerical results reveal and confirm a good agreement between the numerical analysis and the experimental results.

For RC slab reinforced with deformed bars, the bond between a deformed bar and its surrounding concrete is assumed to be perfect. Moreover, its bond degradation due to a repetitive loading is not considered. This leads to a smaller rebar strain evolution than the experimental one. Therefore, it is strongly recommended to consider the bond-slip effect and its degradation in the fatigue analysis. The modified steel bar model by Dehestani and Mousavi [17] can be used to simulate the bond-slip effect by adding an equivalent bond strain to reinforcing bar stress-strain relationship. For fatigue analysis, the increasing of slip displacement due to a repetitive loading can be calculated by the expressed function of the initial slip and number of cycles in Oh and Kim [35].

For RC slabs reinforced with plain bars, the bond-slip degradation effect between the reinforcing bar and its surrounding concrete is ignored in this method. Even though the reduction of rebar stiffness due to the bond-slip effect is considered as the major effect on the RC element behaviors at first cycle, the bond-slip degradation effect is required to obtain an accurate fatigue behavior. To simulate this degradation, the crack bridging degradation model for smooth fiber reinforced concrete by Zhang et al. [12] can be employed in the case of plain reinforcing bar. By using the material properties of used plain bar, the bond degradation equation can be integrated in this numerical method.

CHAPTER 5

FATIGUE ANALYSIS OF STRENGTHENED RC SLABS WITH FRP SHEETS

5.1 Introduction

RC slabs is considered as one of the most common structural systems. However, one of the major drawbacks of this system is its critical resistance to punching shear. In RC bridge, a slab is subjected to repetitive cyclic loading due to heavy traffic. Therefore, to increase their punching shear capacity and extended their fatigue life, a suitable strengthening technique is required such as externally bonded FRP sheets. Numerical simulation of FRP strengthening is a useful tool to predict its improvement.

This chapter presents a proposed numerical method based on bridging stress degradation concept to analyze three full scale RC slabs reinforced with plain bars under moving load. two of them are strengthened with externally bonded FRP sheets in longitudinal and transverse directions on the slab bottom surface. This numerical method considers the bond-slip effect between plain reinforcing bar and its surrounding concrete. For accurate numerical results, the interfacial bond behavior between FRP sheet and concrete surface with its degradation due to fatigue loading is also implemented. The propagation of cracked elements is used for updating the numerical model in further cycles until failure according to bridging stress degradation and the degradation of interfacial bond element.

The propagation of cracked elements, center displacement evolution, cracking pattern and FRP strain will be provided in this chapter. The verification of numerical results will be conducted using the experimental results.

5.2 Geometry and numerical model

Three slabs (S0, S330, S450) reinforced with plain bars are analyzed under repetitive moving load using the proposed numerical results. These slabs were simply supported over the transverse direction. In the longitudinal direction, these slabs were supported by two steel I-beam to simulate an elastic reaction behavior. **Fig. 5.1** shows slab geometry and reinforcement arrangement.

Slabs S330 and S450 are strengthened with externally bonded FRP sheets in longitudinal and transverse directions. The FRP sheets of two different spaces were externally bonded to the tension face of the slab in two perpendicular directions, parallel to the internal tension reinforcement. The details of the analyzed slabs are listed in **Table 5.1**. **Fig. 5.2** shows the numerical model of strengthened RC slabs.

The loading pattern and load levels are the same as those used in the experiments by Mitamura et al. [8]. Concrete was made using Hiroshi Portland cement, fine aggregate (5mm or less) and coarse aggregate (up to 20 mm). SR365 round steel was used for reinforcing the RC slabs. For FRP sheets, carbon FRP with width of 100 mm and thickness of 1.2 mm were used for strengthening. Epoxy resin adhesive was used to bond these sheets with the bottom surface of RC slab. **Table 5.2** shows the materials properties for concrete, reinforcing bar, FRP and adhesive material.

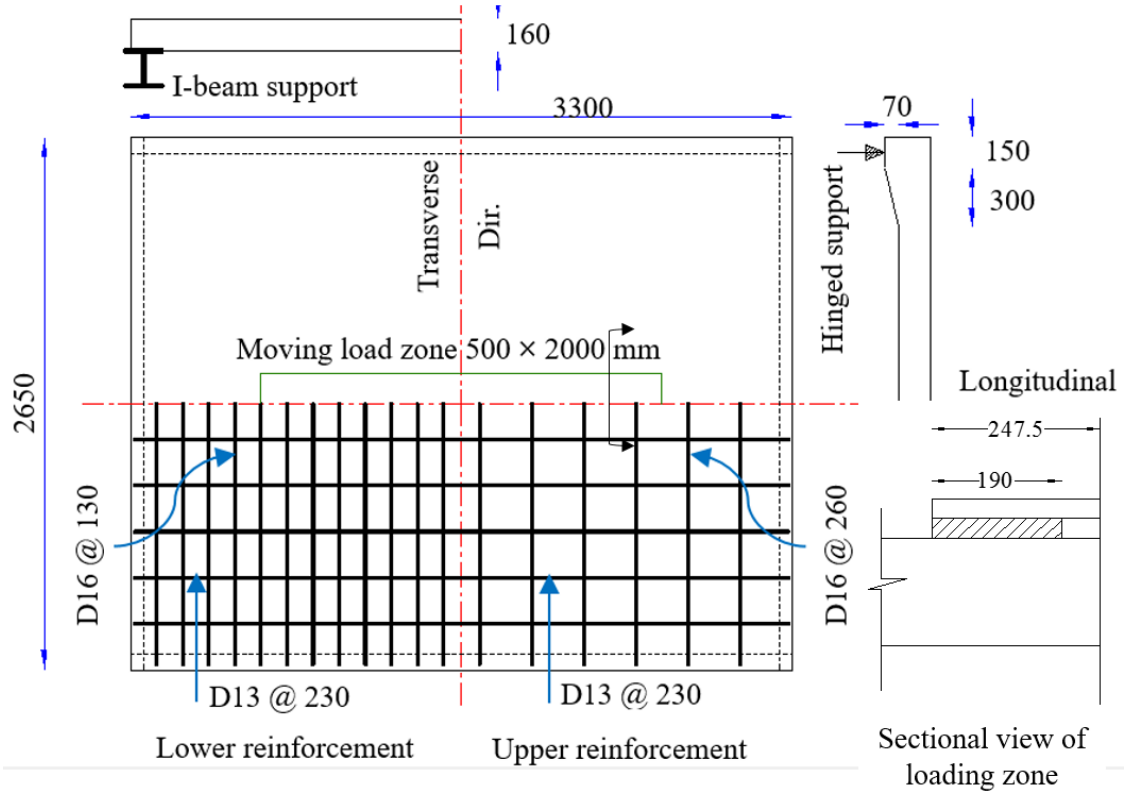

Fig. 5.1 RC slab geometry, upper and lower reinforcing bars arrangement (all dimensions in mm)

Table 5.1 Details of analyzed RC slabs

ID	Slab dimensions (mm)	FRP sheets			
		Width (mm)	Thickness (mm)	Longitudinal spacing (mm)	Transverse spacing (mm)
S0	3300 × 2650 × 160	Without strengthening			
S330		100	1.2	330	330
S450		100	1.2	450	400

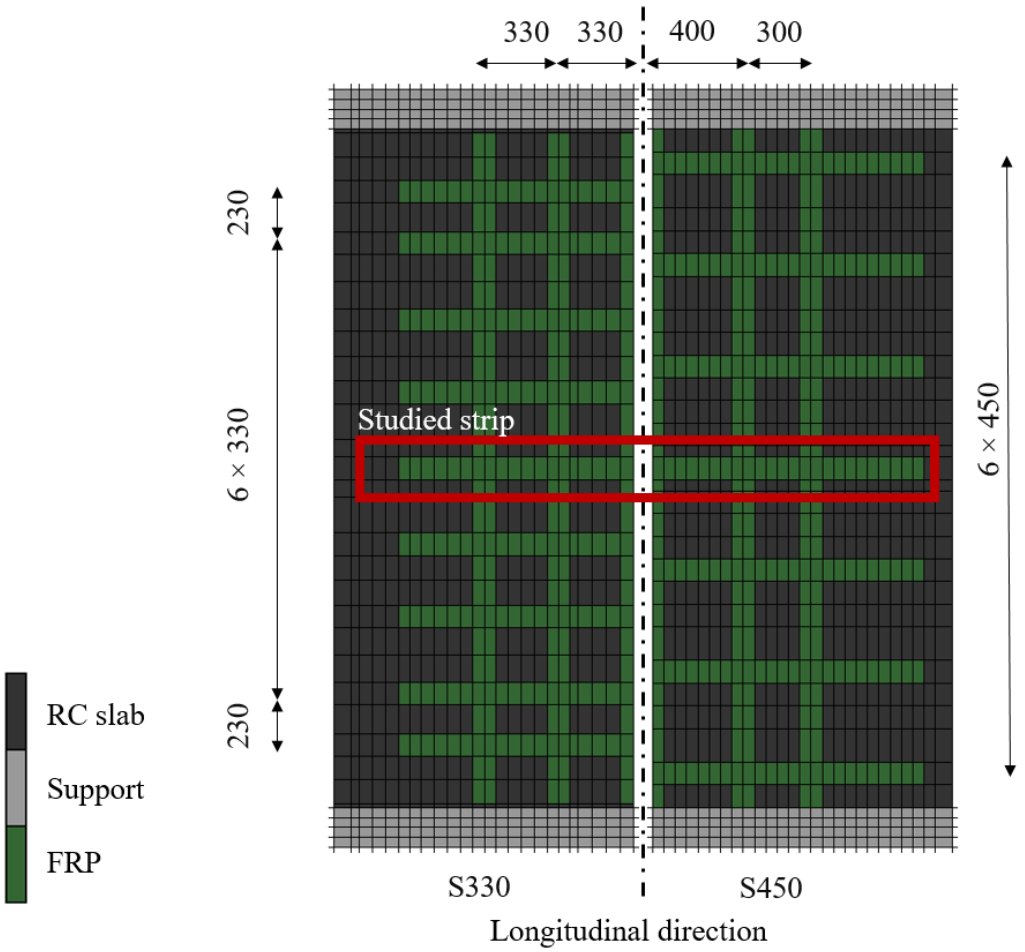

Fig. 5.2 FRP configuration (dimensions in mm)

Table 5.2 Materials properties [8]

Material	Young's modulus (GPa)	Poisson's ratio	Strength (MPa)	
			Tension	Compression
Concrete	26.133	0.2	3.3	45.26
Reinforcing steel bar	187	0.3	235 (Yield)	
FRP	171	0.3	3320 (Tensile)	
Adhesive	2.66	0.3	35	56

The measurements contain the applied load magnitude, displacement of the slab at slab center, and strain in the reinforcing bars and FRP sheets. The strain in the carbon FRP sheets was measured by strain gauges attached at midwidth of the sheets.

All slabs are analyzed under a moving load by two parallel wheels. This loading was simulated by moving a constant load level along the longitudinal direction as shown in **Fig. 5.1**. This load level is constant at every cycle and is applied as a surface load with contact area dimensions of 190 × 400 mm. The applied moving load starts at the center of slab elements following the moving path as shown in **Fig. 5.3**. The loading technique is the same as that in Chapter 4. After 100,000 cycles, the moving load level increases according to **Table 5.3**. The loading pattern for all slabs is shown in **Fig. 5.4**.

For fatigue analysis, the cracked elements were propagated with increasing number of cycles due to the degradation of their bridging stress as mentioned in the previous chapter, Chapter 4. At different moving load locations, the output-cracked elements were stored to be used in updating the numerical model for the next cycle step. Moreover, the output-cracked elements were updated before and after increasing the moving load level.

In other hand, RC slab without FRP strengthening, S0, and strengthened RC slab, S450, were analyzed under static loading to check the improvement of FRP strengthening on the ultimate static loading capacity. Static load was located at the center of the slab. A half of slab model was analyzed due to its symmetry in the longitudinal direction. The applied load was distributed on the area with dimensions of 200 x 190 mm. strengthened RC slab, S450, was analyzed considering two cases to evaluate a simplified isotropic material approach for FRP sheets as shown in **Fig. 5.5**. For first case, FRP elements was modeled as an isotropic material with linear stress-strain relationship. For second case, Orthotropic was used to define FRP sheets. In this case, Young's modulus of FRP and adhesive material were used for sheet-length and sheet-width directions as shown in **Fig. 5.5 (b)**.

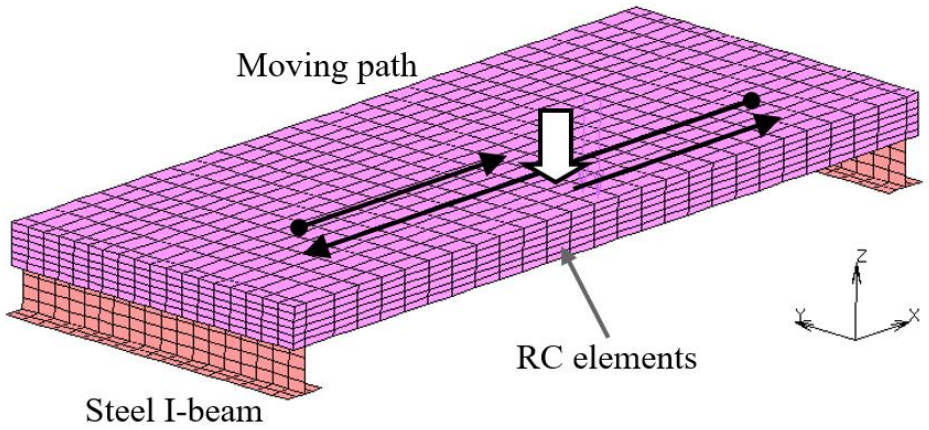

Fig. 5.3 Moving load path

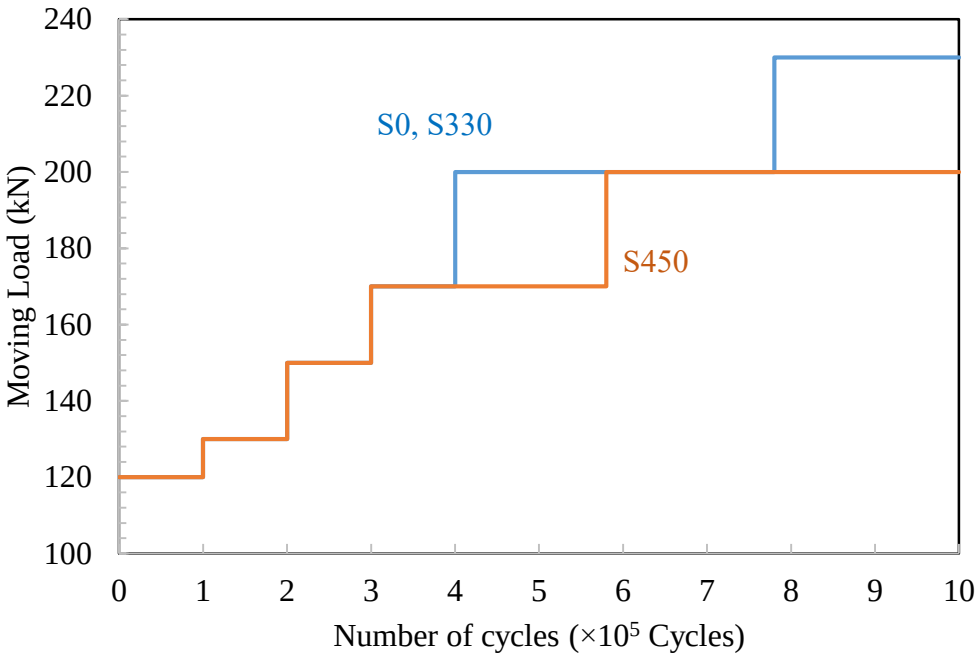

Fig. 5.4 Moving load pattern

Table 5.3 Applied moving load for all analyzed slabs

Moving load (kN)	Number of cycles (Cycles)	
	S0 and S330	S450
120	100,000	100,000
130	200,000	200,000
150	300,000	300,000
170	400,000	580,000
200	780,000	930,000

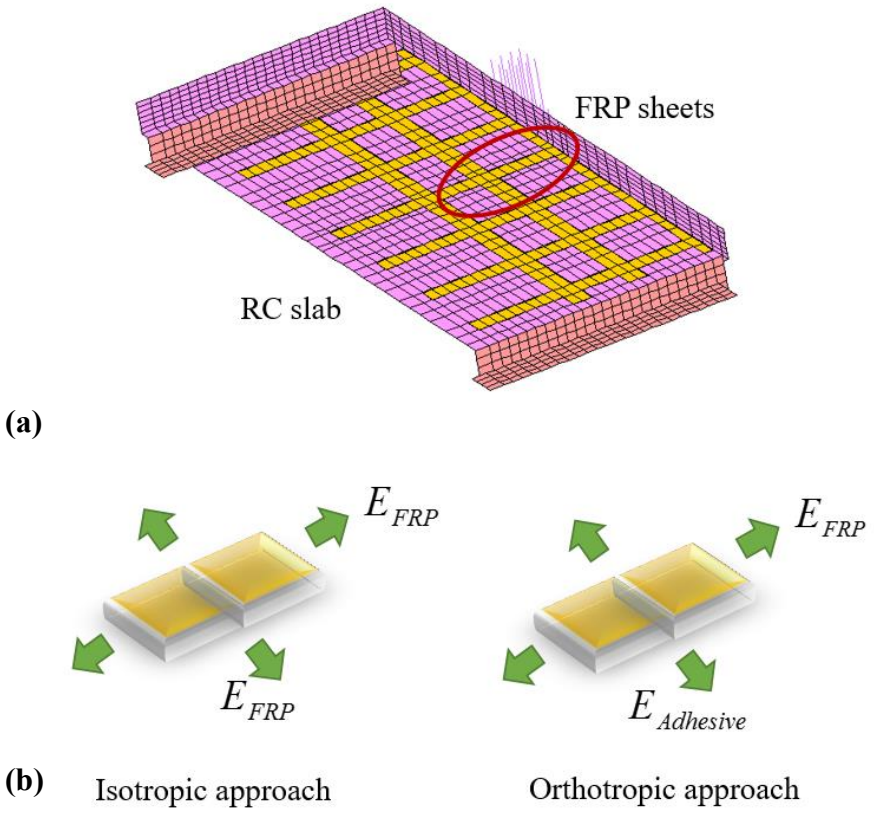

Fig. 5.5 (a) Strengthened RC slab **(b)** Isotropic and Orthotropic approaches

5.3 Static analysis results

Fig. 5.6 shows the load-center displacement relation for RC slab without strengthening, S0, and strengthened RC slab, S450. RC slab without strengthening shows a larger center displacement than that in the strengthened slab. Strengthened RC slab, S450, shows a significant improvement in slab strength and stiffens than that without strengthening, S0. The reason is that the FRP sheets works as an additional reinforcement to increase slab stiffens resulting a small deformation.

The improvement of FRP strengthening in strengthened RC slab, S450, is significant after cracking load due to restricting cracks opening by FRP sheets. For strengthened RC slab, the load-center displacement for isotropic and orthotropic approaches are shown in **Fig. 5.6**. Strengthened RC slab considered isotropic approach shows a slight higher stiffness than that considered orthotropic approach due to the effect of its higher stiffness in the width direction of FRP sheets.

Finally, according to the comparison between for isotropic and orthotropic approaches, modeling FRP sheets with isotropic approach is acceptable as a simplified method in the numerical analysis.

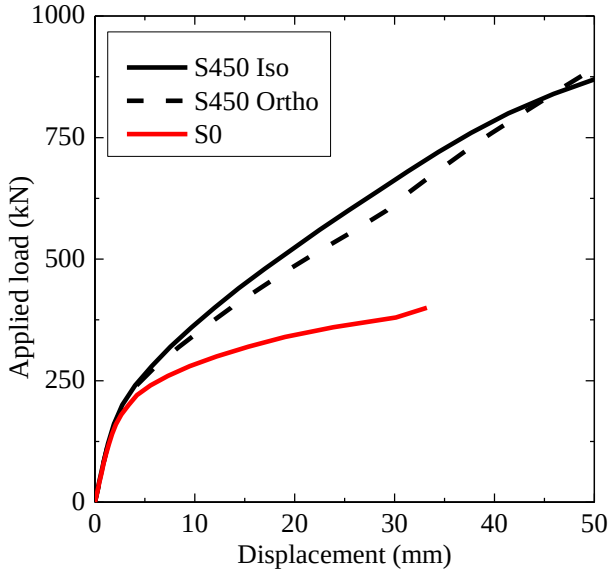

Fig. 5.6 Load-center displacement curves

5.4 Fatigue analysis results

This section presents the numerical fatigue results of al analyzed RC slabs, S0, S330 and S450. The following numerical results shows the propagation of cracked elements, center displacement evolution, cracking pattern, FRP strain and an explanation of fatigue failure mechanism.

5.4.1 Propagation of cracked elements

Fig. 5.7 shows the propagation of cracked elements of the RC slabs under a moving load at different numbers of cycles. This figure shows the one fourth of a slab model is shown due to the geometrical symmetry in both directions. The cracked zone caused by first cycle is indicated by blue. The cracked zones caused by further cycles are indicated by other colored elements. In the transverse direction (T.D.), the propagation of cracked elements is extended from the center of the loading area. For the longitudinal direction (L.D.), the cracked elements are distributed over the movement zone due to the movement effect of the applied load along the longitudinal direction.

To explain the effect of the FRP strengthening on the propagation of the cracked elements, the size of the cracked elements is observed in **Fig. 5.7**. At first cycle, strengthened RC slabs S330 and S450 show a smaller cracked zone than that in RC slab without strengthening, S0. Moreover, the thickness of the cracked zone of strengthened RC slabs is smaller than that in RC slab without strengthening. By increasing number of cycles, the cracked elements are propagated due to the bridging stress degradation.

Strengthened RC slab with larger sheets space, S450, shows a localized cracking propagation at strengthening zone. For strengthened RC slab with short sheets spaces, intensive FRP strengthening leads to a uniformly propagation of the cracked elements. The reason is that the concrete strain is effected by close FRP sheet strain.

Table 5.4 shows the percentages of cracked elements volume. RC slabs without strengthening, S0, shows a smaller percentage than other slabs at first cycles. These percentages are increased with increasing number of cycles. At fatigue failure, the percentages of cracked elements volume for all slabs are almost same.

The average degradation ratio can be defined as the ratio of the difference between the cracked elements volume at fatigue failure and first cycle by mm^3 to the fatigue life by cycles. The average degradation ratios for all analyzed slabs are listed in **Table 5.4**. RC slab without FRP strengthening shows a higher degradation ratio than those in strengthened RC slabs. The reason is that the FRP strengthening leads to restrict the crack opening resulting a decreasing of concrete tensile strain. According to equation (2.20), this leads to a significant decreasing of the bridging stress degradation.

5.4.2 Center displacement evolution

Fig. 5.8 shows the center displacement evolution versus the number of cycles for all slabs compared with the experimental results. According to propagation of cracked elements and its degradation, increasing number of cycles leads to a decreasing of slab stiffness and an increasing of its deformation. Therefore, center displacement is increased by increasing number of cycles.

Increasing moving load level leads to a significant increasing of concrete and rebar strain. This leads to a sharp increasing of center displacement at these load increases.

RC slabs without FRP strengthening, S0, shows a higher center displacement than those in the strengthened slabs, S330 and S450. The reason is that FRP strengthening leads to restrict the crack opening resulting a significant decreasing of slab strain and its deformations. Moreover, the center displacement evolution of RC slab without FRP strengthening, S0, shows a higher slope than those in strengthened RC slabs, S330 and S450. The main reason is that RC slab without FRP strengthening shows a higher degradation ratio than those in strengthened RC slabs as shown in **Table 5.4**.

For RC slab without FRP strengthening, the center displacement evaluations for first part, from 1 to 100,000 cycles, and last part, from 300,000 to 400,000 cycles, show a higher slope than other parts. The reason can be explained by the bridging stress degradation equations **(2.20)**. For the first part, the difference between logarithmic 100,000 and logarithmic 1 is larger than other parts. Therefore, the bridging stress degradation of this part is larger than other parts. For last part, the tensile strain, $\varepsilon_{t\max}$, rapidly increases before fatigue failure due to a significant increasing of major crack opening. According to the bridging stress degradation equations **(2.20)**, this leads to a decreasing of concrete tensile strength resulting a decreasing of slab stiffness.

This figure shows a good agreement between the experimental and numerical results for RC slab without FRP strengthening, S0. For strengthened RC slabs, there is an acceptable agreement between the experimental and numerical results at lower number of cycles. The difference between experimental and numerical results is significant at higher number of cycles. The reason can be explained as the following. The degradation of interfacial bond stiffness, E_b, according to equation **(2.46)** is assumed as a uniformly degradation for all interfacial bond elements according to the maximum bond stress rang, $\Delta\tau$. This leads to an increasing of the concrete strain at bottom surface resulting a larger displacement. This assumption not results an accurate displacement evolution. But, it is acceptable for predicating a fatigue life.

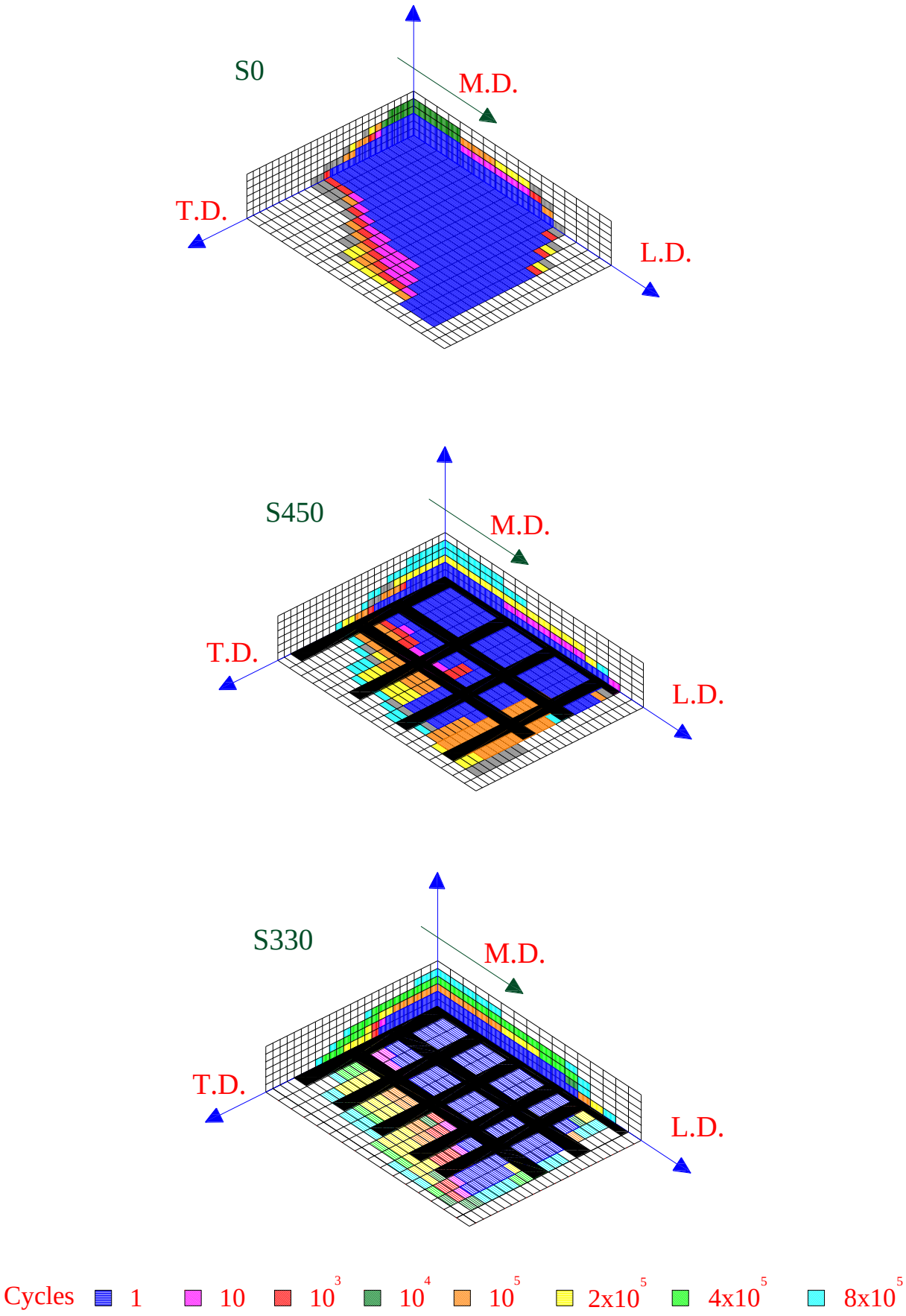

Fig. 5.7 Propagation of cracked elements for analyzed slabs

Table 5.4 The percentages of cracked elements volumes of analyzed slabs

Slab ID	Cracked elements volume %			Average degradation ratio (mm^3
	N = 1	N = 400,000	N = 900,000	
S0	22%	49.1%	———	9479.6
S450	8.33%	32.21%	41.6%	458.7
S330	10.7%	33.6%	50.5%	618.8

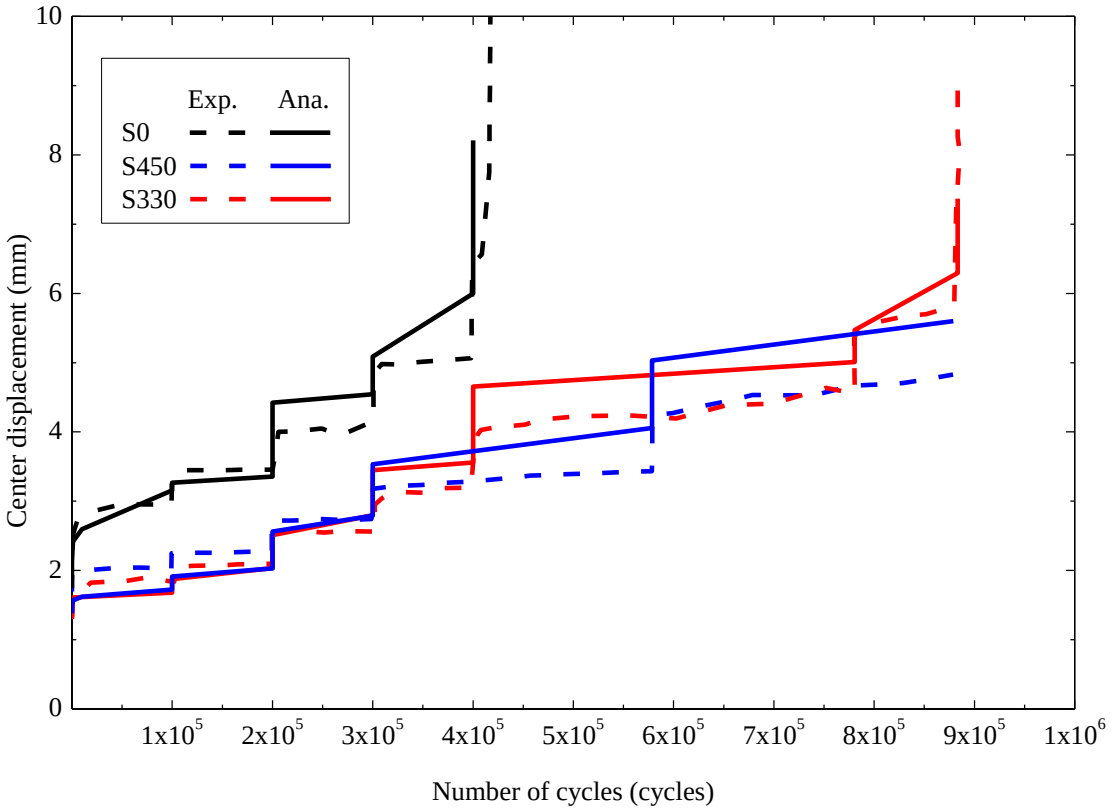

Fig. 5.8 Center displacement evolutions

The reason is that the fatigue life is mainly effected by the behavior of the major crack. In most cases, a maximum degradation of interfacial bond stiffness locates at the major crack. moreover, the predicting of fatigue life according to this assumption is expected to be slight shorter fatigue life.

5.4.3 Cracking pattern and strain distribution at fatigue failure

The cracking pattern on bottom surface of RC slabs without strengthening, S0, under a moving load at fatigue failure is compared with the experimental results as shown in **Fig.5.9 (a)**. This figure shows a half slab of experimental cracking pattern in the left side. In the right side, the numerical cracking pattern for first and second crack sets are shown respectively in the upper and lower slab quarter due to its geometrical symmetry in the longitudinal and transverse directions.

The major crack started at slab center, thereafter extending to the supporting corners. When the applied load starts to move in longitudinal direction, other diagonal cracks propagated between the moving load locations and the supporting corner. Hence, second crack sets are propagated perpendicularly to the existing cracks. Increasing number of cycles leads to cracks propagation and increasing of existing cracks opening due to bridging stress degradation of cracked concrete according to equation **(2.20)**.

According to **Fig. 5.8 (a)**, the ordination of numerical cracking pattern shows a similar angle to that in the experimental one. Therefore, there is an acceptable agreement between numerical and experimental results.

To examine the crack opening in the numerical model, the maximum principal strain distribution at fatigue failure on bottom surface of RC slab S0 is shown in **Fig. 5.9 (b)**. This figure shows only a half slab due to the symmetry in longitudinal direction. The maximum principal strain can be used as an indication for cracking width.

According to **Fig. 5.9 (b)**, the higher principal strain locates at the center of slab. This strain gradually decreases with closing to surrounding supports. According to experimental cracking pattern in **Fig. 5.9 (a)**, the larger cracking width locates at the major cracking which indicated by red line. This observation agrees with the numerical result of maximum principal strain distribution in **Fig. 5.9 (b)**.

According to previous explanation, applying moving load leads to propagate diagonal cracks. Increasing number of cycles results in an increasing of cracking width for major cracks. These major cracks are expected to be a primary reason of fatigue failure.

Fig. 5.10 shows the numerical and experimental cracking pattern for strengthened RC slabs, S450, at fatigue failure due to moving load. In the experimental results, the cracks are widely distributed than that without strengthening, S0. This observation is founded in the numerical cracking pattern which shows a widely cracked zone. The reason is that the fatigue life of strengthened RC slab, S450, is longer than that without strengthening, S0. This leads to propagates more cracks due to the effect of bridging stress degradation under higher number of cycles. Moreover, adding FRP sheets leads to increase the surrounding concrete strain due to its higher tensile strength. The cracks orientation and cracked zones are similar to that in experimental results. Therefore, there is an acceptable agreement between numerical and experimental cracking pattern.

In **Fig. 5.10**, the black colored area indicates to the debonding zone between FRP sheets and concrete surface. This figure shows that the debonding zones between the FRP sheets and concrete surface are effected with the location of the corresponded major cracks. The reason is that the cracking width of the major cracks is larger than that in other cracks. This results a separation in adhesive material due to its lower shear strength.

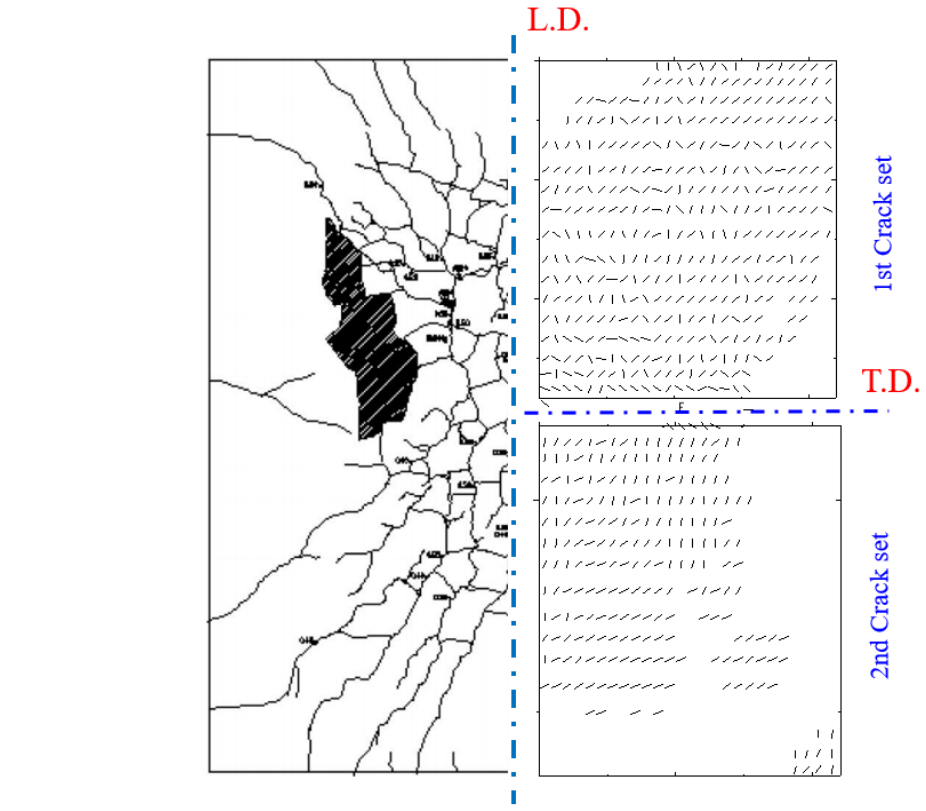

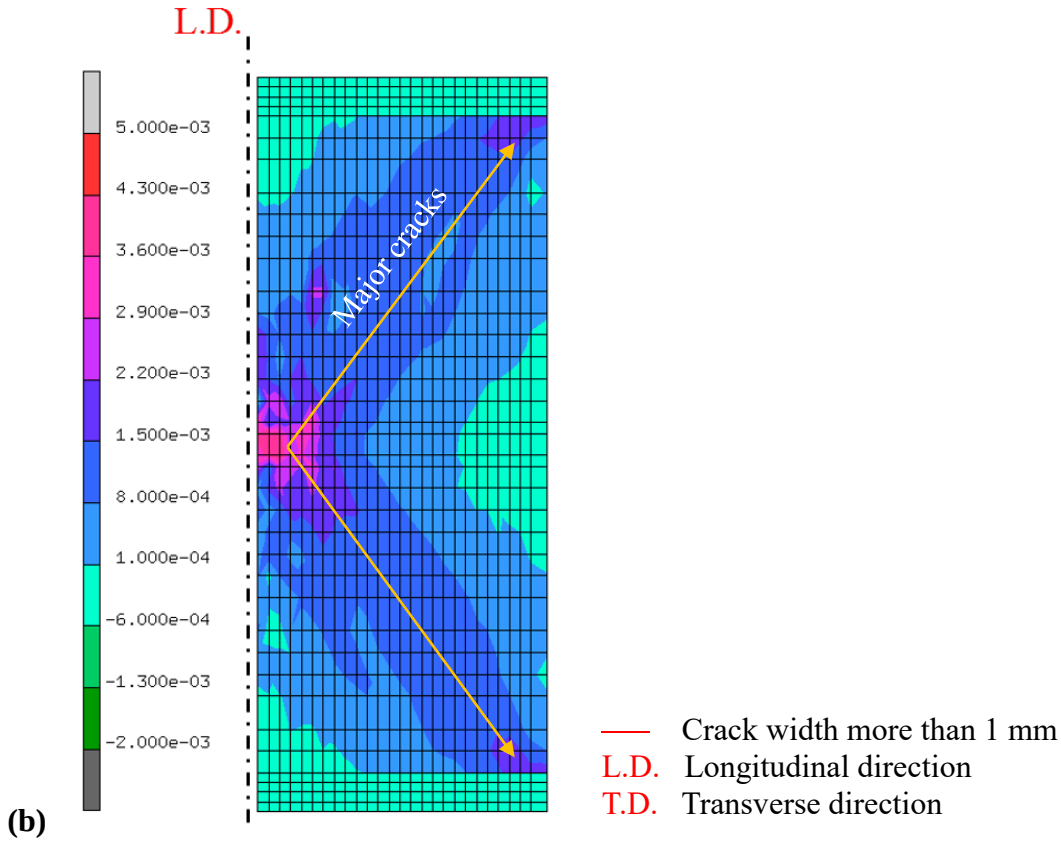

Fig. 5.9 (a) Numerical and experimental [8] cracking pattern **(b)** maximum principal strain distribution at fatigue failure for RC slab S0

The maximum principal strain distribution on bottom surface of strengthened RC slab, S450, at fatigue failure is shown in **Fig. 5.11 (a)**. The higher concrete strain locates at the major crack indicating a higher cracking width in this zone. Concrete strain distribution of strengthened RC slab, S450, is smaller than that in RC slab without strengthening, S0. The reason is that the FRP sheets works as an additional reinforcement. This leads to decrease the strain and stress of reinforced concrete elements. In other words, FRP strengthening leads decrease the major crack opening or maximum tensile strain. According to equation **(2.20)**, the decreasing of tensile strain of concrete leads to a decreasing of its bridging stress degradation. Therefore, FRP strengthening extend the RC slab fatigue life.

The shear strain distribution for interfacial bond elements at fatigue failure is shown in **Fig. 5.11 (b)**. Interfacial bond elements simulate the sliding behavior of adhesive material between the concrete surface and FRP sheets. According to the proprieties of interfacial bond element in Chapter 2, the initial debonding corresponds the shear strain equaling to 0.005.

In **Fig. 5.11 (b)**, there is no observed debonding zone in the numerical result of shear strain distribution of strengthened RC slab, S450. This observation is different than that in the experimental one. The possible reason is that the debonding is mainly effected by the cracking behavior. The smeared cracks element approach is used in this study to simulate the concrete behavior under tension. This approach assumes that the cracking width displacement will be uniformly distributed in the concrete element. Therefore, the maximum concrete strain of numerical result is smaller than that in the experimental one. This leads to decrease the possibility of interfacial debonding.

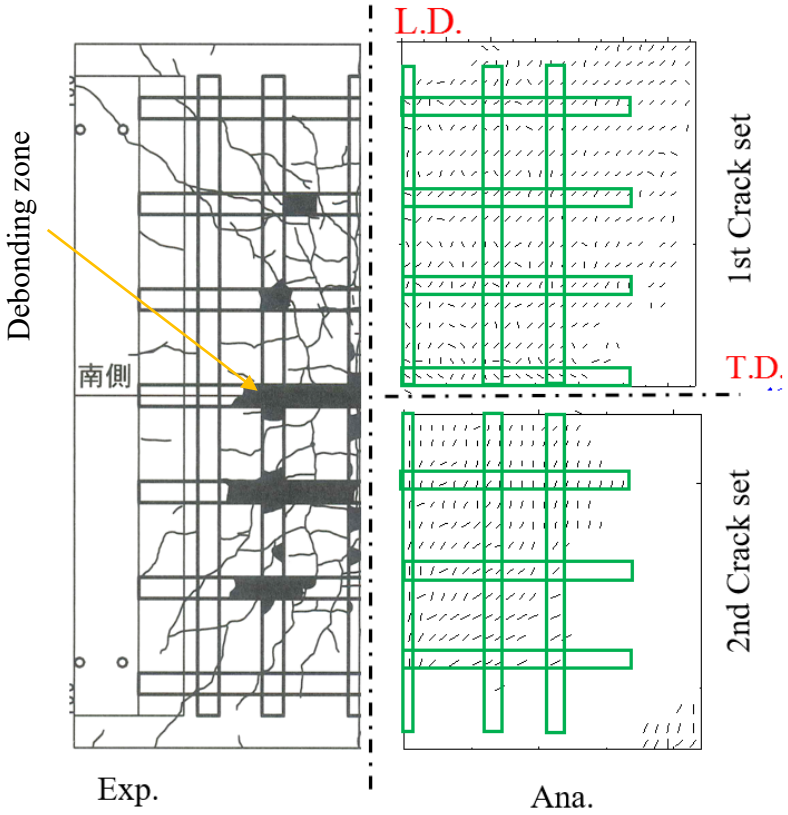

Fig. 5.10 Numerical and experimental [8] cracking pattern at fatigue failure for S450

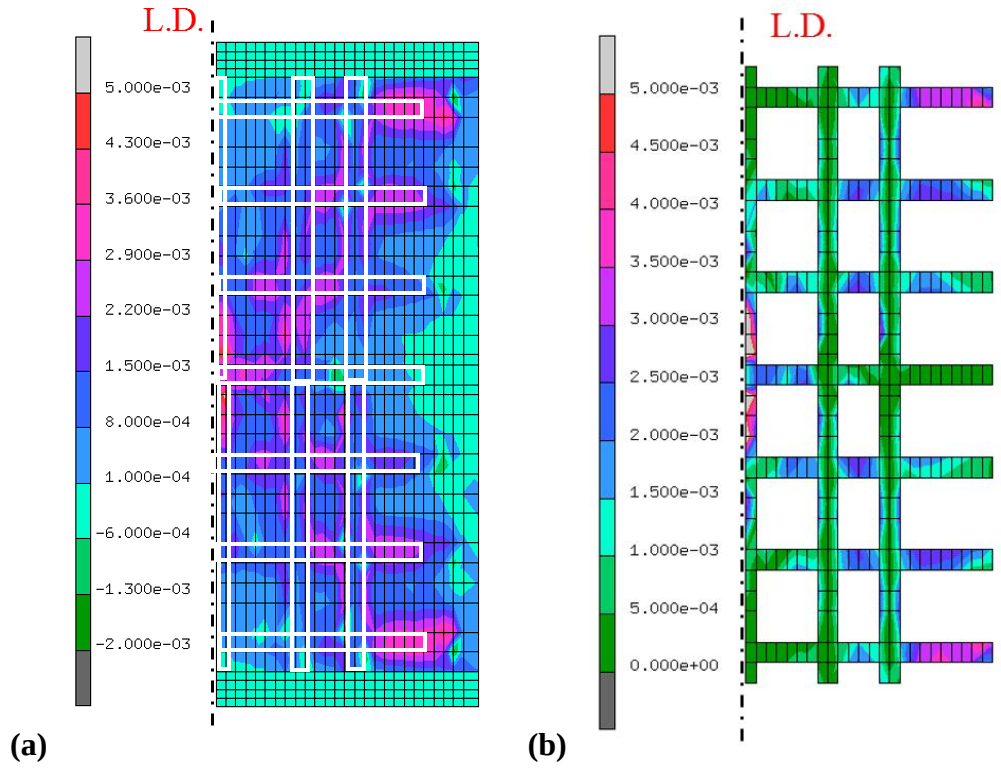

Fig. 5.11 (a) maximum principal strain distribution **(b)** Shear strain distribution for interfacial bond elements at fatigue failure for S450

The shear strain distribution of interracial bond elements in **Fig. 5.11 (b)** can be used as an indication of the debonding location between the concrete surface and FRP sheets. This figure shows that the higher shear strain is localized at the corresponded zone between FRP sheets and the major cracks. This observation agrees with the location of debonding zone in the experimental one in **Fig. 5.10**.

Fig. 5.12 shows numerical and experimental cracking pattern for strengthened RC slab, S330, with extensive FRP sheets at fatigue failure. The orientation of numerical cracking pattern is almost similar to the experimental one indicating an acceptable agreement. This figure shows an extensive cracking pattern with wide distribution. The reason is that the concrete strain is influenced by the surrounding FRP sheet strain. Therefore, strengthened RC slab with small-spacing FRP sheets shows a widely distribution of cracking pattern than that with larg-spacing FRP sheets due to its extensive-FRP-sheets strengthening. This observation can be also shown in numerical results for both slabs (S450 and S330).

For the cracking pattern of numerical and experimental strengthened RC slabs, the orientation of the distributed cracks is redirected at strengthened zones to be nearly perpendicular to the direction of FRP sheets. The reason is that the higher strain of FRP sheets leads to increase the horizontal component of concrete strain, which parallel to FRP sheets. This leads to redirect the principal stain direction resulting a changing orientation of crack orientation.

Fig. 5.13 (a) shows the principal strain distribution for strengthened RC slab, S330, of bottom concrete surface at fatigue failure. This figure shows that the higher strain distribution

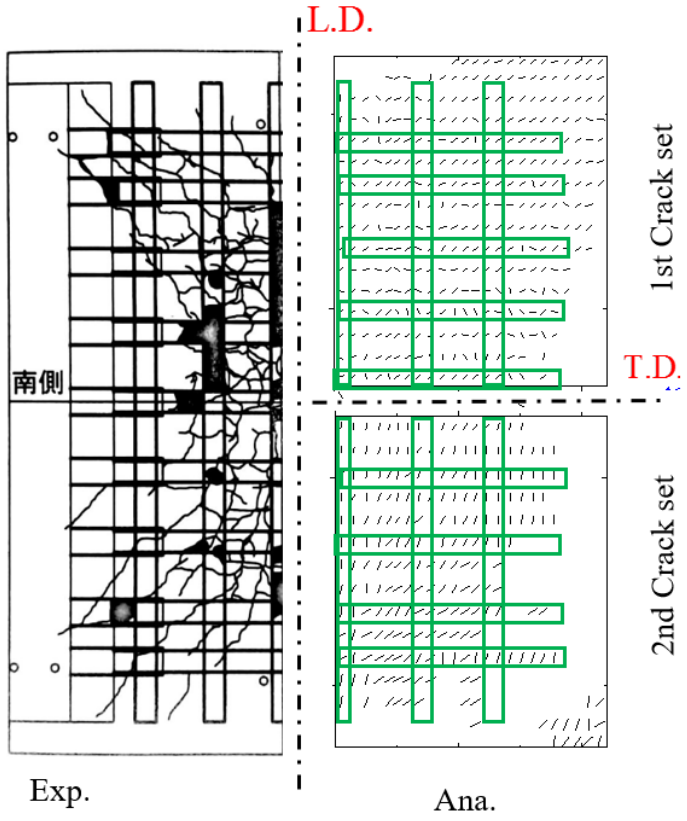

Fig. 5.12 Numerical and experimental [8] cracking pattern at fatigue failure for S330

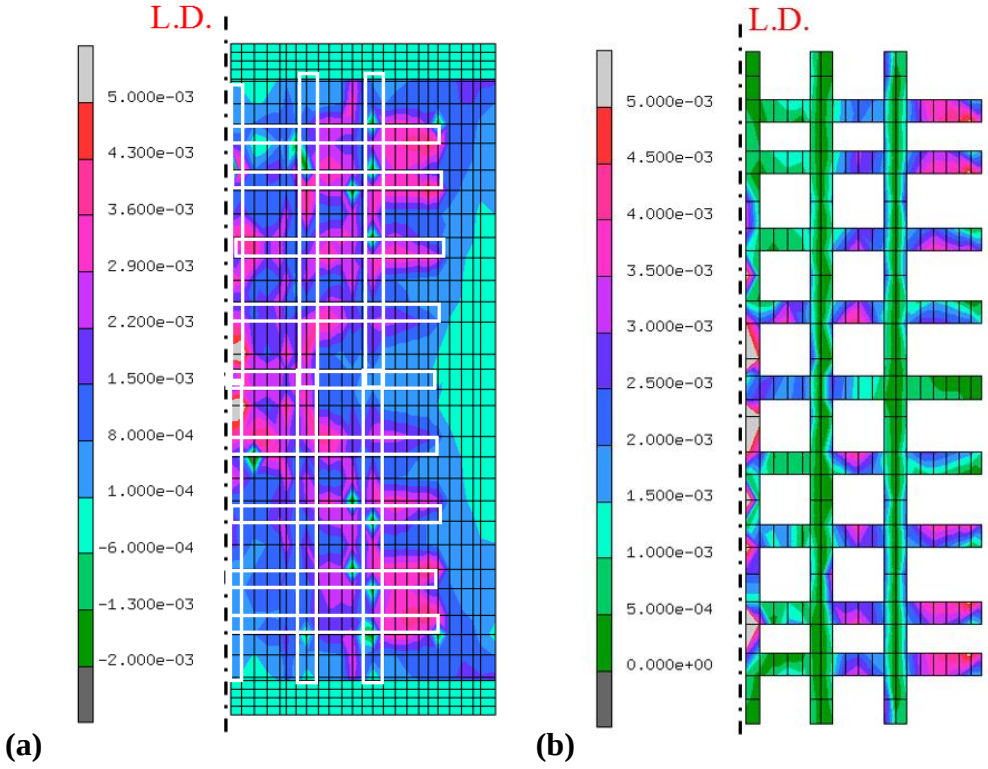

Fig. 5.13 (a) maximum principal strain distribution **(b)** Shear strain distribution for interfacial bond elements at fatigue failure for S330

is localized by the location of FRP sheets. Strengthening FRP sheets leads to increase the surrounding concrete zone. Moreover, strengthened RC slab with smaller sheet spacing, S330, shows a higher strain distribution at fatigue failure than that with larger sheet spacing, S450, due to the effect of higher strain of FRP sheets.

Fig. 5.13 (b) shows the shear strain distribution for interfacial bond elements at fatigue failure. The higher shear strain can be used as an indication for debonding behaviors. Higher shear strain locates at the location of major cracks. The reason is that the major cracks provides a larger cracking opening resulting a higher shear strain.

This figure shows that the shear strain distribution of strengthened RC slab s is significantly larger of than that with larger sheet spacing, S450, due to the effect of higher strain of FRP sheets.

5.4.4 Transverse FRP sheet strain

Fig. 5.14 and **5.15** show numerical and experimental transverse strain distribution of FRP sheet at slab center for strengthened RC slabs S330 and S450 at different moving load level, respectively. The horizontal axis shows the transverse length starting from slab center. The location of longitudinal FRP sheets is indicated by dashed-green box to observe their effect on the center transverse sheet.

The numerical and experimental maximum strain values locate at the loading position. Increasing moving load level leads to increase numerical and experimental FRP sheet strain. This increasing is significant at the punching zone than that other parts. The reason is that the bridging stress degradation of concrete is influenced by the maximum tensile strain, which locates in the punching zone. This leads to crack opening localization at slab center resulting a higher strain of surrounding FRP sheets.

According to these figures, strengthened RC slab with large spacing sheets, S450, shows a higher FRP sheet strain than that with smaller sheet spacing, S330, at same moving load level. The reason is that the tensile force of FRP sheet is influenced with its spacing. FRP sheets with large spacing needs to covers a larger area.

In the numerical results, transverse FRP strain shows a significant decreasing at overlapping location with the longitudinal sheets. The reason is that the tensile force in perpendicular sheet leads to strain shrinkage at overlapping location as shown in **Fig. 5.16**. Therefore, there a difference between the numerical and experimental results at overlapping location. This observation cannot be founded in the experimental results due to the effect of separated layers with different strain. In the numerical analysis, the overlapping element between longitudinal and transverse sheets sharing same strain distribution.

In other parts, the good agreement between numerical and experimental results is provided. Moreover, in the overlapping locations, the extension lines between numerical results pass the experimental results.

5.4.5 Fatigue behavior improvement due to FRP strengthening.

In this section, the improvement of fatigue behavior of strengthened RC slabs due FRP sheet is provided. The comparison of concrete strain for RC slab without strengthening and strengthened RC slabs is presented.

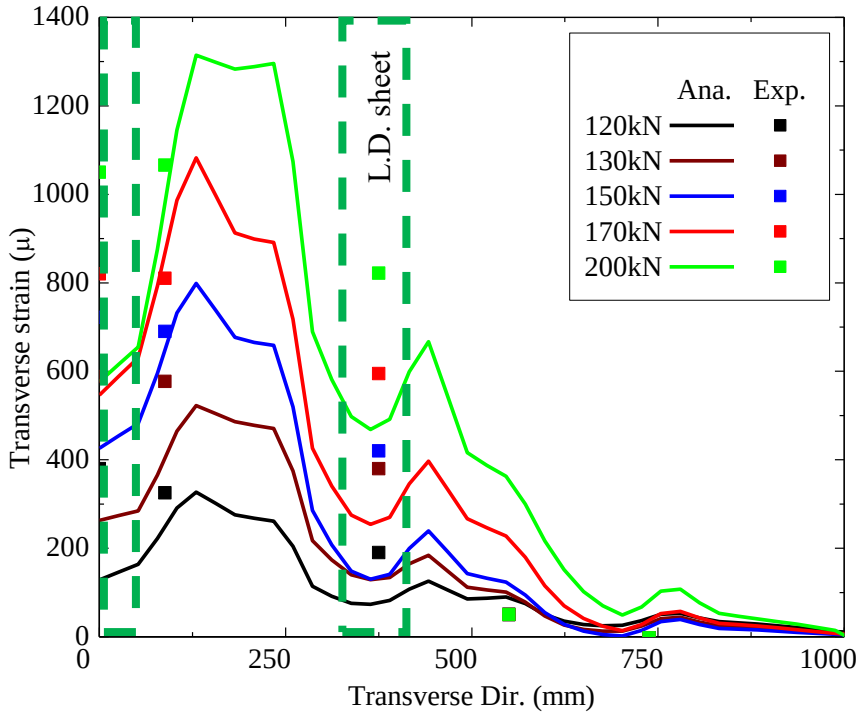

Fig. 5.14 Transverse FRP strain at slab center for S330

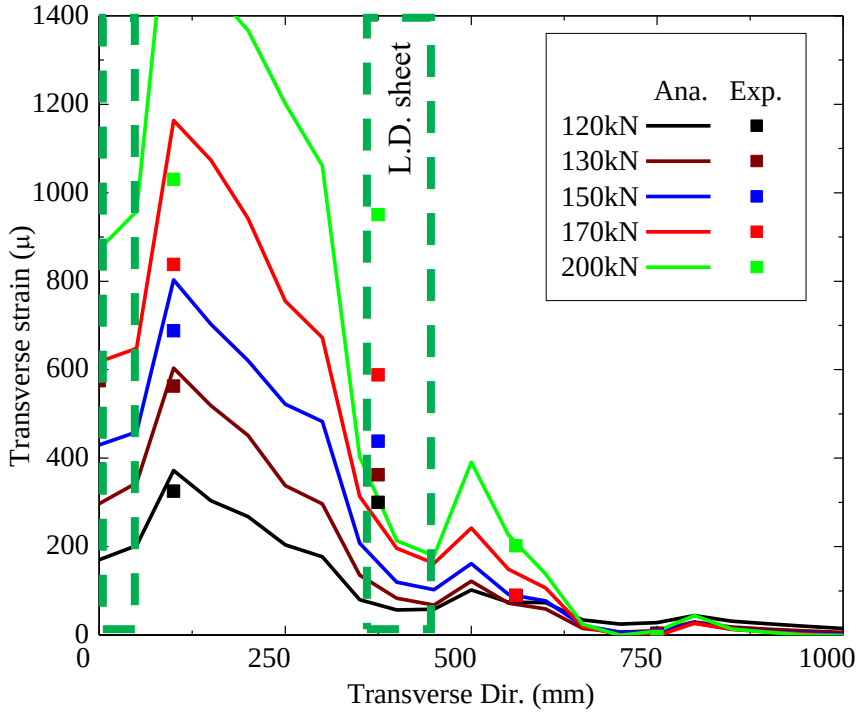

Fig. 5.15 Transverse FRP strain at slab center for S450

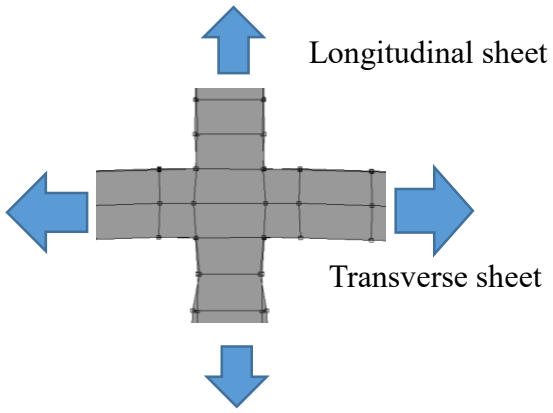

Fig. 5.16 Longitudinal and transverse FRP sheets overlapping

Fig. 5.17 shows the transverse strain distribution of concrete on the bottom slab surface at slab center for all analyzed slabs. RC slab without strengthening, S0, is indicated by black. Strengthened RC slabs S330 and S450 are indicated by red and blue, respectively. The cracking strain level is indicated by horizontal green line. Yellow vertical line indicates to the punching zone. The punching zone on bottom surface is assumed to be as a linear extension of loading zone with a slope equaling 1:1.

At first cycle (120kN), RC slab without strengthening, S0, shows a higher strain distribution than those in strengthened RC slabs at punching zone indicating a localized crack at this zone. By increasing number of cycles, RC slab without FRP strengthening, S0, shows a localized increasing in transverse strain at punching zone. Strengthened RC slabs, S330 and S450, show a smaller concrete strain at higher number of cycles than that without strengthening, S0, indicating to the improvement of FRP strengthening on the concrete strain. This improvement is significant at punching zone. In other part, Strengthened RC slabs shows a slightly larger concrete strain than that without strengthening due to the effect of higher FRP sheet strain for RC slabs S330 and S450.

According to previous explanation, FRP strengthening can extended the fatigue life of RC slabs under moving load by restricting the major cracks opening. This leads to decrease the maximum concrete strain, ε_{tmax}, in equation **(2.20)** resulting a smaller bridging stress degradation of cracked concrete than that without strengthening. Moreover, this strengthening type decreases the effect of crack opening localization due to the punching shear at fatigue failure.

To explain the improvement of FRP strengthening due to other transverse sheets, transverse strain of concrete at different sheets location is observed for strengthened RC slab, S450, as shown in **Fig. 5.18**. At the same section locations, concrete strain is present for RC slab without strengthening, S0, to check the improvement of these sheets on the concrete strain and crack opening. The locations of studied sections are indicated by red, blue and green as shown in **Fig. 5.18**.

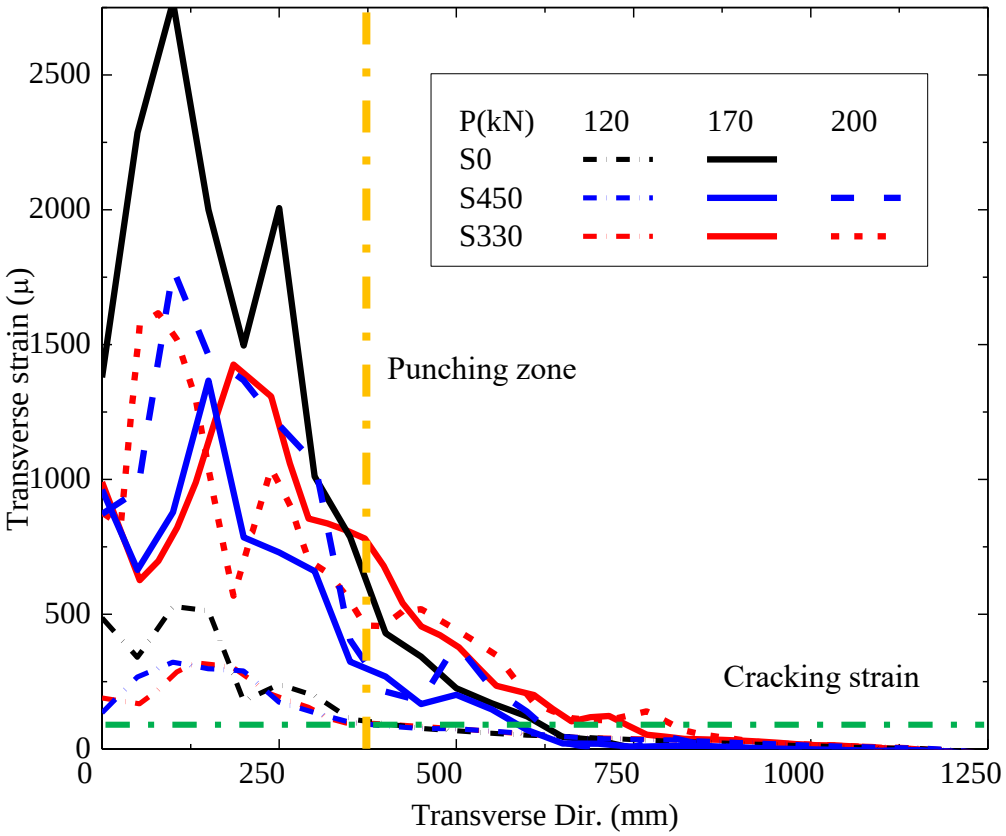

Fig. 5.17 Transverse strain distribution of concrete on the bottom slab surface at slab center

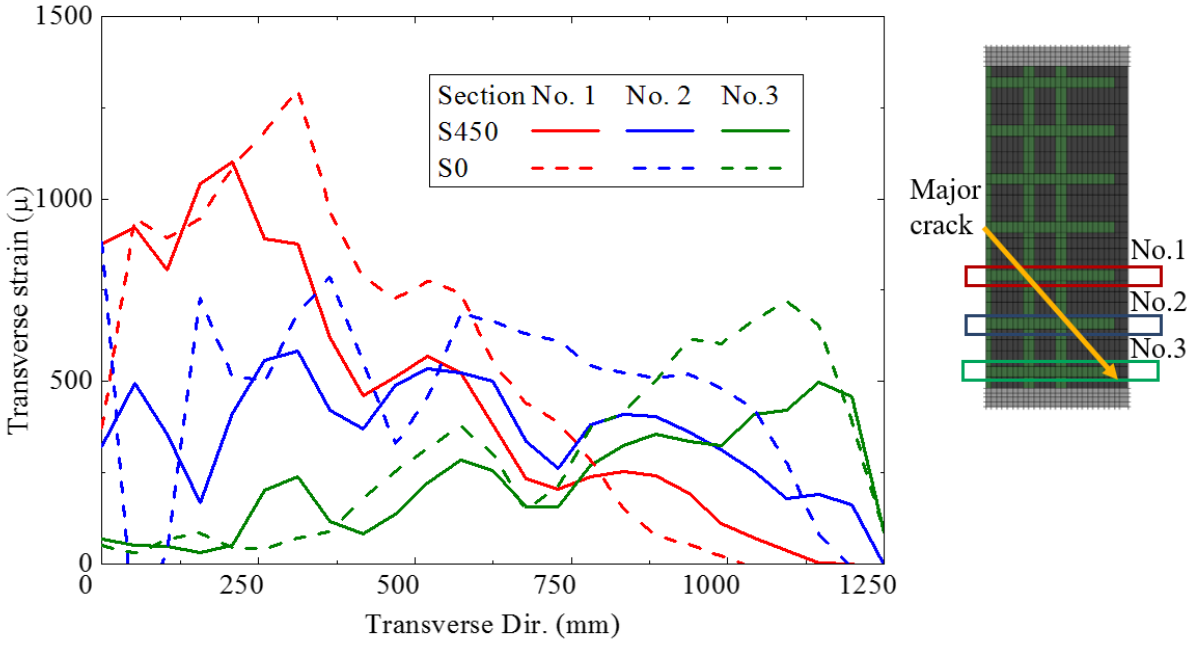

Fig. 5.18 Transverse strain distribution of concrete at different sheet location for S450 and S0 at fatigue failure

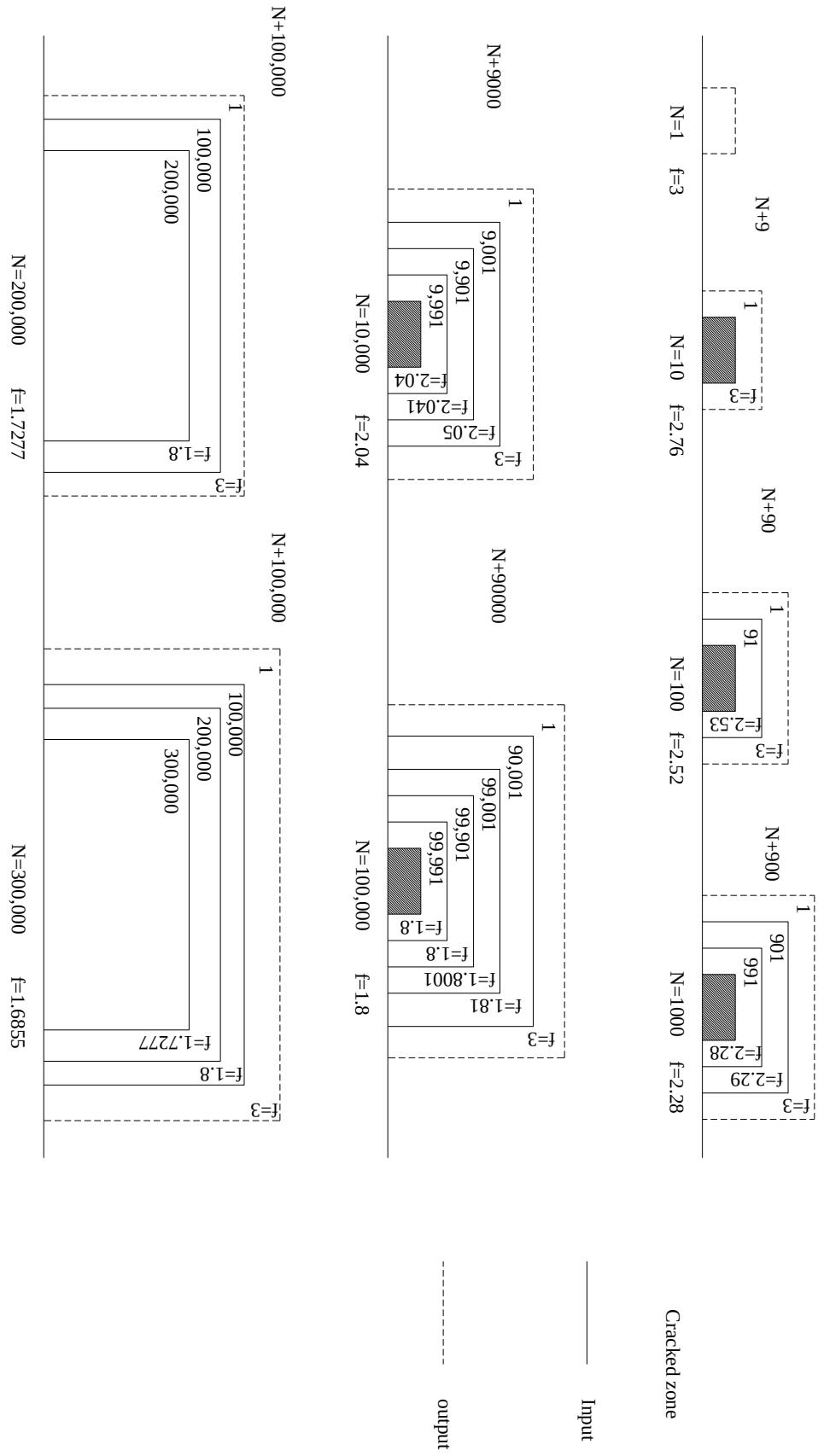

Fig. 5.19 Cracked zone propagation according to separated cracked zones concept for strengthened RC slab S450

At fatigue failure, RC slab without strengthening, S0, (which indicated by dash lines) shows a higher localized concrete strain at the location of major crack. The location of major crack for all sections can be shown in **Fig. 5.18**. For all sections, strengthened RC slab, S450, shows a smaller concrete strain than that without FRP strengthening, S0. This reduction of concrete strain is significant for the nearest section to the slab center.

According to this explanation, the improvement of FRP strengthening is significant at slab center due to its larger crack opening. FRP sheets can restrict this cracks to extended RC slab fatigue life.

5.5 The separated and uniform cracked zones on fatigue analysis

To study the effect of cracked zone separation on fatigue analysis, strengthened RC slab, S450, is analyzed using an FEM based on bridging stress degradation concept. This slab is analyzed according to two cases; uniform cracked zone concept and separated cracked zone concept. In the uniform cracked zone concept, the propagated and existing cracked elements are modified according to bridging stress degradation concept using a constant number of cycle equaling the older one. For the separated cracked zone concept, the propagated cracked elements are deteriorated by a different number of cycle than that in the existing cracked elements. The number of cycle of is related to its cracking age. The separation is started from the number of cycle equaling 100,000. The reason is that the effect of separated cracked zones can be neglected in logarithmic scale due to the small changes in the number of cycles. The separated cracked zone can be shown in **Fig. 5.19**.

Fig. 5.20 shows the center displacement elevation for numerical and experimental results. This figure shows that the separated and uniform cracked zone concepts provide almost same values. In other words, there is no difference between both concepts.

The reason can be explained as following. For number of cycles less than 100,000, the difference between concrete tensile strength in all cracked zones is very small. Therefore, the cracked zones can be used as a one cracked zone. For number of cycles larger than 100,000, the difference between concrete tensile strength in all cracked zones is significant. Therefore, the separated cracked zone is important to define as a different material. But, the oldest cracked zone (at 100,000) is very large comparing with other zones. So, the effect of these zones in the degradation calculation is very small. Moreover, the effect of the location of the oldest cracked zone on the slab stiffness is significant than that other zones.

Also, for plain concrete, the effect cracking tip is more important than that at cracking base. For reinforced concrete elements as a smeared reinforcement, the effect of the crack base is significant as shown in **Fig. 5.21**. Therefore, the influence of the bridging stress degradation on the oldest cracked zone is significant than that in the other propagated zones. Finally, the uniform cracked zones concept is acceptable in this loading case.

5.6 Conclusions and summary

This chapter presented a numerical analysis of FRP strengthened RC slabs reinforced with plain bars moving load to verify the proposed numerical method and predict the fatigue improvement of these slabs. One RC slab without strengthening and two strengthened RC slab were studied to present the effect of the FRP strengthening on fatigue behavior. The propagation of cracked elements, center displacement evolution, cracking pattern and FRP strain were provided in this study.

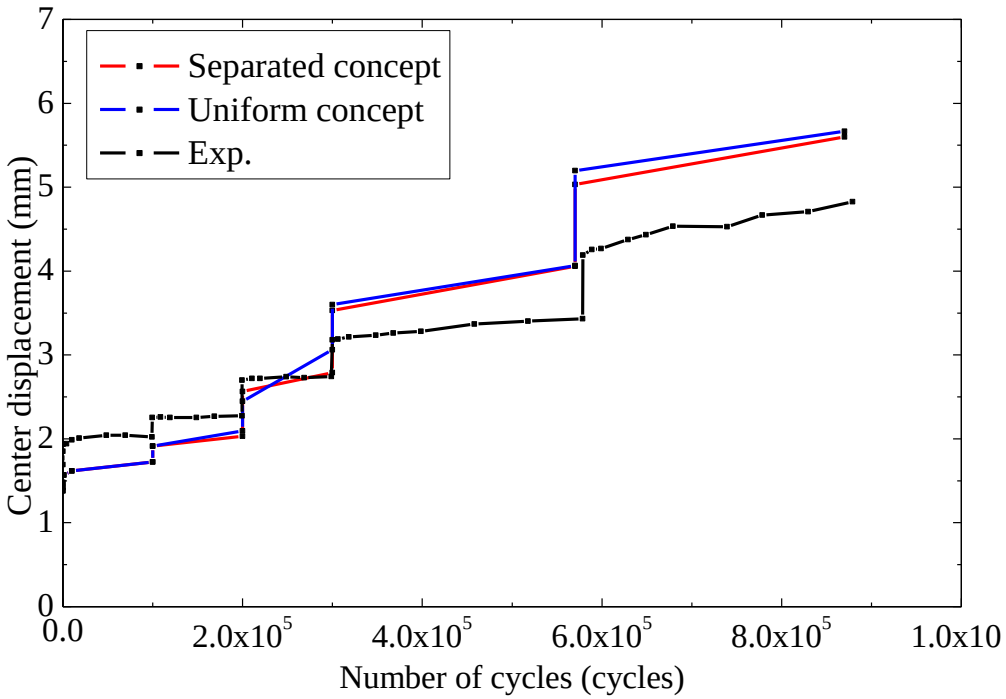

Fig. 5.20 Comparison between separated and uniform cracked zones concepts on the center displacement evolutions

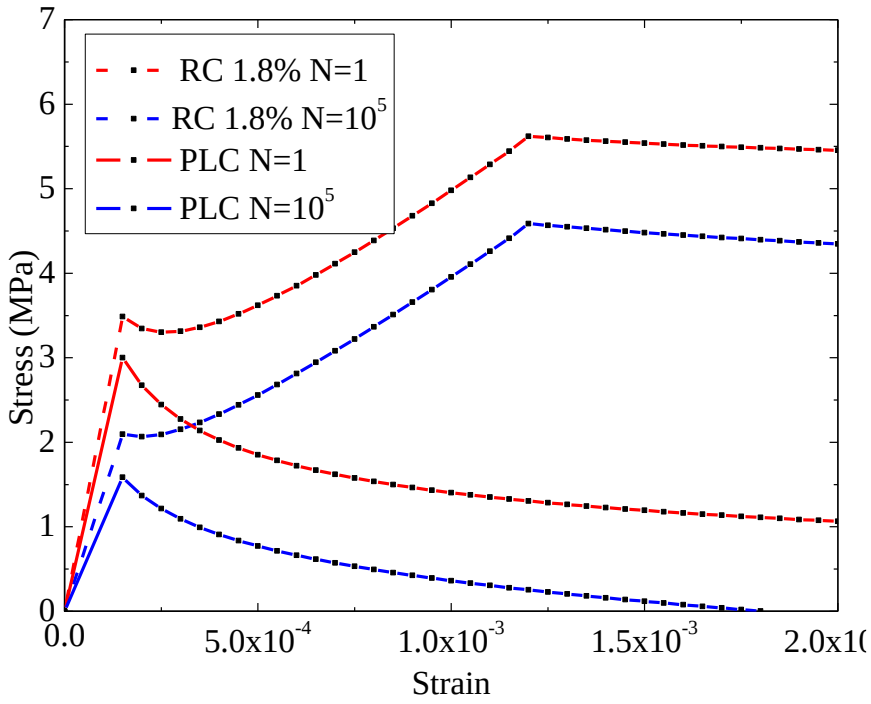

Fig. 5.21 Bridging stress degradation for plain and reinforced cracked concrete elements

Static analysis was conducted for RC slab without strengthening, S0, and strengthened RC slab, S450. Strengthened RC slab shows an improvement in the slab stiffens and ultimate static load. This improvement is significant after cracking load.

In strengthened RC slab, 450, FRP sheets was modeled by two approaches; simplified isotropic and orthotropic. Simplified isotropic provided acceptable results. Therefore, this approach can be used in the numerical analysis.

This study showed a numerical method based on bridging stress degradation concept to predict the fatigue behavior of strengthened RC slabs with FRP sheets under an increasing moving load.

The interfacial bond degradation between FRP sheets and its surrounding concrete due to fatigue load is considered. Moreover, the bond effect between plain reinforcing bars and its surrounding concrete was considered in this study.

This method showed a good agreement with the experimental results. Therefore, this method can be used to evaluate the improvement of FRP strengthening on the fatigue behavior of the existing RC slabs reinforced with plain bars.

This method assumed that the bridging stress degradation of major cracks is considered to be the primary cause of fatigue failure. For strengthened slabs, FRP sheets play an important role to restrict the crack opening of theses cracks. This leads to a smaller degradation ratio, a longer fatigue life and a smaller deformation.

At fatigue failure, FRP sheets leads to widely cracking distribution. Moreover, the orientation of distributed cracks was redirected to be almost perpendicular to the direction of FRP sheets. The reason is that FRP sheets leads to increase concrete strain in the sheet direction due to its higher strain.

Extensive FRP strengthening at slab center is predicable to provide a longer fatigue life. The major crack opening in slab center is larger than other zone.

To study the effect of cracked zone separation on fatigue analysis, strengthened RC slab, S450, is analyzed according to two cases; uniform cracked zone concept and separated cracked zone concept. According to the results, the uniform cracked zones concept is acceptable in this loading case.

To reach an optimum design of FRP strengthening for RC slabs under a moving load, the parametric study is required to show the effect of the following parameters on the fatigue behavior.

A. Sheet thickness.

B. Sheet spacing.

C. Sheet width.

CHAPTER 6

CONCLUSIONS AND FUTURE WORKS

6.1 Major conclusions

This study presented a new proposed numerical method based on bridging stress degradation concept for 3D fatigue analysis to predict the fatigue behaviors of RC slabs reinforced with plain bars under a moving load. A numerical analysis was conducted for the follows.

- Plain concrete beams under fixed pulsating load.
- RC beams under static, fixed pulsating and moving load.
- RC slabs reinforced by plain and deformed bars under a moving load.
- Strengthened RC slabs with FRP sheets under a moving load.

For all structures, applying fatigue loading leads to a propagating of the cracked elements due to the degradation of their bridging stress. This leads to a significant decreasing of their structural stiffness, an increasing of concrete strain and its crack opening, and an increasing of their deformations.

RC beams presents a longer fatigue life and wide propagation of the cracked elements than plain concrete beams. The plain concrete beams under fatigue loading lead to a localized crack propagation at critical beam sections.

RC beam under a moving load shows a wide propagation of the cracked elements than that under fixed pulsating load due to the effect of load movement. Therefore, this leads to longer fatigue life, larger center displacement and higher reinforcing bar strain.

For RC slab reinforced with plain reinforcing bars, the modified reinforcing bar model according to the bond-slip effect between plain reinforcing bar and its surrounding concrete by adding equivalent bond strain to plain bar strain in smeared reinforced concrete elements. This effect is significant after concrete cracking.

For RC slab under moving load, the propagation of cracked elements due to its bridging stress degradation is considered as the primary cause of fatigue failure. Therefore, applying higher moving load level leads to increasing of maximum tensile strain in concrete. According to the degradation equation, this leads to a significant bridging stress degradation resulting a higher degradation ratio and shorter fatigue life.

According to plain reinforcing bar model, RC slab reinforced with plain bars leads to higher concrete strain and higher crack opening than that reinforced with deformed bars. This leads to significant decreasing of bridging stress of concrete. Therefore, this slab shows a higher degradation ratio and shorter fatigue life than that reinforced with deformed bars.

For strengthened RC slabs with FRP sheets, the interfacial bond degradation between FRP sheets and its surrounding concrete due to fatigue load is considered. This interfacial bond was modeled by 8-node orthotropic thin element to simulate the vertical and horizontal debonding as sheet opening and sliding, respectively.

For strengthened RC slabs, FRP sheets leads to restrict the crack opening of theses cracks. This leads to a decreasing of maximum tensile concrete strain resulting a significant decreasing of the effect of bridging stress degradation than that in RC slab without strengthening. Therefore, strengthened RC slabs shows a smaller degradation ratio and longer fatigue life than that without strengthening.

At fatigue failure, FRP sheets leads to redirect the orientation of distributed cracks. Higher FRP sheet strain results in an increasing of its surrounding concrete strain in sheet direction resulting perpendicular cracks on this sheet.

The improvement of FRP strengthening is significant at slab center due to its larger crack opening in this zone. Therefore, extensive FRP strengthening at slab center is predicable to provide a longer fatigue life.

6.2 Future works

The following ideas can be used as future works or farther improvement.

- Development the numerical method to predict the fatigue behavior of RC slabs under moving load based on the bond degradation between rebar and its surrounding concrete.
- Fatigue life prediction of post degraded RC slabs due to a repetition of moving loads.
- Monitoring the cracks propagation and opening of existed RC bridge slabs based on the bridging stress degradation.

APPENDIX A- PUBLICATION LISTS

Part 1: Journal papers:

1. Drar, Ahmed Attia M., Takashi Matsumoto, Toshiro Hayashikawa, and Xingwen He. "Development of a Numerical Model to Predict the Fatigue Behaviors of RC Slabs." *Journal of Structural Engineering, JSCE*, vol. (71) A2, no. 2 (2015): I_805-I_812.
2. Drar, Ahmed Attia M., and Takashi Matsumoto. "Fatigue Analysis of RC Slabs Reinforced with Plain Bars Based on the Bridging Stress Degradation Concept." *Journal of Advanced Concrete Technology* 14, no. 1 (2016): 21-34.
3. Drar, Ahmed Attia M., and Takashi Matsumoto. "Fatigue analysis of FRP strengthening RC slabs reinforced with plain bars under moving load", *sustainable civil infrastructures journal*. (under preparing).
4. Drar, Ahmed Attia M., and Takashi Matsumoto. "Fatigue analysis of FRP strengthening RC slabs reinforced with plain bars based on bridging stress degradation concept", *material and structure journal*. (under preparing).

Part 2: Conference papers:

5. Drar, A. A. M., Matsumoto, T., Hayashikawa, T., and He, X. (2014). "Developing a numerical model for fatigue life prediction of plain concrete beams" JSCE Hokkaido brunch No. 71, Papers report collection No. A-31, (2014), Muroran, Japan.
6. Drar, A. A. M., Matsumoto, T., Hayashikawa, T., and He, X. (2015). "Development of a numerical model to predict the fatigue behaviors of RC slabs" JSCE, Applied Mechanics Symposium Conference No. 18, pp 207-208, (2015), Kanazawa, Japan.
7. Drar, A. A. M. and Matsumoto, T. (2015). "Fatigue analysis of RC slabs reinforced with plain bars subjected to moving load" EASEC-14, pp 867-673, Ho Chi Minh City, Vietnam.
8. Drar, A. A. M. and Matsumoto, T. (2015). "Developing a numerical method for fatigue life prediction of RC slabs reinforced with plain bars" 3rd International Conference on Computational Design in Engineering, pp 82, Tokyo.
9. Drar, A. A. M. and Matsumoto, T. (2015). "Fatigue analysis of RC slabs under moving load based on the bridging stress degradation concept" JSCE Hokkaido brunch No. 72, Papers report collection No. A-22, Sapporo, Japan.
10. Drar, A. A. M. and Matsumoto, T. (2016). "Fatigue analysis of FRP strengthened RC slabs reinforced with plain bars under moving load" GeoMEast2017 international conference, Sharm El-sheik, Egypt (accepted).
11. Drar, A. A. M., Matsumoto, T. and Hayashikawa, T. (2016). "Numerical simulation of FRP strengthening for RC slabs reinforced with plain bars under moving load" GJBS, Osaka, Japan (accepted).

REFERENCES

[1] S. Matsui, "Fatigue strength of RC-slabs of highway bridge by wheel running machine and influence of water on fatigue," *Proceedings of JCI,* vol. 9, pp. 627-632, 1987.

[2] P. C. Perdikaris and S. Beim, "RC bridge decks under pulsating and moving load," *Journal of Structural Engineering,* vol. 114, pp. 591-607, 1988.

[3] T. Ueda, M. Zahran, and Y. Kakuta, "Shear fatigue behavior of steel-concrete sandwich beams," *Concrete Library International of JSCE*, vol. 33, pp. 83-111, 1999.

[4] K. Maekawa, K. Toongoenthong, E. Gebreyouhannes, and T. Kishi, "Direct path-integral scheme for fatigue simulation of reinforced concrete in shear," *Journal of Advanced Concrete Technology,* vol. 4, pp. 159-177, 2006.

[5] V. C. Li and T. Matsumoto, "Fatigue crack growth analysis of fiber reinforced concrete with effect of interfacial bond degradation," *Cement and concrete composites,* vol. 20, pp. 339-351, 1998.

[6] P. Suthiwarapirak and T. Matsumoto, "Fatigue analysis of RC slabs and repaired RC slabs based on crack bridging degradation concept," *Journal of structural engineering,* vol. 132, pp. 939-948, 2006.

[7] K. Shakushiro, H. Mitamura, T. Watanabe, and N. Kishi, "Experimental study on fatigue durability of RC slabs rein-forced with round steel bars," *Journal of Structural Engineering, JSCE,* vol. 57(A), pp. 1297-1304, 2011 (in Japanese).

[8] H. MITAMURA, S. OMOTE, and H. NISHI, "Effects of Retrofit with Two CFRP Materials of Different Properties on Fatigue Durability Improvement of RC Slabs," *CERI Monthly Report*, pp. 2-14, 2011.

[9] K. Maekawa, H. Okamura, and A. Pimanmas, *Non-linear mechanics of reinforced concrete*: CRC Press, 2003.

[10] H. Kupfer, H. K. Hilsdorf, and H. Rusch, "Behavior of concrete under biaxial stresses," in *Journal Proceedings*, 1969, pp. 656-666.

[11] J. Zhang, H. Stang, and V. C. Li, "Fatigue life prediction of fiber reinforced concrete under flexural load," *International Journal of Fatigue,* vol. 21, pp. 1033-1049, 1999.

[12] J. Zhang, H. Stang, and V. C. Li, "Crack bridging model for fibre reinforced concrete under fatigue tension," *International Journal of Fatigue,* vol. 23, pp. 655-670, 2001.

[13] S. Wolinski, D. A. Hordijk, H. W. Reinhardt, and H. A. Cornelissen, "Influence of aggregate size on fracture mechanics parameters of concrete," *International Journal of Cement Composites and Lightweight Concrete,* vol. 9, pp. 95-103, 1987.

[14] K. Shakushiro, "Study on Durability of Highway Bridge RC Slabs using Round Bars under Cyclic Loading," *Ph.D. thesis, Muroran Institute of Technology*, 2014.

[15] J. G. Rots and J. Blaauwendraad, "Crack models for concrete, discrete or smeared? Fixed, multi-directional or rotating?," *HERON, 34 (1), 1989*, 1989.

[16] H. Varum, "Seismic assessment, strengthening and repair of existing buildings," *These de doctorat, Aveiro: Civil engineering department, University of Aveiro*, 2003.

[17] M. Dehestani and S. Mousavi, "Modified steel bar model incorporating bond-slip effects for embedded element method," *Construction and Building Materials*, vol. 81, pp. 284-290, 2015.

[18] A. Belarbi and T. T. Hsu, "Constitutive laws of concrete in tension and reinforcing bars stiffened by concrete," *Structural Journal*, vol. 91, pp. 465-474, 1994.

[19] J. Zhao and S. Sritharan, "Modeling of strain penetration effects in fiber-based analysis of reinforced concrete structures," *ACI structural journal*, vol. 104, p. 133, 2007.

[20] J. Melo, C. Fernandes, H. Varum, H. Rodrigues, A. Costa, and A. Arêde, "Numerical modelling of the cyclic behaviour of RC elements built with plain reinforcing bars," *Engineering structures*, vol. 33, pp. 273-286, 2011.

[21] M. Menegotto and P. Pinto, "Method of analysis for cyclically loaded reinforced concrete frames including changes in geometry and non-elastic behavior of elements under combined normal forces and bending moment," *IASBE Proceedings*, 1973.

[22] X. Lu, J. Teng, L. Ye, and J. Jiang, "Bond-slip models for FRP sheet/plate-to-concrete interfaces," in *Proceedings of 2nd international conference of advanced polymer composites for structural applications in construction (ACIC2004). Woodhead Publishing Limited, Cambridge, England*, 2004, pp. 152-61.

[23] X. Lu, J. Teng, L. Ye, and J. Jiang, "Bond–slip models for FRP sheets/plates bonded to concrete," *Engineering structures*, vol. 27, pp. 920-937, 2005.

[24] J. Dai, Y. Saito, T. Ueda, and Y. Sato, "Static and fatigue bond characteristics of interfaces between CFRP sheets and frost damage experienced concrete," in *Proceedings of Fourth International Symposium on Fiber Reinforced Polymer Reinforcement for Reinforced Concrete Structures (FRPRCS-4)*, 2005, pp. 1515-1530.

[25] Y. Yun, Y.-F. Wu, and W. C. Tang, "Performance of FRP bonding systems under fatigue loading," *Engineering Structures*, vol. 30, pp. 3129-3140, 2008.

[26] J. O. Holmen, "Fatigue of concrete by constant and variable amplitude loading," *Special Publication*, vol. 75, pp. 71-110, 1982.

[27] K. Loo, S. Foster, and S. T. Smith, "Fatigue behaviour of CFRP-repaired corroded RC beams," 2010.

[28] T. Matsumoto and V. C. Li, "Fatigue life analysis of fiber reinforced concrete with a fracture mechanics based model," *Cement and Concrete Composites,* vol. 21, pp. 249-261, 1999.

[29] P. Heffernan and M. Erki, "Fatigue behavior of reinforced concrete beams strengthened with carbon fiber reinforced plastic laminates," *Journal of Composites for Construction,* vol. 8, pp. 132-140, 2004.

[30] R. D. Guide, "American Association of State Highway and Transportation Officials," *Washington, DC,* 2002.

[31] F. A. Tavárez, *Simulation of behavior of composite grid reinforced concrete beams using explicit finite element methods*: University of Wisconsin--Madison, 2001.

[32] E. R. Buckhouse, *External flexural reinforcement of existing reinforced concrete beams using bolted steel channels*, 1997.

[33] J. Anthony and B. Wolanski, "Flexural behavior of reinforced and prestressed concrete beams using finite element analysis," *Milwaukee, Wisconsin (May 2004)*, 2004.

[34] K. Shakushiro, "Study on durability of highway bridge RC slabs using round bars under cyclic loading," *Ph.D. thesis, Muroran Institute of Technology,* 2014 (in Japanese).

[35] B. H. Oh and S. H. Kim, "Realistic models for local bond stress-slip of reinforced concrete under repeated loading," *Journal of Structural Engineering*, vol. 133, pp. 216-224, 2007.